Institute of Thermoelectricity, Academy of Sciences and Ministry of Education and Science of Ukraine

Journal of THERMOELECTRICITY

International Research
Founded in December, 1993
published 6 times a year

No. 2 *2014*

Editorial Board

Editor-in-Chief LUKYAN I. ANATYCHUK

Petro I. Baransky
Lyudmyla N. Vikhor
Ivan V. Gutsul
Stepan V. Melnychuk
Bogdan I. Stadnyk
Vilius Ya. Mikhailovsky
Elena I. Rogacheva
Andrey A. Snarskii

International Editorial Board

Lukyan I. Anatychuk, *Ukraine*
Steponas P. Ašmontas, *Lithuania*
Jean-Claude Tedenac, *France*
H.J. Goldsmid, *Australia*
L.P. Bulat, *Russia*
L. Chen, *China*
T. Caillat, *USA*
Yuri Grin, *Germany*
A.I. Casian, *Moldova*
Takenobu Kajikawa, *Japan*
T. Tritt, *USA*
Sergiy O. Filin, *Poland*
M.I. Fedorov, *Russia*
D. Sharp, *USA*
Yuri Gurevich, *Mexico*

Founders - National Academy of Sciences, Ukraine
Institute of Thermoelectricity of National Academy of Sciences and Ministry of Education and Science of Ukraine

Certificate of state registration № KB 15496-4068 ПР

Editorial office manager D. Taschuk

Editors:

L. Vikhor, V. Kramar, V. Katerynchuk, O. Luste, A. Farion, O. Bodnaruk

Approved for printing by the Academic Council of Institute of Thermoelectricity
of the National Academy of Sciences and Ministry of Education and Science, Ukraine

Address of editorial office:
Ukraine, 58002, Chernivtsi, General Post Office, P.O. Box 86.
Phone: +(380-372) 90 31 65.
Fax: +(380-3722) 4 19 17.
E-mail: jt@inst.cv.ua
http://www.jt.inst.cv.ua

Signed for publication 25.04.14. Format 70×108/16. Offset paper №1. Offset printing.
Printer's sheet 11.1. Publisher's signature 9.2. Circulation 400 copies. Order 6.

Printed from the layout original made by “Journal of Thermoelectricity” editorial board
in the printing house of “Bukrek” publishers,
10, Radischev Str., Chernivtsi, 58000, Ukraine

Copyright © Institute of Thermoelectricity, Academy of Sciences
and Ministry of Education and Science, Ukraine, 2014

CONTENTS

Theory

P.V. Gorsky, S.V. Melnychuk. Fundamental constants and similarity criteria in thermoelectricity 5

Material Research

E.I. Rogacheva, A.A. Nikolaenko, O.S. Vodorez, A.Yu. Sipatov, S.N. Grigorov, A.G. Fedorov. Size effects in *GeTe* thin films 11

M.O. Galuschak, I.V. Gorichok, O.S. Krynytsky, D.M. Freik. Thermoelectricity of lead telluride doped with *Sb* and *Bi* 22

E.M. Godzhayev, U.S. Abdurakhmanova. Phase analysis and electrophysical properties of $InGaTe_2$ 29

V.A. Romaka, P. Rogl, Yu.V. Stadnyk, L.P. Romaka, R.O. Korzh, D. Kaczorowski, V.Ya. Krayovskyy, O.I. Lakh. Structural, energy and kinetic characteristics of $Hf_{1-x}Lu_xNiSn$ thermoelectric material 39

Technology

V.A. Barabash, S.A. Glyazer, G.G. Gromov, I.A. Drabkin, L.B. Ershova, S.A. Molchanova. Matching of extruded materials based on bismuth-antimony chalcogenides for a thermoelement 50

Design

L.I. Anatychuk, R.V. Kuz. Effect of air cooling on the efficiency of thermoelectric generator in a diesel-engined car 57

Yu.M. Lobunets. Criteria for performance evaluation of thermoelectric energy converters 65

News

Kin-Ichi Uemura 81

Discussion

M.M. Mamedov. Universal nonequilibrium thermodynamics and the Seebeck effect 82

P.V. Gorsky, S.V. Melnychuk

Institute of Thermoelectricity of the NAS and MES
Ukraine, 1, Nauky Str. Chernivtsi, 58029, Ukraine

P.V. Gorsky

S.V. Melnychuk

FUNDAMENTAL CONSTANTS AND SIMILARITY CRITERIA IN THERMOELECTRICITY

In the paper, for reasons of dimensionality it is shown that all characteristics of thermoelectric materials (TEM) that are important for thermoelectric applications can be expressed through fundamental constants and dimensionless groups depending on material parameters and their application conditions. Therefore, materials possessing identical sets of these dimensionless groups should have identical thermoelectric characteristics. It is demonstrated how this method can be used for the estimation of achievable values of thermoelectric figure of merit of materials based on single crystals.

Key words: fundamental Seebeck coefficient, fundamental electric conductivity, fundamental power factor, fundamental thermal conductivity, fundamental thermoelectric figure of merit, fundamental dimensionless thermoelectric figure of merit.

Introduction

Similarity methods and dimensionality theories are widely employed in the simulation of many "macroscopic" physical objects and phenomena in mechanics, hydro- and aerodynamics [1], thermal physics [2], scattering media optics [3], etc. They are equally widely used in thermoelectricity in the simulation of operating modes of various devices. In so doing, a broad spectrum of various similarity criteria is used. To such criteria one can refer, for instance, the Ioffe criterion or the so-called thermoelectric figure of merit of material which is important in the determination of generator efficiency or refrigerator coefficient of performance. In the description of conditions of heat exchange between any thermoelectric device and the environment of significant importance is the so-called Biot criterion describing convective heat exchange in boundary layer. The Reynolds criterion is one of similarity criteria describing, for instance, the work of generator modules with permeable legs whose channels carry liquid or gas. Dimensionless current in the theory of thermoelectric cooling can serve one of similarity criteria for operating modes of various refrigerators. This list goes on, but it is used exceptionally for solving design and development, rather than material science problems, aside from the fact that the Ioffe factor or the related dimensionless thermoelectric figure of merit are mainly responsible for the choice of thermoelectric material. Moreover, it is assumed that in the microscopic "ab initio" description of the properties of condensed media, such as TEM, the similarity and dimensionality methods are of rather limited application, or not used at all, with the exception of renormalization group method which is well known to experts in theory of phase transitions and critical phenomena [4]. Therefore, the purpose of this paper is to illustrate the way of using these methods to get the estimates of the upper limits of thermoelectric figure of merit of TEM.

Fundamental thermoelectric characteristics and corollaries

We shall call fundamental thermoelectric characteristics the values that have proper dimensions and are expressed only through fundamental constants. In this respect, the simplest way is to introduce the fundamental Seebeck coefficient α_0 as follows:

$$\alpha_0 = k/e. \tag{1}$$

In this formula, k is the Boltzmann constant, e is electron charge modulus. The numerical value of this quantity is 86.25 μV/K.

The fundamental electric conductivity can be introduced equally easily. Its introduction, though, is not so unambiguous, but for reasons of dimensionality it is easy to check that as such one can take, for instance, the value:

$$\sigma_0 = e^2/(ha_B), \tag{2}$$

where h is the Planck constant, a_B is the radius of the first Bohr orbit in hydrogen atom. The numerical value of this quantity is $7.32\cdot10^5$ S/m. This value is about an order higher than the conductivity of bismuth telluride. This choice raises the question as to why as the fundamental length the radius of the first Bohr orbit in hydrogen atom was taken, rather than, say, a similar radius of hydrogen-like exciton in some semiconductor thermoelectric material, or some of lattice parameters of this material, which, at first sight, would be more natural. However, the radius of the first Bohr orbit in hydrogen atom is widely known and is really a fundamental value expressed in turn through other fundamental constants. However, the radius of exciton in thermoelectric material, just as its lattice parameter, is purely individual value determined by specific composition and structure of material, as well as by its manufacturing technique. Therefore, establishment of such peculiar “thermoelectric standard of length” requires, in the first place, some agreement on “standard” thermoelectric material “reproducing” this length and, in the second place, some strictly specified and reliably reproduced requirements to its composition, structure and manufacturing technique.

Thus, having decided upon fundamental electric conductivity in the form of (2), it can be easily understood that the fundamental power factor P_0 is determined as

$$P_0 = \alpha_0^2\sigma_0 = k^2/(ha_B). \tag{3}$$

Its numerical value is $5.44\cdot10^{-3}$ W/(m·K^2)

However, for a complete description of TEM these characteristics are insufficient. One must also introduce the fundamental thermal conductivity κ_0. For this purpose only the Wiedemann-Franz relation is suitable. Using it, we get the expression for κ_0:

$$\kappa_0 = k^2T_0/(ha_B). \tag{4}$$

In this case, as the fundamental temperature T_0, one can take “standard” temperature of normal conditions, i.e. 273.16 K. By virtue of such selection, the numerical value of fundamental thermal conductivity is 1.48 W/(m·K), which is close to thermal conductivity of bismuth telluride parallel to cleavage planes at 300 K.

Now it is an easy matter to introduce a fundamental thermoelectric figure of merit Z_0. Taking into account (3) and (4), it is not difficult to obtain that:

$$Z_0 = 1/T_0. \tag{5}$$

The numerical value of this value is $3.66\cdot10^{-3}$ K^{-1}. Therefore, the fundamental dimensionless thermoelectric figure of merit Z_0T_0 is simply equal to unity.

Thus, thermoelectric characteristics of any TEM under any application conditions can be expressed through fundamental thermoelectric characteristics as follows:

$$\alpha = \alpha_0 f_\alpha\left(\{a_\alpha\}\right), \tag{6}$$

$$\sigma = \sigma_0 f_\sigma\left(\{a_\sigma\}\right), \tag{7}$$

$$\kappa = \kappa_0 f_\kappa\left(\{a_\kappa\}\right), \tag{8}$$

$$P = P_0 f_\alpha^2\left(\{a_\alpha\}\right) f_\sigma\left(\{a_\sigma\}\right), \tag{9}$$

$$Z = \frac{f_\alpha^2\left(\{a_\alpha\}\right) f_\sigma\left(\{a_\sigma\}\right)}{T_0 f_\kappa\left(\{a_\kappa\}\right)}, \tag{10}$$

$$ZT = \frac{T f_\alpha^2\left(\{a_\alpha\}\right) f_\sigma\left(\{a_\sigma\}\right)}{T_0 f_\kappa\left(\{a_\kappa\}\right)}. \tag{11}$$

In formulae (6) – (11), f_α, f_σ, f_κ are certain dimensionless functions depending on the sets of dimensionless groups $\{a_\alpha\}$, $\{a_\sigma\}$, $\{a_\kappa\}$, or similarity criteria, comprising both material parameters and characteristics of its application conditions. From this standpoint, the basic task of thermoelectric materials science (in its theoretical part) is to develop a detailed theory for said dimensionless functions.

As regards Eq. (11), at first sight it may seem an absurd tautology adding nothing to understanding the heart of the matter, as there are relationships (6 – 10). Nevertheless, imagine certain, though hypothetical, TEM for which the dimensionless functions f_α, f_σ, f_κ are such that in a certain temperature range the relationship $\frac{f_\alpha^2\left(\{a_\alpha\}\right) f_\sigma\left(\{a_\sigma\}\right)}{f_\kappa\left(\{a_\kappa\}\right)}$ is a weakly varying function of temperature close to unity. Then for the dimensionless thermoelectric figure of merit of such hypothetical TEM in the mentioned temperature range the following simple formula is valid:

$$ZT = T/T_0. \tag{12}$$

In the authors' opinion, it is already something more than "mere nothing". Let our hypothetical TEM fulfill the above specified conditions, say, in the temperature range from 523 to 773 K (it is a typical "generator" range). Then its dimensionless thermoelectric figure of merit in the above temperature range should linearly increase from 1.92 to 2.83. In case it could be created, it would be a fairly good TEM. It is interesting to compare its characteristics to the experimental data for some real generator TEM. This data [5] shows that the dimensionless thermoelectric figure of merit of even fairly good nanostructured and composite TEM at a temperature of 523 K, is at least a factor of 1.23 – 1.92 lower compared to our hypothetical TEM. Moreover, in practice there is either a decrease in dimensionless thermoelectric figure of merit with temperature, or the existence of maximum, rather than its monotonous increase. Exactly the latter fact, on the one hand, necessitates creation and use of functionally-graded TEM, and, on the other hand, causes the very possibility of this [6]. Hence, our requirement to dimensionless functions f_α, f_σ, f_κ, simple at first sight, in fact, is a rather strict requirement to TEM which is far from being satisfied so far. At this point, however, we finish discussion of only small fraction of general considerations related to the use of methods of similarity and dimensions in theory of thermoelectricity and pass on to some specific examples.

Some specific examples of constructing model dimensionless functions and their corollaries

We begin with the simplest widely known case of calculating Seebeck coefficient of a semiconductor with isotropic square law of dispersion and power law of energy dependence of relaxation

time in impurity region. The above characteristic is a function of only two dimensionless parameters, namely $\eta = \zeta/kT$, where ζ is chemical potential of carrier gas, and power exponent r in the law of energy dependence of relaxation time, i.e. in this case $\{a_\alpha\} = \{\eta, r\}$. The respective model function is given by [7]:

$$f_\alpha\left(\{\eta, r\}\right) = \frac{(2r+5)F_{r+3/2}(\eta)}{(2r+3)F_{r+1/2}(\eta)} - \eta. \tag{13}$$

In this formula, $F_n(\eta)$ are the Fermi integrals. Note that braces, along with round brackets on the left side of formula (13), just as in subsequent similar formulae, will be used by the authors not in the least in order to artificially complicate or "cloud" material presentation, but in order to emphasize that in each specific case the respective dimensionless parameters are by no means casual, but make a certain unified closed set, clearly and unambiguously caused by selected model approach.

Consider some corollaries from relationship (13). For this purpose we will take into account the fact that according to general principles of quantum mechanics, power exponent r can vary from -0.5 to 3.5. Let us analyze from this standpoint possible limits of change in the value of Seebeck coefficient of thermoelectric material $Bi_{0.5}Sb_{1.5}Te_3$. Using equation determining chemical potential, i.e. parameter η, in the form [7]

$$n_0 = \frac{8\sqrt{2}\pi\left(m^* kT\right)^{3/2}}{h^3} F_{1/2}(\eta), \tag{14}$$

we will get that, for instance, at hole concentration $n_0 = 3.2\cdot10^{19}$ cm^{-3}, density-of-state effective mass $m^* = 0.94\, m_0$, temperature $T = 300$ K and $r = -0.5$, which corresponds to dominating at this temperature charge carrier scattering on the deformation potential of acoustic phonons $\alpha = 172$ μV/K. This theoretical value with an error less than 10 % is in agreement with the experimental data [8] for $Bi_{0.5}Sb_{1.5}Te_3$. However, if it were $r = 3.5$ (this case corresponds to a hypothetical TEM where there is ultimately strong energy filtration of charge carriers), the value of Seebeck coefficient would be 480 μV/K. And this, with unvaried electric conductivity, would mean increase in the figure of merit of TEM by a factor of 7.79. However, such strong filtration is hardly realizable in any TEM. Therefore, it seems more correct to consider a case of charge carrier scattering on random potential of chaotically distributed charged impurities whose concentration will be considered to be equal to charge carrier concentration which corresponds to single ionization of impurity centres. To determine the mean free path of charge carriers in this case, it is necessary to know transport cross-section. From among relatively simple formulae that determine it and have correct asymptotics at low and high energies, the Conwell-Weiskopf formula in the authors' opinion is the most correct. It is based on the angular dependence (defined by Rutherford formula) of differential cross-section of charged particle scattering on unscreened Coulomb potential, which is identical both in classical and quantum case. The energy dependence of relaxation time in this case is given by:

$$\tau(\varepsilon) = \frac{16\pi\sqrt{2m^*}\left(\chi\varepsilon_0\right)^2 \varepsilon^{3/2}}{e^4 N_i \ln\left[1 + \left(4\pi\chi\varepsilon_0 / e^2 N_i^{1/3}\right)^2 \varepsilon^2\right]}, \tag{15}$$

In this formula, N_i is impurity concentration which in case of single ionization is taken to be equal to major-carrier concentration, m^* is charge carrier effective mass, χ is relative dielectric constant of TEM, and ε_0 is absolute dielectric constant of vacuum.

In the calculation of relaxation time based on this formula, quite a reasonable physical assumption is made that in a crystal there is no sense to consider impact parameters exceeding half the

average distance between scattering centres. Using this formula, from the condition of coincidence of the observed and calculated values of electric conductivity for $Bi_{0.5}Sb_{1.5}Te_3$ we get that the effective relative dielectric constant of this TEM is of the order of 44. Such estimation based on the data of [7, 8] also seems to be reasonable. In this case the calculated value of Seebeck coefficient is 272 μV/K. And it means thermoelectric figure of merit increase as low as 2.5 times. Taking into account that the figure of merit of our TEM at 300 K is $2.6 \cdot 10^{-3}$ K^{-1}, the predicted value of dimensionless thermoelectric figure of merit of TEM at 300 K provided that it is increased by a factor of 2.5, will be 1.95. It is shown that such or somewhat higher values of dimensionless thermoelectric figure of merit are attainable in good bulk nanostructured TEM obtained of nanopowders by hot pressing or electric spark plasma sintering techniques [9, 10]. It is considered that such values of thermoelectric figure of merit are attainable in good bulk nanostructured TEM obtained from nanopowders by hot pressing or electric spark plasma sintering. But this case also corresponds to sufficiently strong energy filtration of charge carriers. At first sight it may seem that the necessary energy filtration can be achieved by increasing the number of scattering centres in material, hence, by suppressing "harmful" in terms of Seebeck coefficient value charge carrier scattering on deformation potential of acoustic phonons. But the Conwell-Weiskopf formula implies that with increase in the number of impurities, the mean free path of charge carriers ceases to depend on energy. Moreover, conductivity increase does not compensate the drop in squared Seebeck coefficient, even though the contribution of lattice thermal conductivity is considered to be small, and thermoelectric figure of merit of material can be considered as the integral characteristic of a subsystem of free charge carriers in it. In this case, for the dimensionless thermoelectric figure of merit the following formula is valid:

$$ZT = \alpha^2 / L, \tag{16}$$

where L is the Lorentz number. In the case of simple isotropic parabolic zone this formula with regard to known relationships [7] yields the following expression:

$$ZT = \left[\frac{(2r+5)F_{r+3/2}(\eta)}{(2r+3)F_{r+1/2}(\eta)} - \eta \right]^2 \left[\frac{(r+7/2)F_{r+5/2}(\eta)}{(r+3/2)F_{r+1/2}(\eta)} - \frac{(r+5/2)^2 F^2_{r+3/2}(\eta)}{(r+3/2)^2 F^2_{r+1/2}(\eta)} \right]^{-1}. \tag{17}$$

Therefore, it is exactly "harmful" effect that we get. It is illustrated in Fig. 1.

From Fig. 1 it is seen that with increase in the degeneracy degree of free carrier gas, i.e. doping impurity concentration, the dimensionless thermoelectric figure of merit of material drops, and with increase in power exponent r, it increases. However, high values of r correspond to strong energy filtration of charge carriers in material.

Thus, to achieve even the value of 1.95 at 300 K for single crystal is problematic. This result differs radically from that in [11] according to which the thermoelectric figure of merit of TEM at $r = 1.5$ can reach 3. The difference is due to the fact that [11] does not take into account the difference of r from 1.5 at low charge carrier energies. Therefore, to achieve so high figure of merit, it is necessary to use

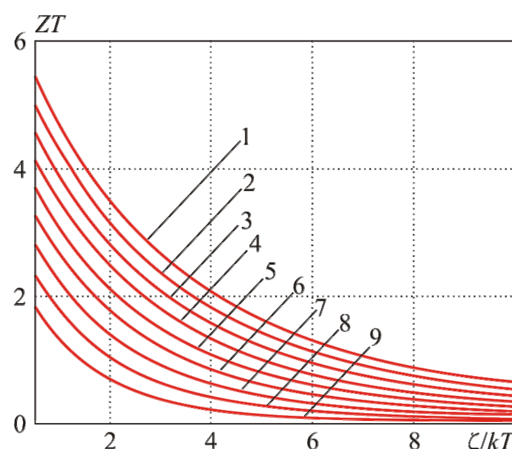

Fig. 1. Dependnece of dimensionless thermoelectric figure of merit of material on the degeneracy degree of free carrier gas with different energy dependences of relaxation time. Curves 1 – 9 are constructed for r from – 0.5 to 3.5 with increment 0.5.

special additional measures for creation in TEM of a kind of quantum-mechanical "filtration barriers", which is by no means always realizable in practice. Therefore, fundamental physical restrictions on power exponent *r* caused, in particular, by its drop at low energies, embound the achievable thermoelectric figure of merit of TEM based on a single crystal. Thus, it turns out that whereas the lower limit of dimensionless thermoelectric figure of merit of TEM determined by formula (12) might be attainable in a single crystal, the achievement of upper limit, at least at this stage, seems to be doubtful.

Conclusions

1. All thermoelectric characteristics of materials can be expressed through fundamental values of these characteristics and dimensionless groups comprising material parameters and characteristics of their application conditions.
2. The increase in thermoelectric material figure of merit is restricted by Seebeck coefficient drop with increase in charge carrier concentration and the energy dependence of charge carrier scattering factor.
3. For essential increase in the figure of merit of TEM based on single crystals it is necessary to create conditions whereby there is strong charge energy filtration of charge carriers.

References

1. L.I. Sedov, *Mechanics of Continuous Medium*, *Vol. 1-2* (Moscow: Nauka, 1976).
2. *Fundamentals of Thermal Engineering: Handbook*, ed. by V.A. Grigoryev and V.M. Zorin, Vol. 1, 2 (Moscow: Energoatomizdat, 1988).
3. A. Ishimaru, *Wave Propagation and Scattering in Random Media, Vol. 1, 2* (New York: Academic Press, 1978).
4. J. Zaiman, *Models of Disorder* [Russian translation] (Moscow: Mir, 1982), 592 p.
5. S. Fan, J. Zhao, J. Guo, Q. Yan, J. Ma, and H.H. Hang, *p*-type $Bi_{0.4}Sb_{1.6}Te_3$ Nanocomposites with Enhanced Figure of Merit, *Appl. Phys. Lett.* 96 182104/1-3 (2010).
6. LI. Anatychuk, L.M. Vikhor, *Thermoelectricity, Vol. IV, Functionally Graded Thermoelectric Materials* (Kyiv-Chernivtsi: Institute of Thermoelectricity, 2012), 180 p.
7. B.M. Goltzman, V.A. Kudinov, and I.A. Smirnov, *Semiconductor Thermoelectric Materials Based on* Bi_2Te_3 (Moscow: Nauka, 1972), 320 p.
8. L.D. Ivanova, Yu.V. Granatkina, A. Dauscher, B. Lenoir, and H. Sherrer, Influence of the Purity and Perfection of Czochralski-grown Single Crystals of Bismuth and Antimony Chalcogenides Solid Solution on Their Thermoelectric Properties, *Proc. of 5th European Workshop on Thermoelectrics (Pardubice, Czech Republic, 1999), 175 – 178.*
9. P.V. Gorsky, V.P. Mikhalchenko, On the issue of the mechanism for increasing the thermoelectric figure of merit of the bulk nanostructured materials, *J. Thermoelectricity* **5**, 5 – 9 (2013).
10. L.I. Anatychuk, P.V. Gorsky, V.P. Mikhalchenko, Impact of size effects on the properties of thermoelectric materials, *J. Thermoelectricity* **1**, 5 – 11 (2014).
11. L.P. Bulat, V.S. Zakordonets, The Theoretical Analysis of Thermoelectric Materials Figure of Merit, *J. Thermoelectricity* **2**, 15 – 23 (1995).

Submitted 03.01.2014.

E.I. Rogacheva[1], A.A. Nikolaenko[1], O.S. Vodorez[1], A.Yu. Sipatov[1], S.N. Grigorov[1], A.G. Fedorov[2]

[1]National Technical University "Kharkiv Polytechnic Institute"
21, Frunze Str., Kharkiv, 61002, Ukraine;
[2]Institute for Scintillation Materials NAS of Ukraine, 60, Lenin Ave., Kharkiv, 61001, Ukraine

SIZE EFFECTS IN *GeTe* THIN FILMS

Dependences of electric conductivity σ, the Seebeck coefficient S, the Hall coefficient R_H, charge carrier mobility μ_H and thermoelectric power $P = S^2\sigma$ on the thickness d (d = 5 – 210 nm) of GeTe thin films grown by thermal evaporation in vacuum of GeTe crystals with subsequent condensation on (001) KCl substrates at temperature T_S = 520 K have been studied. For films of different thickness the temperature dependences of σ, R_H and μ_H in the range of 80 – 300 K have been obtained and power coefficient ν in the dependence $\mu_H(T)$ has been determined. Electron microscopy and electron diffraction methods have been used to show that the films possess a rhombohedral structure corresponding to a low-temperature α-modification of GeTe and grow with the preferred orientation (111) and (111) $(\bar{1}11)$ || (001) KCl. It has been established that with a growth of film thickness to ~ 100 – 150 nm, the values of σ, μ_H and ν are monotonously increased, the dependences $R_H(d)$, S(d) and P(d) have the form of curves with a peak at ~ 75 nm, and with further increase of d the kinetic coefficients are practically unvaried. The dependence of properties on the thickness of films testifies to manifestation in GeTe films of classical size effect. Theoretical calculation of the dependence σ(d) made in the framework of the Fuchs-Sondheimer theory is in good agreement with the experimental data. It has been established that the concentrations of holes in the films are lower, and S and P values are higher than in the bulk crystal. Maximum P values are achieved at d ~ 75 nm.

Key words: germanium telluride, thin films, thickness, temperature, thermoelectric properties, classical size effect.

Introduction

Germanium monotelluride is well known as a promising medium-temperature thermoelectric (TE) material of *p*-type [1-3]. It is a narrow-gap degenerate semiconductor with a multi-valley structure of energy bands and a high degree of deviation from stoichiometry. Within a wide homogeneity range (50.3 – 51.5 at.% *Te*) displaced towards *Te* excess with respect to stoichiometric composition, *GeTe* has three polymorphous modifications, namely high-temperature (β) and two low-temperature (α and γ). At temperatures lower than ~ 670 K the fcc lattice of *NaCl* type in β-*GeTe* is transformed into rhombohedral (α-*GeTe*) or rhombic one (γ-*GeTe*). The low-temperature α- and γ- modifications exist in the range of compositions close to homogeneity region on the side of *Ge* and *Te*, respectively, and in the range of compositions 50.5 – 50.9 at.% *Te* there is an eutectoid decomposition β → α + γ. Considerable deviation from stoichiometry determines high concentration of intrinsic defects (for the most part doubly ionized cation vacancies) and *p*-type charge carriers (~ 10^{20} – 10^{21}cm^{-3}). Among the disadvantages of *GeTe* as a TE material is too high concentration of holes exceeding the optimal value almost by an order. The problem of *p* reduction is generally solved by doping [1-4].

System dimension is another parameter permitting control of the physical properties, including TE ones [5-7]. For instance, it is known that if film thickness d is comparable to mean free path of charge carriers, there is the so-called classical size effect, manifested in the dependence of the kinetic properties of films on their thickness [5, 6]. This effect arises due to the fact that with a reduction of d the contribution of surface scattering of charge carriers to the resulting scattering is increased and becomes comparable to the contribution of bulk scattering.

A great many works have been devoted to the study of *GeTe* films. Some works ([8-10]) investigated the mechanism of growth and crystalline structure of *GeTe* films deposited onto glass, mica, (001) *NaCl*, (001) *KCl*, (001) *SnTe*, (111) BaF_2 and other materials at different substrate temperatures T_s. It was shown that depending on substrate temperature the films can be amorphous, textured or epitaxial, and that substrate type does not play a defining role in the determination of structural state of the films. Some works studied the electrical properties of *GeTe* films as a function of various factors (evaporator temperature, substrate type and temperature, thermal treatment, initial substance composition, condensation rate, etc.) [11-18]. It was established that substrate temperature determines not only the structural state of the film, but also the electrophysical and TE parameters. For instance, according to work [13] that investigated *GeTe* films on mica, *Te* content in the charge practically does not affect the electrical properties of the films, and hole concentration p in the films is primarily dependent on T_s: at low substrate temperatures p in the film is factor of 1.5 – 2 greater than p in the initial substance, and at high T_s, – on the contrary, it is reduced by a factor of 3 – 4. The authors of [14] showed that the electrical properties and structure of *GeTe* films are determined not only by substrate temperature, but also by condensation rate, as well as the duration and temperature of annealing, and are practically independent of charge composition. Considerable attention was given to investigation of the character of change in the electrical properties of *GeTe* when going from amorphous to crystalline state [7, 11, 16, 17]. In the interpretation of experimental results, especially the data related to hole concentration in thin films, the majority of explanations was reduced to the assumption of not only quantitative, but also qualitative change in defective structure with a change in technological parameters, as well as to possibility of re-evaporation processes at condensation.

As regards study of the kinetic properties of *GeTe* thin films as a function of thickness d, there is work [11] which studies the dependences of resistivity ρ, the Hall coefficient R_H and charge carrier mobility μ_H on the thickness of *GeTe* crystalline films obtained by electron-beam evaporation of *GeTe* crystals with subsequent condensation on the glass at $T_s = 425$ K. In the range of thickness $d = 8 \div 40$ nm the authors of [11] who observed a reduction of ρ and R_H and increase in μ_H with a growth of d attributed this fact to structural imperfection of films at low thicknesses. In [19] we reported the observed dependence of electrical conductivity σ and μ_H on the thickness of *GeTe* films obtained by thermal evaporation in vacuum of *GeTe* crystals and subsequent condensation on the surface of (001) *KCl* at 520 K. We attributed the existence of such dependence to classical size effect manifestation.

The purpose of this work is a more detailed study of classical size effect in *GeTe* thin films obtained by thermal evaporation in vacuum through measurement of the galvanomagnetic and TE properties.

Experimental procedure

GeTe thin films of thickness $d = 5 – 210$ nm were prepared by thermal evaporation in vacuum ($\sim 10^{-5} – 10^{-6}$ Pa) of *GeTe* crystals. As a charge for sputtering we used polycrystalline *GeTe* obtained by direct melting of initial components in evacuated quartz ampoules. The rate of films condensation was 0.1 – 0.3 nm/s. As the substrates we used glass at $T_s = 300 \pm 10$ K and *KCl* (001) cleavages at

T_s = 300 ± 10 K and T_s = 520 ± 10 K. To prevent interaction with the air atmosphere, the films were coated with a layer of Al_2O_3 10 – 20 nm thick which was deposited onto the surface of films by electron-beam evaporation method. Film thickness was determined by a pre-calibrated quartz resonator located close to the substrates. Calibration of the resonator for films of $d > 100$ nm was performed by means of interferometer, and for films of $d < 100$ nm – with the use of *X*-ray diffractograms of small-angle scattering for one-layer films by comparison of experimental and calculated diffractograms. In this case, near the primary beam there is *X*-ray diffraction, namely the Kissing oscillations by the period of which one can determine film thickness to an accuracy of 0.1 nm. The calculated film thickness was varied for matching the calculated curve to the experimental one. Diffraction curves were obtained on DRON-2 diffractometer in CuK_α-radiation in $\Theta - 2\Theta$ scanning mode. As an example, Fig. 1 shows calculated and experimental diffraction curves for films with d = 77 nm and d = 105 nm.

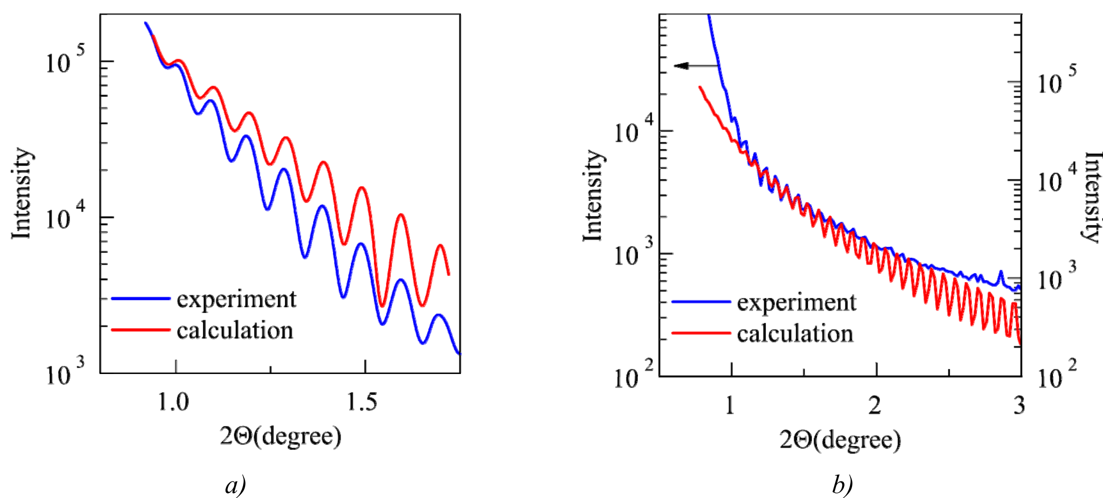

Fig. 1. Experimental and calculated diffractograms of small-angle X-ray scattering of GeTe films: a) – d = 77 nm, b) – d = 105 nm.

Electron microscope investigations of the films were performed on radiographic electron microscope PEM-125K. The temperature dependences of R_H and σ were obtained by method of direct current through the sample and constant magnetic field with induction 1 T in the temperature range of 80 – 300 K. The measurements of σ and R_H were made in two modes: cooling (300 – 80 K) and heating (80 – 300 K), which prompted a conclusion of practical absence of the temperature hysteresis. The Hall mobility of charge carriers and hole concentration p was calculated by the formulae $\mu_H = \sigma \cdot R_H$ and $p = 1/R_H \cdot e$, respectively, where e is electron charge. The Seebeck coefficient S was measured by compensation method with respect to copper. The error of measurement of R_H, σ and S did not exceed ± 5 %. Measurement of the electrophysical properties of the bulk crystal *GeTe* used as a charge showed that crystal has hole conductivity and the following set of electrophysical parameters: $p = 5.7 \cdot 10^{20}$ cm^{-3}, μ = 55 cm^2/V·s, σ = 5820 Ω^{-1}cm^{-1}, S = 32 μV/K. All the measurements were made on as-prepared films.

Experimental results

Electron-microscopic study of *GeTe* structure has shown that films deposited onto glass and (001) *KCl* surface at T_s = 300 K are amorphous. With the investigation in electron microscope they were crystallized under the effect of electron beam. Fig. 2 shows an electron micrograph of crystalline fragment in amorphous die and its microdiffraction pattern. Crystal growth is of dendritic nature.

Crystalline structure of small crystals corresponds to the structure of low-temperature α-modification of *GeTe* (rhombohedrally distorted structure of *NaCl* with parameters a = 0.5986 nm, $\alpha = 88.35^{o}$ [3, 4]).

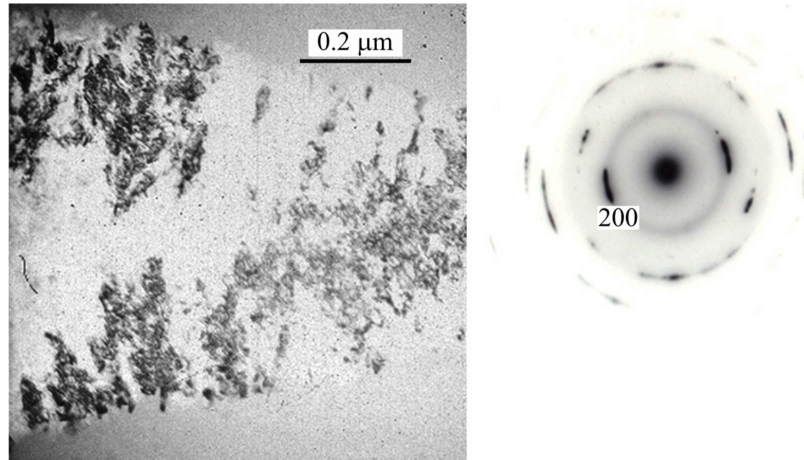

Fig. 2. Crystallization of amorphous GeTe film with d = 40 nm.

According to the results of electron-microscopic study, on (001) *KCl* substrate heated to temperature T_s = 520 K, α-*GeTe* film grows by island mechanism with the preferred orientation of (111) and $(\bar{1}11)$ α-*GeTe* || (001) *KCl*, and full healing of the film occurs at $d \approx 20$ nm (Fig. 3). The film with d = 7 nm (Fig. 3, *a*) is at the island growth stage, when isolated chips of α-*GeTe* have a distinct crystallographic faceting and grow together mechanically, without a variation of faceting, mutual arrangement and orientation. The angles between the faces of interlocked crystals are practically unrounded. The above described growth form is typical of substance condensation by the mechanism of "vapor-crystal without coalescence of contacting particles" [20]. The α-*GeTe* film with d = 23 nm (Fig. 3, *b*) is almost continuous and has plane intercrystalline boundaries faceting the grains. The results obtained are mostly consistent with the data of [7-9].

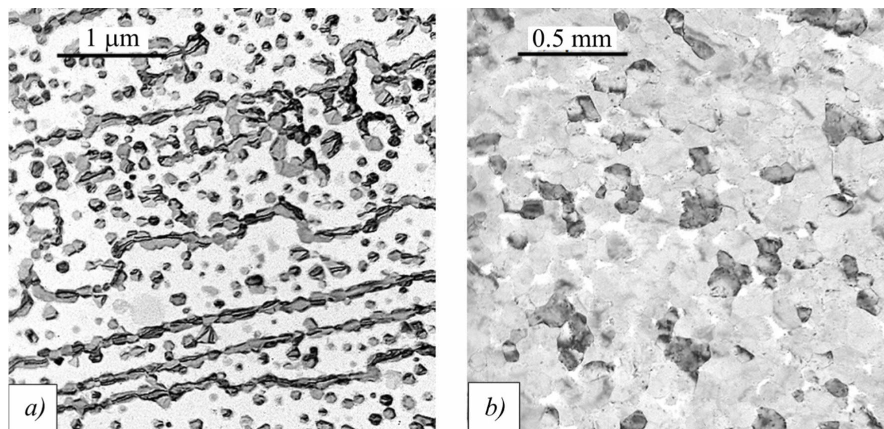

Fig. 3. Electron micrographs of GeTe films deposited onto (001) KCl substrates at temperature T_s = 520 K. Film thicknesses: d = 7 nm (a) and d = 23 nm (b).

Films deposited on (001) *KCl* at T_s = 520 K at d < 25 nm proved to be nonconducting, which agrees with the presence of island structure with small thicknesses.

Fig. 4, *a – d* shows the temperature dependences of σ, μ_H and R_H for *GeTe* polycrystal of which the films were manufactured and for some *GeTe* films (d = 208, 170 and 30 nm). For films of other thickness the dependences σ(T), $\mu_H(T)$, $R_H(T)$ were of similar type. From Fig. 4, *a* it is clear that the

choice of measurement mode (heating-cooling or cooling-heating) does not affect the general type of dependence $\sigma(T)$ and the values of σ. It points to the absence of temperature hysteresis and testifies to sufficiently equilibrium measurement conditions.

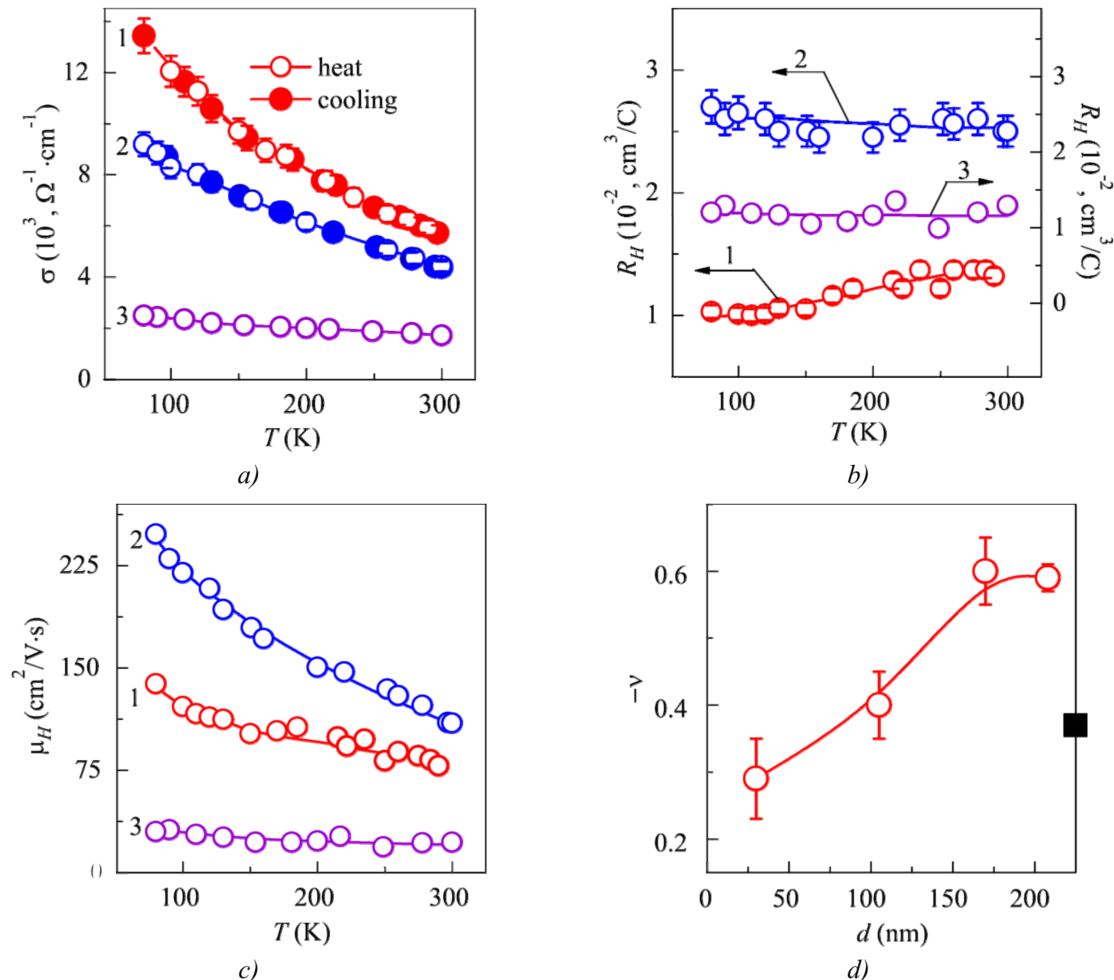

Fig. 4. Temperature dependences of electric conductivity σ (a), the Hall coefficient R_H (b), the Hall mobility of charge carriers μ_H (c) of GeTe thin films and power coefficient ν in the dependence $\mu_H \sim T^\nu$ as a function of thickness of GeTe films (d): 1 – polycrystal; 2 – film, d = 208 nm; 3 – film d = 30 nm. (d): Black square on the axis is the value of coefficient ν for polycrystal.

As can be seen, for all investigated samples, with a rise in temperature, the values of σ and μ_H are reduced, and the values of R_H are practically unvaried with temperature for the films and slightly increase for *GeTe* polycrystal. Such type of the temperature dependences of galvanomagnetic properties is characteristic of degenerate semiconductors. The observed R_H increase with temperature for *GeTe* polycrystal is generally related to a complex structure of *GeTe* valence band consisting of two subbands with different density of states and redistribution of holes in the subbands with a rise in temperature [3, 4, 21-24].

On the assumption of the power type of the temperature dependence of charge carrier mobility ($\mu_H \sim T^\nu$) based on the experimental data (Fig. 4, *c*) the power coefficients ν were determined by construction of log-log plots ($\ln\mu_H - \ln T$). Fig. 4, *d* shows the dependence of ν on the thickness of films. It is seen that with a growth of *d* the power coefficient increases from $\nu = -0.3 \pm 0.05$ for a film with $d = 30$ nm to $\nu = -0.6 \pm 0.05$ for a film with $d = 170$ nm, following which it is practically

unvaried. This testifies to increase with growth of film thickness of phonon scattering contribution (for metals and strongly degenerate semiconductors $\nu = -1.0$) as compared to scattering on crystal lattice defects ($\nu = 0$). For polycrystal $\nu = -0.4 \pm 0.05$, and this indicates that as a result of charge carrier scattering on the grain boundaries polycrystal proves to be more defective than "thick" textured film.

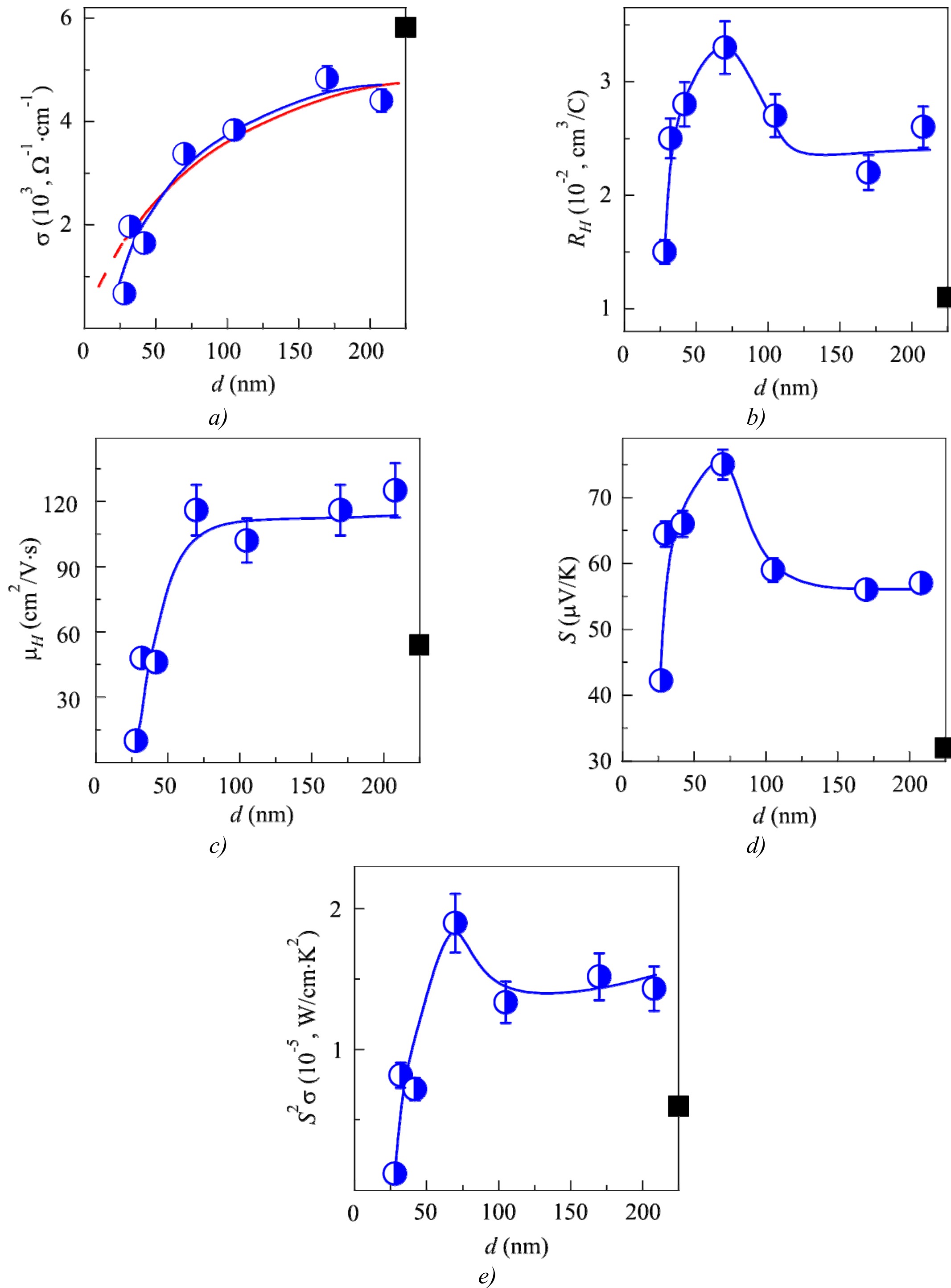

Fig. 5. Dependences of electric conductivity σ (a), the Hall coefficient R_H (b), the Hall mobility of charge carriers μ_H (c), the Seebeck coefficient S (d) and thermoelectric power $P = S^2{\cdot}\sigma$ of GeTe films at 300 K. Black squares are the values of σ, μ_H, R_H, S and P for the bulk polycrystal of GeTe; red line in Fig. 5 (a) – theoretical calculation of $\sigma(d)_{theor}$ using the Fuchs-Sondheimer theory.

Fig. 5 shows the dependences of σ, R_H, μ_H, S and TE power $P = S^2\sigma$ on the thickness of films at room temperature. Analysis of the dependences σ(d), $R_H(d)$, $\mu_H(d)$, $S(d)$ and $P(d)$ shows the following.

1) Over the entire investigated thickness range σ is monotonously increased with a growth of d, and charge carrier mobility quickly grows to ~ 100 nm, then being practically unvaried;

2) S, R_H and P vary with thickness in a more complicated way as compared to σ and μ_H: up to d ~ 75 nm there is fast growth of S, R_H and P with increase of film thickness, then these values drop to d ~ 100 nm, following which S, R_H and P do not vary;

3) the values of the Hall coefficient in the bulk crystal are lower than in the films. For instance, for a film of thickness d ~ 75 nm R_H is increased as compared to a crystal by a factor of ~ 3.5. It means that in the films it is possible to get lower charge carrier (hole) concentrations than in polycrystal;

5) the values of the Seebeck coefficient and thermoelectric power in the bulk crystal are considerably lower than in the films. Maximum values of S and P correspond to films of thickness d ~ 75 nm.

Analysis of the results

1. First of all, we should state the fact that in the films under study there is a classical size effect related to increase of the share of charge carriers scattered on the film surfaces, as its thickness is reduced. In the bulk crystals the role of the surface serving as structural imperfection is minor, and free path of charge carriers l is mainly determined by scattering of the latter in the bulk of the crystal. As the film thickness is reduced, the contribution of surface scattering is increased, leading to a respective change of properties.

The Fuchs-Sondheimer theory of classical size effect [25-27] which was developed for metals is based on the use of the Boltzmann kinetic equation and the boundary conditions on the film surface. The theory has two independent parameters: 1) relationship d/l where l is free path of charge carriers, and 2) specularity parameter R characterizing the share of electrons elastically reflected from the film surface. The value of R lies between 0 (for fully diffuse scattering) and 1 (for fully specular scattering).

According to the Fuchs-Sondheimer theory [25, 26], the formula for calculation of the dependence of electric conductivity σ on film thickness d is given by:

$$\sigma(d) = \frac{3}{4}\sigma_\infty \frac{d}{l}\ln\left(\frac{l}{d}\right)\left(\frac{1+p}{1-p}\right), \ \frac{d}{l} << 1, \tag{1}$$

where σ_∞ is infinitely thick sample conductivity and d is film thickness.

It should be noted that the theory comprises a number of simplifications (consideration is given to a metal with a spherical Fermi surface and isotropic free path; it is assumed that specularity parameter is a constant equal for both Fermi surfaces and trajectory-independent). However, despite the fact that the theory is rather approximate, in many cases for metals there is a good agreement between theory and experiment, though in very thin films, even if they are continuous, the conductivity is generally reduced much faster than it follows from the theory [25-27].

When establishing the dependence of the kinetic coefficients on the film thickness in semiconductors, we must take into account the availability in them of a near-surface space charge. The authors of a number of works tried to do it (see, for instance, [1]), but up to date the theory of size effect for transport phenomena in semiconductors has not been developed yet.

In this connection, we have performed a theoretical calculation of dependence σ(d) using formula (1) of the Fuchs-Sondheimer theory. As σ_∞ value, the electric conductivity value for the bulk

polycrystal was taken ($\sigma_\infty = 5820\ \Omega^{-1}\cdot\text{cm}^{-1}$). The resulting theoretical dependence $\sigma(d)_{theor}$ (shown in Fig. 5, *a* as a red line) practically coincides with a line drawn through the experimental points by least-squares method, with the following values of specularity parameter *p* and hole free path *l*: $R = 0.5 \pm 0.01$ and $l = (680 \pm 10)$ nm. It is seen, however, that the first point corresponding to the smallest thickness lies below the theoretical curve, which is quite explainable, if, apart from the size effect, we take into account the influence of structural factor on the electric conductivity values. The influence of structural factor is due to the fact that *GeTe* films grow on halide crystals according to island mechanism [20], and with a growth of *d* there is a transition from the film with isolated islands that are formed as a result of nucleation and growth of individual condensate particles to the structure with channels connecting these islands and determining charge transfer along the entire film. After the formation of a continuous film the influence of structural factor on σ and μ_H is considerably reduced; nevertheless, in the region of small thicknesses it is important to take into account the *d*-dependence of film structure. Fig. 5 shows *d*-dependences, starting from the thicknesses, when a continuous film is formed. Therefore, the role of structural factor will not be as important as in the case of ultrathin films. As noted above, with very small thicknesses, even in continuous films, the conductivity is generally reduced much faster than follows from the theory [25-27]. Apparently, for this reason the first point on the dependence $\sigma(d)$ lies below the theoretical curve.

2. Comparing the results of the present work and the data of [11] that studied *GeTe* crystalline films grown on the glass at $T_s = 425$ K, it can be seen that films prepared on (001) *KCl* substrates at $T_s = 520$ K (the present work) have higher values of σ (almost 2 fold) and μ_H (almost 8 fold). This testifies to the fact that with selected type ((001) *KCl*) and temperature ($T_s = 520$ K) the substrates of *GeTe* film are structurally more perfect and this provides considerable opportunities for revealing classical size effect and its theoretical description.

3. The fact that curves $R_H(d)$ and $S(d)$ are practically identical shows that dependences $S(p)$ correspond to a semiconductor with one sort of charge carriers. It is known [3, 4, 21] that dependences of the electrical properties of *GeTe* on hole concentration are of abnormal type, and this is because from the standpoint of present-day ideas of the band structure of *GeTe*, the valence band of the latter consists of two subbands with different density of states divided by the energy gap. With a change of hole concentration in the range of $(1.8 - 7.5)\cdot 10^{20}$ cm^{-3}, the Seebeck coefficient drops with a growth of hole concentration in conformity with the ideas of the band theory of degenerate semiconductors with one sort of charge carriers. In this case the Fermi level is in the zone of light holes which are responsible for crystal conductivity. However, with further increase in hole concentration, the Fermi level goes over to the overlap region of valence subbands, and, alongside with light holes, heavy holes start to participate in conductivity, and their ever increasing contribution results in the growth of *S*. In the range of thicknesses $d = 30 - 75$ nm the hole concentration is reduced from $p = 4.5\cdot 10^{20}$ cm^{-3} to $p = 1.9\cdot 10^{20}$ cm^{-3} and these *p* values show that light holes take part in conductivity and dependence $S(p)$ corresponds to the dependence for semiconductors with one sort of carriers. A reduction in carrier concentration results in the growth of the Seebeck coefficient whose maximum value is achieved close to $d = 75$ nm.

There is a good correlation between the values of R_H and *S* corresponding to dependence $S(p)$ established in [21].

4. It is rather difficult to predict the type of R_H and *S* dependence on the thickness of *GeTe* films caused by classical size effect, with regard to specific features of *GeTe* band structure and the presence of high concentration of intrinsic defects. The non-monotonous type of dependences $R_H(d)$ and $S(d)$ shows that, apart from the size effect, the type of dependences is evidently affected by other factors,

too. It can be assumed that at the first condensation stages of *GeTe* films there is partial tellurium reevaporation, as a result of which the concentrations of charged cation vacancies and *p*-type charge carriers are reduced (to $p = 1.9 \cdot 10^{20}$ cm^{-3} at $d = 75$ nm). This effect can be due to peculiarities of *GeTe* evaporation, as well as the change in thermodynamic equilibrium conditions (and, accordingly, to the change in equilibrium concentration of vacancies) in thin layers as compared to the bulk crystal. Subsequent reduction of R_H with the variation of *d* from 75 nm to ~ 100 nm shows that some additional factor starts to take effect, increasing the number of *p*-type charge carriers. It can be supposed that close to $d = 75$nm the extreme low value of cation vacancies is achieved, and then, alongside with nonstoichiometrtic vacancies, there appear other acceptor-type defects, such as charged twin boundaries formed in the process of film growth [9]. The relaxation phenomena must not be ruled out, taking into account that measurements were performed on as-prepared films.

5. It should be noted that dependence on the thickness of *GeTe* films of another important TE parameter, namely TE power, which significantly determines the efficiency of TE power converter, also is of a non-monotonous type (Fig. 5, *e*), and it should be taken into account when using films in TE devices.

Conclusions

The method of thermal evaporation in vacuum was used to grow *GeTe* films on (001) *KCl* substrates at temperature $T_s = 520$ K in the range of thicknesses $d = 5 - 210$ nm. The electron microscopy and electron diffraction methods were used to show that the films possess a rhombohedral structure corresponding to low-temperature α-modification of *GeTe* and grow with the preferred orientation (111) and $(\bar{1}11)$ α-*GeTe* || (001) *KCl*.

It is established that with a growth of film thickness to $d \sim 100 - 150$ nm the values of conductivity σ, charge carrier mobility μ_H and power coefficient ν in the temperature dependence μ_H are monotonously increased, and *d*-dependences of the Hall coefficient R_H, the Seebeck coefficient *S* and TE power $P = S^2\sigma$ have the form of curves with a peak at ~ 75 nm; with further growth of *d* the kinetic coefficients are practically unvaried. The dependence of properties on the thickness of films testifies to manifestation of classical size effect in *GeTe* films. There is a good agreement between the experimental dependence σ(*d*) and the results of theoretical calculation in the framework of the Fuchs-Sondheimer theory.

From the resulting data it follows that using the method of thermal evaporation of *GeTe* polycrystals in vacuum with the working technological parameters, one can prepare *GeTe* thin films with the values of hole concentration lower than in the bulk polycrystal and higher values of TE power.

This work was supported by the Ukrainian State Foundation for Fundamental Research (grant № UU 42/006-2011) and by the CRDF (grant № UKP2-7074-KK-12).

References

1. L.I. Anatychuk, *Thermoelements and Thermoelectric Devices, Handbook* (Kyiv: Naukova Dumka, 1979), 766 p.
2. M.A. Korzhuyev, *Germanium Telluride and its Physical Properties* (Moscow: Nauka, 1986), 103 p.
3. N.Kh. Abrikosov, L.E. Shelimova, *Semiconductor Materials Based on $A^{IV}B^{VI}$ Compounds* (Moscow: Nauka, 1975), 195 p.

4. E.I. Rogacheva, O.S. Vodorez, and O.N. Naschekina, Influence of nonstoichiometry defects on the mechanism of impurities dissolution and thermoelectric properties of germanium monotelluride, *J. Thermoelectricity* **4**, 22 – 31 (2011).
5. Yu.F. Komnik, *Physics of Condensed Metal Films* (Moscow: Nauka, 1979), 270 p.
6. Z.V. Stasyuk and A.I. Lopatinsky, Size Kinetic Effects in Metal Thin Films. Classical Effects (Review), *Physics and Chemistry of the Solid State* **2** (4), 521 – 542 (2011).
7. E.I. Rogacheva, O.N. Nashchekina, S.I. Ol’khovskaya, and M.S. Dresselhaus, Size effects in thin *PbSe* films, *J. Thermoelectricity* **4**, 25 – 32 (2012).
8. S.K. Bahl and K.L. Chopra, Amorphous Versus Crystalline *GeTe* Films. I. Growth and Structural Behavior, *J. Appl. Phys*. **40** (10), 4171 – 4178 (1969).
9. J. Stoemenos and R. Vincent, Twinning Faults in Epitaxial Films of Germanium Telluride and *GeTe-SnTe* Alloys, *Phys. stat. sol.* (*a*) **11**, 545 – 558 (1972).
10. V.I. Shtanov, T.V. Shtanova, L.V. Yashina, R.Ts. Bondokov, and I.V. Saunin, Growth of Polycrystalline *GeTe* Films on $Pb_{1-x}Sn_xTe$ (x = 0.05 or 0.2) and BaF_2 Substrates, *Mendeleev Commun*. **14** (4), 136 – 137 (2004).
11. S.K. Bahl and K.L. Chopra, Amorphous Versus Crystalline *GeTe* Films. III. Electrical Properties and Band Structure, *J. Appl. Phys*. **41** (5), 2196 – 2212 (1970).
12. A.G. Mikolaichuk, A.N. Kogut, and M.I. Ignativ, Electrical Properties of Thin Films of Germanium Telluride and Selenide, *Izvestiya VUZ. Fizika* 7, 103 – 105 (1970).
13. O.G. Vasilkova, V.E. Lebedeva, P.P. Konstantinov, E.Ya. Lev, and L.M. Sysoyeva, Electrical Properties of *GeTe* Films, *Inorganic Materials* **12** (6), 1000 – 1003 (1976).
14. B.B. Anisimov, A.A. Gabedava, Sh.Z. Dzhamagidze, T.I. Yefimova, Yu.A. Maltsev, and R.R. Shvangiradze, Effect of Condensation and Annealing Conditions on the Electrical Properties and Structure of *GeTe* Films, *Inorganic Materials* **14** (8), 1417 – 1421 (1978).
15. S. Kumar, D. Singh, S. Sandhu, and R. Thangaraj, Structural, Electrical and Optical Properties of Thermally Evaporated *Ge-Te*, *Ge-Sb-Te*, and *Sb-Te* Thin Films, *Phys. Stat. Sol. A* **209** (10), 2014 – 2019 (2012).
16. P. Kumar, R. Thangaraj, and T.S. Sathiaraj, Electrical and Optical Study of Phase Transitions in Thermally Evaporated *GeTe* Films, *Phys. Stat. Sol. A* **208** (4), 838 – 842 (2011).
17. K.-H. Kim, Y.-K. Kyoung, J.-H. Lee, Y.-N. Ham, and J.S. Choi, Evolution of the Structural and Electrical Properties of *GeTe* under Different Annealing Conditions, *J. Electronic Materials* **42** (1), 78 – 82 (2013).
18. J. Liu and M.P. Anantram, Low-Bias Electron Transport Properties of Germanium Telluride Ultrathin Films, *J. Appl. Phys*. **113**, 063711-1-063711-6 (2013).
19. G.O. Nikolaenko, O.I. Rogacheva, Thickness Dependences of Galvanomagnetic Properties of *GeTe* Films, *Bulletin of Lviv University. Physics series* 48, 85 – 90 (2013).
20. L.S. Palatnik, M.Ya. Fuks, and V.M. Kosevich, *Formation Mechanism and Substructure of Condensed Films* (Moscow: Nauka, 1972), 320 p.
21. N.A. Yerasova, V.I. Kaidanov, I.A. Chernik, L.M. Sysoyeva, E.Ya. Lev, and N.V. Kolomoyets, Electrophysical Properties of *GeTe* at Low Temperatures, *Semiconductors* **3** (9), 1289 – 1292 (1969).
22. A.A. Andreyev, L.M. Sysoyeva, and E.Ya. Lev, Temperature Dependence of the Hall Effect and Electric Conductivity in *GeTe*, *Physics of the Solid State* **7** (8), 2558 – 2559 (1965).

23. B.F. Gruzinov, P.P. Konstantinov, B.Ya. Moyzhes, Yu.I. Ravich, and L.M. Sysoyeva, Kinetic Effects in Cubic and Rhombohedral Phases of *GeTe*, *Semiconductors* **10** (3), 497 – 503 (1976).
24. N.V. Kolomoyets, E.Ya. Lev, and L.M. Sysoyeva, Electrical Properties and Model of Valence Band of Germanium Telluride, *Physics of the Solid State* **6** (3), 706 – 713 (1964).
25. K. Fuchs, The Conductivity of Thin Metallic Films According to the Electron Theory of Metals, *Proc. Cambridge Philos. Soc*. **34**, 100 – 108 (1938).
26. E.H. Sondheimer, The Mean Free Path of Electrons in Metals, *Adv. Phys*. **1**, 1 – 42 (1952).
27. E.H. Sondheimer, The Influence of a Transverse Magnetic Field on the Conductivity of Thin Metallic Films, *Phys. Rev*. **80**, 401 – 406 (1950).
28. J.R. Schrieffer, Effective Carrier Mobility in Surface-Space Charge Layers. *Phys. Rev*. **97**, 641 – 646 (1955).
29. R.F. Greene, Surface Transport Theory, *J. Phys. Chem. Solids* **14**, 291 – 298 (1960).
30. J.N. Zemel, Surface Transport Theory. *Phys. Rev*. **112**, 762 – 765 (1958).
31. A. Amith, Galvanomagnetic Properties of Semiconductor Thin Films and Surface Layers, *J. Phys. Chem. Solids* **14**, 271 – 290 (1960).

Submitted 30.05.2014.

M.O. Galuschak[1], I.V. Gorichok[2], O.S. Krynytsky[1], D.M. Freik[2]

[1]Ivano-Frankivsk National Technical University of Oil and Gas,
15, Karpatska Str., Ivano-Frankivsk, 76018, Ukraine;
[2]Vasyl Stefanyk Precarpathian National University,
57, Shevchenko Str., Ivano-Frankivsk, 76018, Ukraine

THERMOELECTRICITY OF LEAD TELLURIDE DOPED WITH *Sb* AND *Bi*

X-ray investigations of antimony and bismuth doped lead telluride have been performed and its thermoelectric parameters (the Seebeck coefficient α *and electric conductivity* σ*) have been measured. It has been established that more optimal properties for use in thermoelectric generators are inherent in PbTe:Sb samples with impurity content 0.3 at.% whose electric conductivity is* $\sigma \approx 700\ (\Omega\cdot cm)^{-1}$*, and the Seebeck coefficient* $\alpha \approx 300\ \mu V/K$*, assuring thermoelectric power* $\alpha^2\sigma$ *higher than 50* $\mu W/cm\ K^2$*.*

Key words: lead telluride, thermoelectric properties, doping.

Introduction

As a result of many experimental and theoretical investigations [1-3] it has been shown that impurities of V group elements, especially *Sb* and *Bi*, make it possible to improve considerably the parameters of lead telluride which is widely used for creation of thermoelectric power converters working in the temperature range of (500 – 800 K).

Apart from other parameters, the effect of impurity on thermoelectric characteristics of crystals is essentially dependent on the manner of preparation of samples under study. The majority of known works, in particular, [2, 3], study single-crystal samples or samples cut of polycrystal ingots. However, thermoelectric converters mostly employ thermoelements made by meta-ceramic methods. Therefore, investigation of samples obtained by compaction of power *PbTe*:*Sb* (*Bi*) is of considerably greater practical interest.

This paper studies structural and thermoelectric properties of samples obtained by compaction of powder *PbTe*:*Sb* and *PbTe*:*Bi* with impurity concentration in the range of (0.0 – 1.0) at.% *Sb* (*Bi*).

Experimental procedure

Lead telluride, impurity-free and doped with bismuth and antimony in the amount of 0.1, 0.3 and 1.0 at.%, was synthesized by alloying in quartz ampoules evacuated to pressure of $2\cdot10^{-4}$ Pa. As the precursor components, purified *Pb*, *Te*, *Sb* and *Bi* were used. The obtained ingots were crushed in agate mortar and, after fractionation of size (0.05 – 0.5) mm, were compacted under pressure of 0.5 GPa. The obtained cylinder-shaped samples with d = 5 mm and $h \approx 8$ mm were annealed in the air at temperature T = 500 K for 5 hours.

The value of the Seebeck coefficient S and electric conductivity σ was determined by standard procedure detailed in [1]. The sample was located between two copper rods placed in the oven which heated it to given temperature. Temperature gradient on the sample ($\approx 10\ ^\circ$C) was created by additional oven on one of the copper rods. The temperature was measured by two chromel-alumel thermocouples placed in openings in the sample. Electrical conductivity was determined by measuring

voltage drop on the sample generated by DC voltage source. In so doing, one of the legs of each thermocouple was used as current lead.

For *X*-ray investigations the ground material was applied as a uniform layer on the amorphous film using amorphous glue for *X*-ray transmission experiments and fixed by another film in a special bath. Arrays of experimental intensities and reflection angles from the investigated samples were obtained on automatic diffractometer STOE STADI P (produced by "STOE & Cie Gmbh", Germany) with a linear precision position detector PSD according to the scheme of modified Guinier geometry by transmission method (CuK_{α_1} -radiation; concave Jogann-type *Ge*-monochromator (111); 2θ/ω-scanning, angle interval $10.000 \leq 2\theta \leq 125.185$ with a step 0.015°2θ; detector step 0.480 °2θ, scanning time in step 100 – 230 s, temperature of exposure $T = (297.6 \pm 0.3)$ K, $U = 40$ kV, $J = 35$ mA). Primary processing of experimental diffraction arrays, calculations of theoretical diffractograms of known compounds for the purpose of phase identification, specification of unit cell parameters was performed with the use of programs STOE Winxpow (version 3.03) and Powdercell (version 2.4).

Experimental Results

PbTe:*Sb*. The results of *X*-ray phase investigations are presented in Fig. 1. Diffraction lines from individual components (lead, tellurium) or their oxides were not discovered.

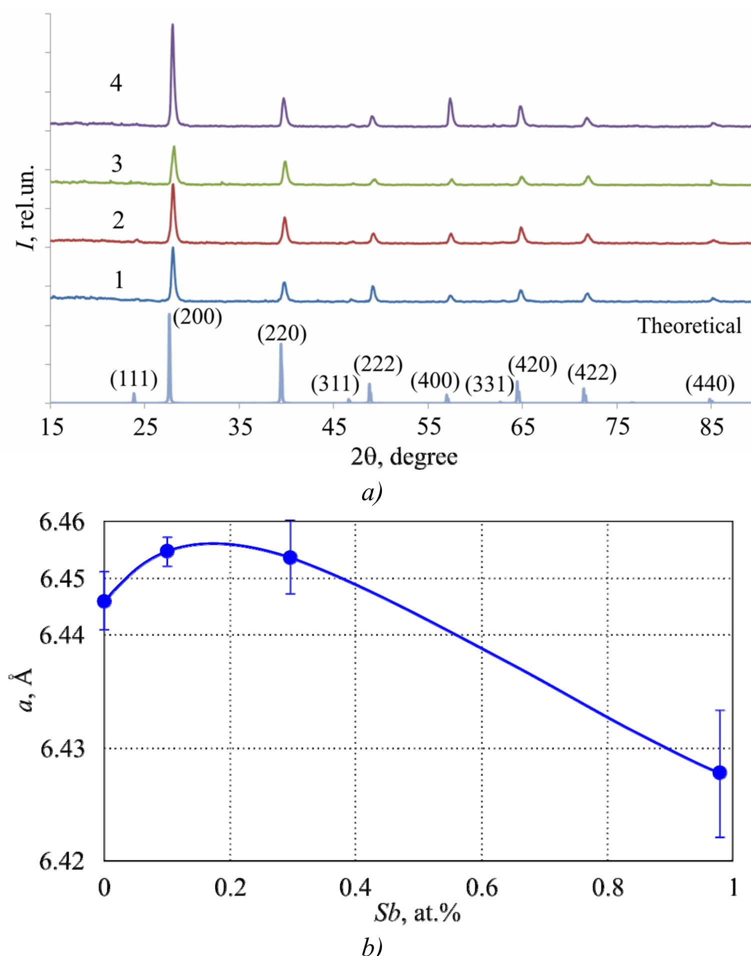

Fig. 1. (a) Comparative diffractograms of lead telluride with different content of antimony impurity (1 – sample 12-1 PbTe; 2 – sample 12-2 PbTe + 0.1 at.% Sb; 3 – sample 12-3 PbTe + 0.3 at.% Sb; 4 – sample 12-4 PbTe + 1 at.% Sb); (b) unit cell period a *of PbTe:Sb samples under study versus Sb impurity content.*

Comparison of the obtained diffractograms to the theoretical one shows a relative amplification of some and attenuation of other intensities of diffraction reflection line. Also, conspicuous is a non-monotonous change of lattice parameter (*a*) with increase in the number of introduced antimony atoms (Fig. 1, *b*). Up to impurity concentration 0.2 at.% *Sb* the (*a*) value of *PbTe* is increased, and at concentration > 0.3 at.% *Sb*-decreased.

Thermoelectric samples were of *n*-type conductivity (Fig. 2). Electric conductivity of lead telluride doped with 0.3 at. % *Sb* is $\sigma \approx (700 - 800)\ (\Omega \cdot cm)^{-1}$.The Seebeck coefficient is reduced with increasing the amount of impurity introduced, but the absolute value remains rather high ($\alpha \approx (250 - 300)$ μV/K at $T \approx 500$ K). Impurity concentration increase to 1.0 at.% *Sb* brings about a considerable reduction of both the Seebeck coefficient and the electric conductivity of samples under study.

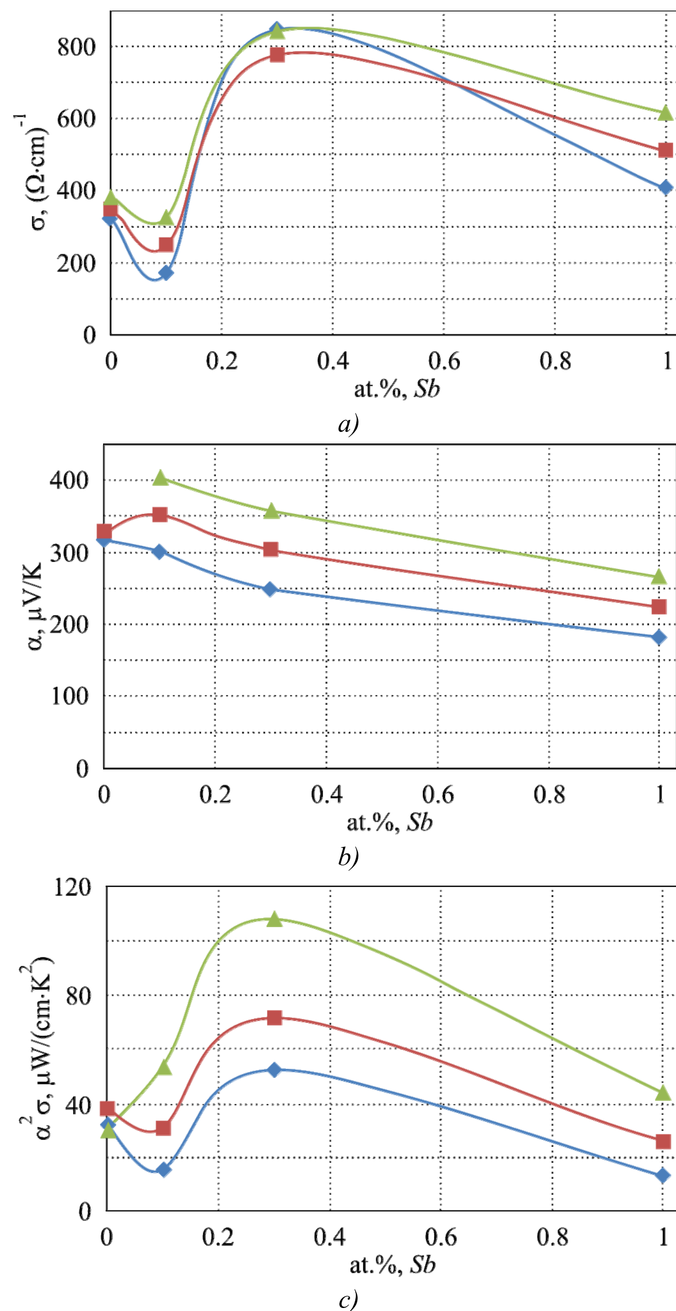

Fig. 2. Electric conductivity – a), the Seebeck coefficient – b), specific thermoelectric power – c), of doped PbTe versus Sb content at different temperatures T, K: 400 K – ♦, 500 K – ■, 600 K – ▲.

PbTe:Bi. The results of *X*-ray studies are presented in Figs. 3 – 4. Impurity-free lead telluride (sample 13-1) is characterized by the existence of one phase of structural type *NaCl* with parameter of face-centered cubic unit cell $a = 6.4595(3)$ Å and space group *Fm*-3*m*. This unit cell parameter is in good agreement with precision structural studies performed by neutron diffraction on *PbTe* samples with the purity of precursor substances > 99.999 at.% [4].

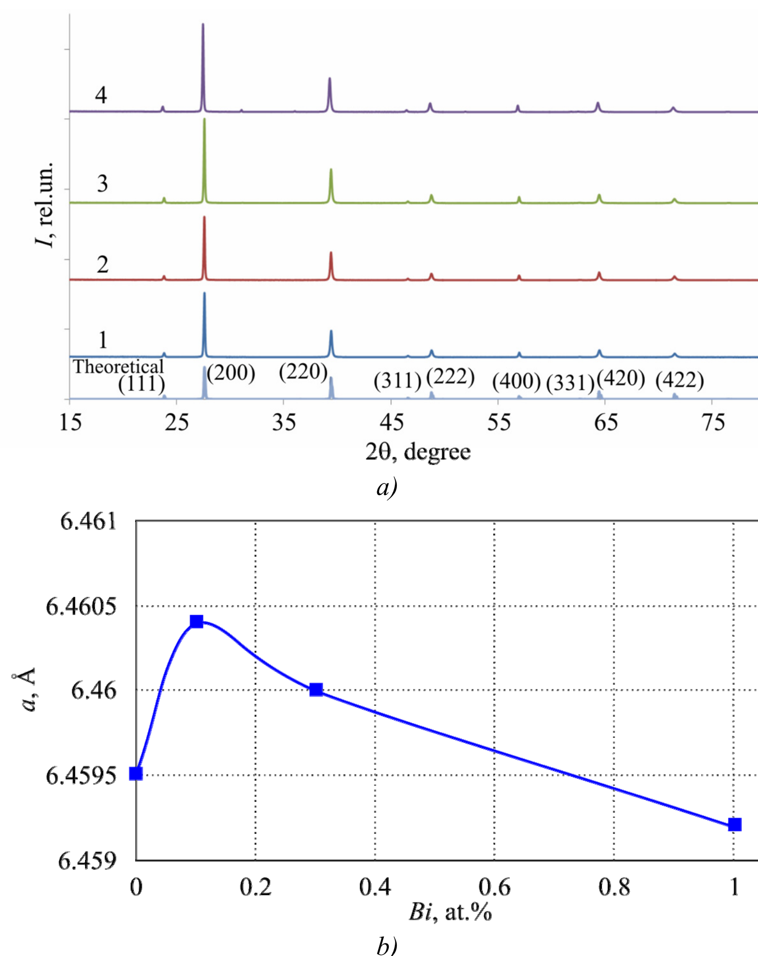

Fig. 3. (a) Comparative diffractograms of lead telluride with different content of bismuth impurity (1 – sample 13-1 PbTe; 2 – sample 13-2 PbTe + 0.1 at.% Bi; 3 – sample 13-3 PbTe + 0.3 at.% Bi; 4 – sample 13-4 PbTe + 1 at.% Bi); (b) unit cell period a of PbTe:Bi samples under study versus Bi impurity content.

Analysis of diffractograms of doped samples brings us to the conclusion about the existence in them of other phase inclusions, namely $Pb_{1-x}Bi_x$ (structural type *Cu*, space group *Fm*-3*m*) (Fig. 4). However, taking into account the precision of *X*-ray phase analysis which is generally ~ 3 – 5 %, and in the case for substances with high-symmetry lattice (cubic, tetragonal, hexagonal syngonies) with small unit cell parameters from 1 %, one can unambiguously state that an additional phase is present only in sample 13-4 for which the content of phase $Pb_{1-x}Bi_x$ is ≈ 1.4 mas. %. The unit cell parameter of this phase in sample 13-4 is 4.9626(5) Å. For pure *Pb* (purity 99.999 %) parameter $a = 4.951$ Å [4], and for the phase $Pb_{0.85}Bi_{0.15}$, according to [5], $a = 4.9650$ Å. That is, in our case for $Pb_{1-x}Bi_x$ phase parameter a has intermediate value, and phase composition is probably ≈ $Pb_{0.9}Bi_{0.1}$.

Like for other *PbTe* based materials in our study [6], synthesized according to a similar procedure, on the diffractograms there is a relative amplification of some and attenuation of other reflex intensities as compared to theoretical diffractogram of *PbTe*. It is most apparent in the variation of peak ratio of diffraction reflection I(200)/I(220).

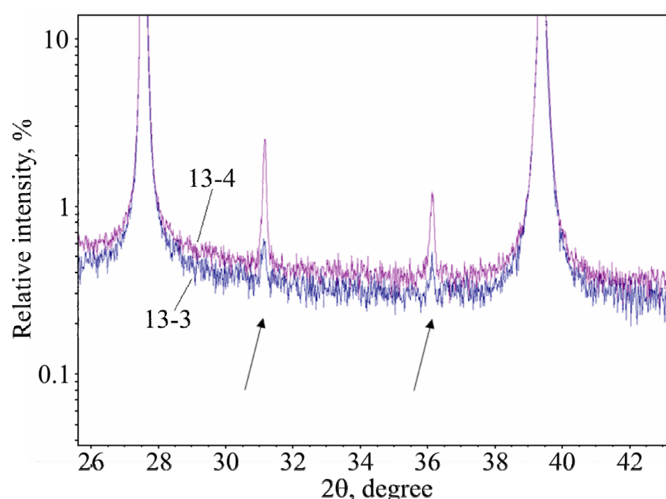

Fig. 4. Comparison of experimental diffractograms of samples 13-3 and 13-4. Reflexes from $Pb_{1-x}Bi_x$ phase (Cu structural type, Fm-3m space group) are arrowed. For better visualization the ordinate axis is represented on a logarithmic scale.

When comparing the unit cell parameters of the basic phase for samples with different *Bi* concentration, one can see certain growth of a value (Fig. 3, *b*) with bismuth content 0.1 at.% and its subsequent reduction with increasing impurity content.

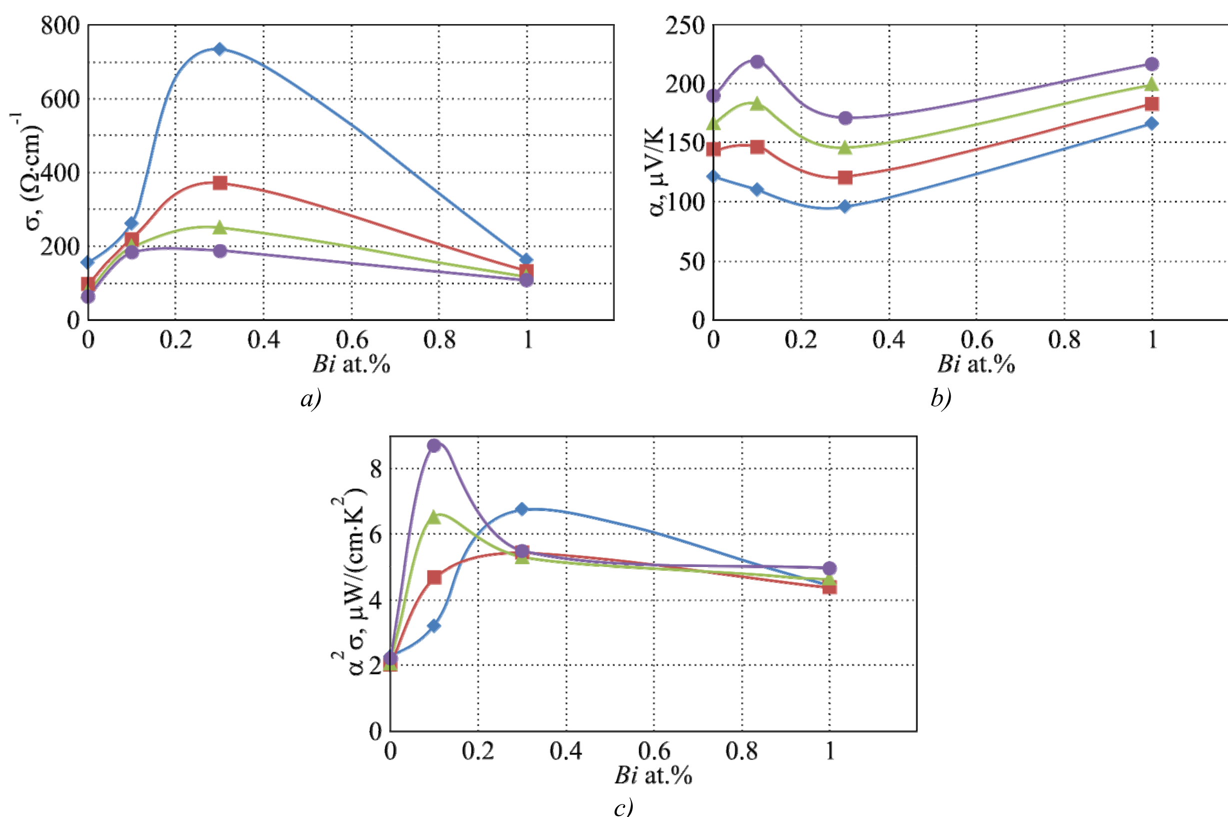

Fig. 5. Electric conductivity – a), the Seebeck coefficient – b), specific thermoelectric power – c), of doped PbTe versus Bi content at different temperatures T, K: 100 K – ♦, 200 K – ■, 300 K – ▲, 400 K – ●.

The results of measuring the Seebeck coefficient and electric conductivity are represented in Fig. 5, *a* and Fig. 5, *b*, and thermoelectric power calculated on their basis – in Fig. 5, *c*. All the samples had *n*-type conductivity. Electric conductivity grows from the values of $\sigma \approx 100 - 200\ (\Omega\cdot\text{cm})^{-1}$ for

impurity-free to σ ≈ 600 $(\Omega\cdot cm)^{-1}$ for lead telluride doped with 0.3 at.% *Bi*. The Seebeck coefficient for a sample with such impurity concentration has a minimum. Analyzing the thermoelectric power of samples under study it is seen that for sample 13-2 with impurity content 0.1 at.% *Bi* it is the highest.

Analysis of the investigation results

The relative change in the intensity ratios of diffraction reflection line in materials under study with different impurity content (Fig. 1, 3) is attributable to the presence of orientation direction of crystallites that was formed in the process of melt crystallization and was not completely destroyed in the process of powder preparation for analysis [6]. The non-monotonous concentration dependence of lattice constant of *PbTe*:*Bi* and *PbTe*:*Sb* is attributable to different mechanisms of impurity atoms (*Bi*, *Sb*) inclusion into lead telluride crystal lattice with different doping levels. Assuming that *n*-type of the obtained impurity-free *PbTe* is caused by tellurium vacancies, then introduction of up to 0.3 at.% *Sb* or 0.1 at.% *Bi* results in their filling with impurity atoms, which accounts for the growth of unit cell parameter. At concentration equal to 0.1 at.% in the case of *Bi* and 0.3 at.% in the case of *Sb* all tellurium vacancies are filled with impurity atoms, which predetermines maximum value of parameter a. At concentrations > 0.1 at.% *Bi* (> 0.3 at.% *Sb*) both the cation and anion sublattices are completed, where considerable concentrations of vacancies are absent, and certain reduction in the value of unit cell parameter is due to the fact that the sum of ionic radii Bi^{3+} (Sb^{3+}) and Bi^{3-} (Sb^{3-}) is somewhat smaller, though not much, than the sum of ionic radii Pb^{2+} и Te^{2-}. Thus, according to [7] r_{ion} (Sb^{3+}) + r_{ion} (Sb^{3-}) = 2.98 Å, r_{ion} (Bi^{3+}) + r_{ion} (Bi^{3-}) = 3.33 Å, whereas r_{ion} (Pb^{2+}) + r_{ion} (Te^{2-}) = 3.36 Å.

It should be noted that on condition of implementation of the represented mechanism of impurity inclusion into lead telluride crystal lattice, at concentrations of antimony atoms < 0.3 at.% and bismuth atoms < 0.1 at.% their arrangement in a vacant anion site will result in reduction of the Hall concentration of carriers per unit. However, because of high dielectric permittivity, the efficiency of carrier scattering by charged centres in *PbTe* is lower as compared to lattice deformations caused by point defects. That is, with identical concentrations of tellurium vacancies that cause relatively strong lattice deformation, carrier scattering is much more active compared to that of impurity ions, the lattice deformations in the neighbourhood of which should be smaller. This statement is partially confirmed by the results of [8] where it is shown that the Coulomb potential of tellurium vacancies has a considerably smaller effect on carrier mobility than its short-range component. Thus, it can be assumed that reduction of carrier concentration is compensated by their mobility increase, which results in electric conductivity growth in the sample with 0.3 at.% *Sb* or 0.1 at.% *Bi* as compared to undoped material.

With impurity content about 1 at.%, a large concentration of antimony (bismuth) ions in both sublattices results in reduction of carrier concentration and increased importance of ionized impurity scattering mechanism due to considerable growth of the number of scattering centres, which accounts for reduction of samples conductivity.

It should be also noted that in case of implementation of another possible mechanism of impurity inclusion into lead telluride crystal lattice, namely cation sublattice completion, a considerable number of tellurium vacancies should be formed, which will result in reduction of lattice parameter with increasing amount of bismuth introduced, hence, it will be difficult to explain the existence of maximum a value in Figs. 1 and 3.

Taking into account the presence in *PbTe*:*Bi* of additional phase, it is important to determine its influence on the thermoelectric properties of samples. Formation of $Pb_{1-x}Bi_x$ inclusions may be caused

by the presence in synthesized material of superstoichiometric lead which in the undoped *PbTe* results in the origination of a considerable number of tellurium vacancies. In one of our earlier works it was established [9] that additional phases that are formed in synthesized ingots may not be manifested any longer in pressed and annealed sample. Therefore, before attracting the fact of existence of $Pb_{1-x}Bi_x$ inclusions to the explanation of the resulting dependences, one should perform *X*-ray studies of those samples that have been measured, the more so that any abnormal numerical values of α or σ values that might have been caused by the existence of additional phase have not been discovered.

Conclusions

1. X-ray studies have been performed and thermoelectric parameters have been measured of antimony and bismuth doped lead telluride in the range of impurity concentration 0.0 – 1.0 at.% *Sb* (*Bi*).
2. It is shown that doping results in improvement of the basic thermoelectric characteristics of material. In particular, for *PbTe*:*Sb* with impurity content 0.3 at.% the electric conductivity is $\approx 700\ (\Omega\cdot\text{cm})^{-1}$, and the Seebeck coefficient ≈ 300 μV/K. For *PbTe*:*Bi* an optimal impurity concentration is 0.1 at.% of *Bi* whereby $\sigma \approx 600\ (\Omega\cdot\text{cm})^{-1}$ and $\alpha \approx 150$ μV/K.
3. A non-monotonous variation of the unit parameter with increasing content of antimony (bismuth) atoms is established, which is attributable to different mechanisms of impurity inclusion into *PbTe* crystal lattice: up to concentration 0.3 at.% *Sb* (0.1 at.% *Bi*) there is filling with antimony (bismuth) atoms of tellurium vacancies, and at higher concentrations – a simultaneous completion of the anion and cation sublattices.

References

1. D.M. Freik, C.A. Kryskov, I.V. Horichok, et al., Synthesis, Properties and Mechanisms of Doping with *Sb* of Thermoelectric Lead Telluride *PbTe*:*Sb*, *J.Thermoelectricity* **2**, 44 – 52 (2013).
2. L.D. Borisova, Thermoelectric Properties of Impurity Doped *PbTe*, *Phys. stat. sol. (a)* **53**, K19 – K22 (1979).
3. Chr. Jaworski, J. Tobola, E.M. Levin, Kl. Schmidt-Rohr, and J. Heremans, Antimony as an Amphoteric Dopant in Lead Telluride, *Physical Review B* **80**, 125208-1 – 125208-10 (2009).
4. N. Bouad, L. Chapon, R.M. Marin Ayral, F. Bourée Vigneron, J.C. Tédenac, Neutron Powder Diffraction Study of Strain and Crystallite Size in Mechanically Alloyed *PbTe*, *J. Solid State Chem*. **173**, 189 – 195 (2003).
5. G.C. Che, M.Ellner, Phase Diagram of *Bi-Pb-Tl* Ternary System, *Acta Metall. Sin. Engl. Ed. Ser. B*, 5-221 (1992).
6. D.M. Freik, I.V. Horichok, N.I. Dikun, and Yu.V. Lysyuk, Influence of Manufacturing Technique on Thermoelectric Properties of Non-Stoichiometric and Doped Lead Telluride and Solid Solutions on its Basis, *J.Thermoelectricity* **2**, 42 – 53 (2011).
7. B.I. Boltaks, *Diffusion and Point Defects in Semiconductors* (Leningrad: Nauka, 1972), 384 p.
8. D.M. Zayachuk, On the Issue of Dominant Mechanisms of Charge Carrier Scattering in Lead Telluride, *Semiconductors* **31** (2), 217 – 221 (1997).
9. D.M. Freik, S.I. Mudryi, I.V. Horichik, et al., Phase Composition of Thermoelectric Materials Based on Solid Solutions $PbTe\text{-}Sb_2Te_3$, $PbTe\text{-}Bi_2Te_3$, *Physics and Chemistry of the Solid State* **14** (4), 831 (2013).

Submitted 30.05.2014.

E.M. Godzhayev

E.M. Godzhayev, U.S. Abdurakhmanova

Azerbaijan Technical University,
25, Huseyn Javid Ave., Baku, AZ1073,
Republic Azerbaijan

U.S. Abdurakhmanova

PHASE ANALYSIS AND ELECTROPHYSICAL PROPERTIES OF *InGaTe*$_2$

This paper presents the results of research on the temperature dependences of the electric conductivity, the Seebeck coefficient and the thermal conductivity in the temperature range of 300 to 900 K, and the results of calculation of the concentration, the Hall mobility of current carriers and the thermoelectric figure of merit of $InGaTe_2$ *semiconductor compound. Based on the band structure of this phase, the unit cell parameters, the electron and hole effective masses have been calculated and it has been established that the unit cell parameters are in good agreement with the experimental data.*

Key words: $InGaTe_2$ compounds, band structure, effective mass, unit cell parameters, thermoelectric figure of merit.

Introduction

It is known that a search for new semiconductor materials is generally pursued toward the expansion of crystal structure group of already known materials.

In particular, crystal structure interpretation of *TlSe* has revealed that this phase is distinguished by extreme specific features. The lattice of *TlSe* proves to be composed of two independent structural units, namely an octagon with the ionic bond Tl^{1+}-*Se* and a tetrahedron with the covalent bond Tl^{3+}-*Se,* hence chemical formula of *TlSe* should be written as $Tl^{+}Tl^{3+}Se_2$ [1-3]. In subsequent works [4, 5], the substitution of indium and gallium atoms for a three-valence thallium atom in *TlSe* type lattices yilded a new class of semiconductor compounds of $A^{III}B^{III}X_2^{VI}$ type.

X-ray investigations have revealed that one part of these compounds has a chain structure and another part has a layered structure. Compounds with a chain structure are crystallized in tetragonal syngony, space group D_{4h}^{18} (I4/mcm) [2, 3].

The existence of the above compound type is also a reality from the standpoint of electronic structure of component atoms. With formation of $A^{III}B^{III}C_2^{VI}$ type compounds, the outer electron shells of two chalcogen atoms with electron shell $2(s^2p^4)$ at the cost of one $(6p^1)$ electron of univalent thallium (or indium) and one $(5s^2p^1)$ three-valence indium (or gallium) will be completed to a stable $2(s^2p^6)$ configuration.

In papers [3, 4] it was experimentally proved that *Tl* atoms interacting even with the elements of its subgroup (*In*, *Ga*) exhibit univalent state with the outer electron configuration $6s^26p^1$. Univalent state is also typical of indium and gallium elements, even though these elements competing with thallium show normal valence with the outer electron configuration $5s^25p^1$ and $4s^24p^1$, respectively.

The reality of this assumption follows from the fact that $5s^2$ shells of indium and $4s^2$ shells of

gallium as compared to $6s^2$ shell of thallium are less stable, i.e. the probability of univalent state appearance, hence of their occupying octahedral position in lattices of *TlSe* type, all other conditions being equal, is reduced in the sequence $Tl \rightarrow In \rightarrow Ga$. Thus, $TlInX_2^{VI}$, $TlGaX_2^{VI}$ and $InGaX_2^{VI}$ compounds, with their isotructurality, differ in respective anion radicals $[Tl^{3+}X_2^{VI}]^-$, $[In^{3+}X_2^{VI}]^-$ and $[Ga^{3+}X_2^{VI}]^-$ and the energy gap [4].

The existence of ternary compounds of $A^{III}B^{III}X_2^{VI}$ type was confirmed by the methods of differential-thermal, microstructural and *X*-ray phase analyses [6-9]. In later works their electrophysical, thermal, optical and photoelectric properties were studied and it was revealed that these compounds possess high photosensitivity, strain gauge factors and memory-switching properties [11-13], while tellurides and their solid solutions possess high coefficients of thermoelectric figure of merit [14-17]. The energy spectrum of $TlInSe_2(Te_2)$ $TlGaSe_2(Te_2)$ compounds was investigated [22-25], their optical functions were calculated, the origin of the valence band and conduction band, the energy gap, the electron and hole effective masses, the unit cell parameters were determined. However, the data on the research of $InGaSe_2(Te_2)$ compounds is insignificant, though the existence of these compounds was reported as far back as the mid of the last century [4]. In later works [4, 5] their electrophysical properties were studied. In paper [10], perfect crystals $InGaTe_2$ were grown, *X*-ray phase analysis was used to determine the unit cell parameters and it was revealed that $InGaTe_2$, as well as its other structural analogs is crystallized in tetragonal syngony.

In the same paper, the energy spectra were calculated and the origin of the energy gap, the valence band and conduction band was determined. Photoluminescence spectrum and photoelectric properties were investigated, the electronic structure of $InGaTe_2$ was calculated and it was revealed that the resulting data is in good agreement with the data of [22] where the band structure of this phase is interpreted. The optical functions of $InGaTe_2$ are calculated in [23]. However, the data on the investigation of the temperature dependences of the electrical and thermal properties, the results of calculation of the unit cell parameters, the electron and hole effective masses of $InGaTe_2$ is not available.

The purpose of this work is to study the electrophysical properties and calculate the electron and hole effective masses and the unit cell parameters of $InGaTe_2$.

Experimental

The electric conductivity σ, the Hall coefficient R, the Seebeck coefficient α and the thermal conductivity χ_p were measured by the procedure described in [24]. The errors of measurement of σ, R, α and χ were 5, 6, 7 and 4 %, respectively.

The $InGaTe_2$ compound was synthesized by melting the initial components taken in stoichiometric ratio in evacuated to 0.0133 Pa and sealed quartz ampoules.

For the synthesis of $InGaTe_2$ the elements of purity *In* – 000, *Ga* – 99.996, *Te* – 99.997 % were used. The ampoules were first cleaned with a mixture of HF and distilled water. After chemical cleaning the ampoules evacuated to 0.0133 Pa were placed into an oven at 1000 °C for 24 hours, following which they were cooled and filled with highly purified components. For homogenization of the alloy the mixture was held for 24 hours at a temperature of 970 °C. During the process of synthesis the ampoules were often shaken for better agitation of component parts. Them the ampoule with the substance at a rate of 1.33 mm/hour travelled from the high-temperature zone to crystallization zone with the respective temperature 700 °C. The obtained crystals, when cooled to room temperature, were subject to *X*-ray phase analysis. The results of *X*-ray phase analysis are given in Table 1.

Table1

Results of X-ray phase analysis of $InGaTe_2$

θ	d_{calc}, Å	d_{exp}, Å	*Hkl*	$I_{relative}$
$10^0 31$\`	4.2300	4.2217	200	6
$13^0 42$\`	3.2600	3.2554	211	100
$22^0 26$\`	2.9911	2.020	220	14
$23^0 1$\`	1.9685	1.9661	411	33
$23^0 22$\`	1.9439	1.9442	332(402)	29
$24^0 39$\`	1.8770	1.8662	420	18
$25^0 12$\`	1.8102	1.8111	421	11
$27^0 20$\`	1.6788	1.6784	340(500)	22
$30^0 46$\`	1.5072	1.5140	502	10
$32^0 49$\`	1.4227	1.4192	522	9

X-ray phase analysis has shown that $InGaTe_2$ compound is crystallized in tetragonal syngony with the lattice parameters $a = 8.463$ Å, $c = 6.981$ Å. These values agree well with the data $a = 8.412$ Å, $c = 6.875$ Å from [10].

Discussion of the results

The results of investigation of the temperature dependences of the electric conductivity, the Hall coefficient, the Seebeck coefficient and the thermal conductivity, the calculated values of the Hall mobility, free-carrier concentration and the thermoelectric figure of merit of $InGaTe_2$ compound are given in the Table and Fig. 1 – 3. As it follows from Fig. 1 *a*, the electric conductivity with a rise from room temperature to 400 K is relatively weak, and with the onset of intrinsic conductivity the intrinsic carriers quickly become dominant, and the conductivity is exponentially increased. The energy gap determined by the high-temperature slope of dependence $\lg \sigma = f(10^3/T)$ is equal to 0.74 eV.

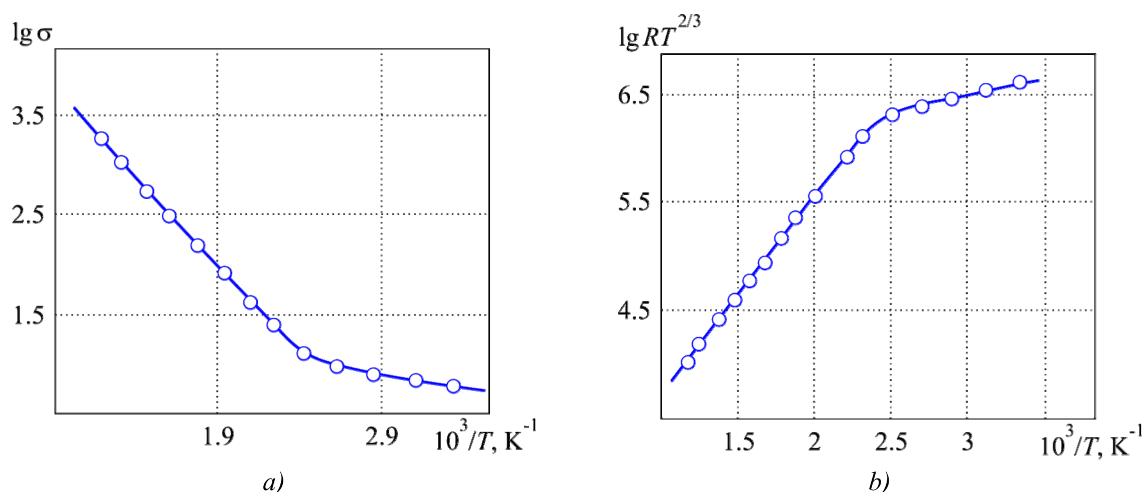

Fig. 1. Temperature dependences of the electric conductivity σ (S/m) (a) and the Hall coefficient R (cm^3/C) (b) of $InGaTe_2$.

The temperature dependence of the Hall coefficient is given in Fig. 1 *b*. As it follows from Fig. 1 *b,* the variation of the Hall coefficient with the temperature agrees well with the variation of the electric conductivity. The value of the energy gap determined by the Hall coefficient, i.e. by the high-temperature slope of dependence $\lg RT^{3/2} = f(10^3/T)$, is equal to 0.76 eV. It is noteworthy that the energy gap 0.56 eV thus defined is not in good agreement with the value found from the experiments with optical absorption or photoconductivity (0.56 eV) [10]. The reason for this discrepancy is that the energy gap itself is a function of temperature. Supposing that all the summands, except for the linear one, in Taylor series expansion of $\Delta E(T)$ with respect to temperature are negligibly small and writing $\Delta E(T) = \Delta E(T = 0) + \beta T$, it becomes apparent that the energy gap determined by the electric conductivity, to a first approximation, is the energy gap at $T = 0$ K and must increase with a rise in temperature.

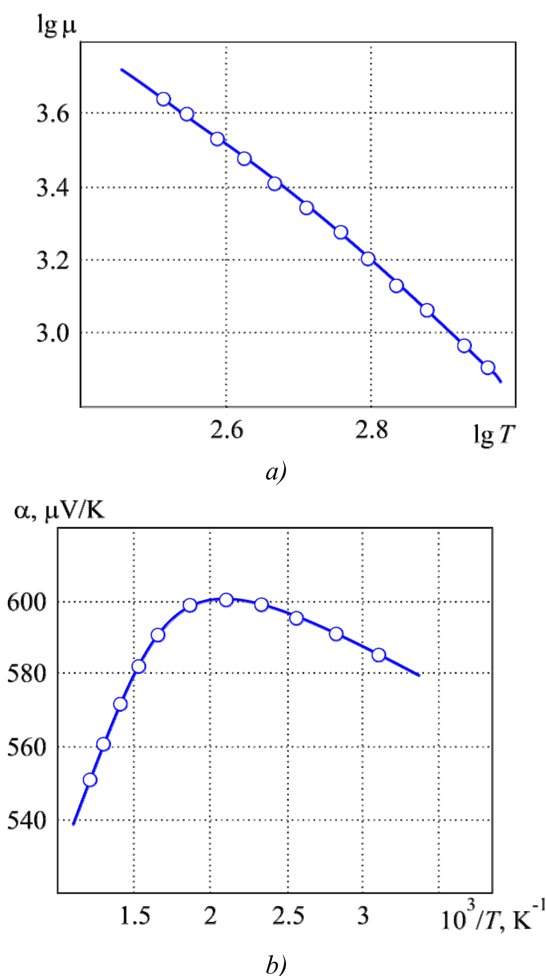

Fig. 2. Dependences of the Hall mobility of carriers μ (cm²/V·s) (a) and the Seebeck coefficient α (b) on the temperature T (K) of $InGaTe_2$.

From the temperature dependence of the Hall mobility (Fig. 2 *a*) it is seen that within the investigated temperature range of 300 to 900 K the mobility drops with a rise in temperature as $T^{-3/2}$, i.e. in this case carrier scattering occurs on the longitudinal acoustic phonons. The temperature dependence of the Seebeck coefficient of $InGaTe_2$ is given in Fig. 2 *b*. As it appears from Fig. 2 *b,* in the temperature range of 300– 500 K the thermoEMF is increased, and with the onset of intrinsic conductivity it is decreased which is a specific feature of ternary compounds of $A^{III}B^{III}X_2^{VI}$ type with a complex energy structure [4, 5, 18-22]. The variation of current carrier concentration with the

temperature in Fig.3a is in good agreement with the variation of the electric conductivity and the Hall coefficient with the temperature (Fig. 1).

Fig. 3 *b* shows the temperature dependence of the thermal conductivity of $InGaTe_2$. As it follows from Fig. 3 *b*, the variation of the thermal conductivity with the temperature occurs by the law T^{-1}.

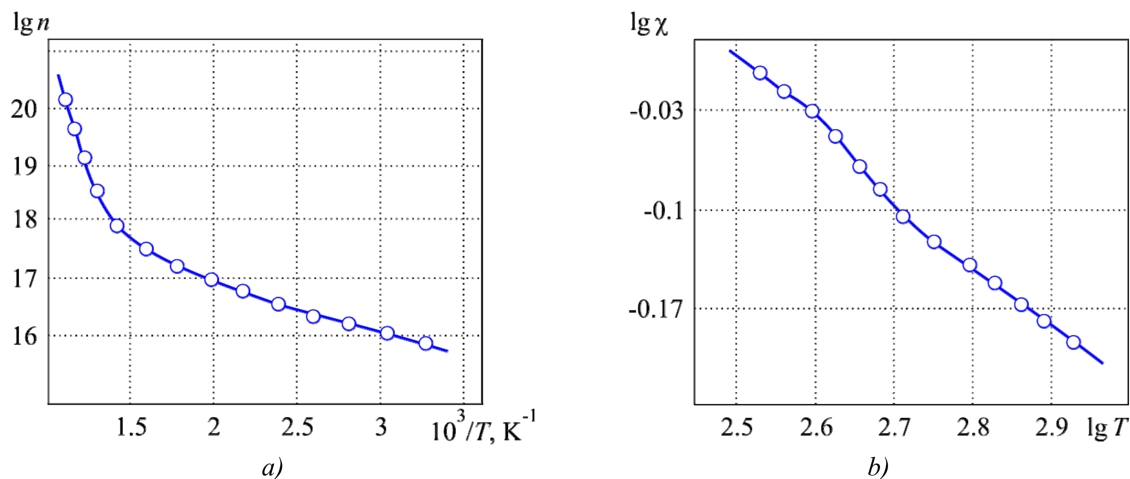

Fig. 3. Temperature dependences of charge carrier concentration n (cm^{-3}) (a) and thermal conductivity coefficient χ (W/m·K) (b) of $InGaTe_2$.

Based on the results of studying the electric parameters and thermal conductivity, the thermoelectric figure of merit of $InGaTe_2$ was determined by the formula

$$Z = \frac{\alpha^2 \sigma}{\chi_p}. \quad (1)$$

The values appearing in (1) are functions of temperature and carrier concentration, causing, accordingly, sharp temperature and concentration dependences of Z.

In the general form the temperature and carrier concentration dependence of *Z* is rather complex. However, with a number of simplifying assumptions of like-sign carriers, the absence of degeneracy, a low value of electronic thermal conductivity, we can establish a relation between Z_{max} and the characteristic parameters of crystals [25].

$$Z_{max} \sim N \frac{m^{*3/2} \mu T^{3/2}}{\chi_p} e^{r+\frac{1}{2}}. \quad (2)$$

Here, *N* is the number of ellipsoids in the Brillouin zone, *m** is the effective mass of carriers, *T* is absolute temperature, *r* is parameter of scattering mechanism, χ_p is lattice thermal conductivity. For $InGaTe_2$ $N = 4$ [4], conductivity is defined by *p*-type conductivity of carriers, the main mechanism is scattering on acoustic phonons with $r = -1/2$, i.e. exponential factor in (2) disappears.

The resulting data on the thermoelectric figure of merit of $InGaTe_2$ is presented in the Table. It is seen that in the temperature range of 500 – 900 K the thermoelectric figure of merit is increased and reaches its maximum value at 900 K.

High thermoelectric figure of merit of $InGaTe_2$ crystal (Table 2) in the specified temperature range is due to a low value of lattice thermal conductivity at mobility values 41 cm^2/V·s.

The low values of χ_p are largely determined by a large mass of atoms forming $InGaTe_2$, and relatively high mobility values are caused by a low value of the effective mass of carriers. Apparently, increase in the thermoelectric figure of merit is promoted by a deeper scattering of phonons as

compared to electrons. However, a gain in μ/χ_p, as a rule, is reduced with a rise in temperature, since due to phonon-phonon scattering the temperature dependence of thermal conductivity is weakened.

Table 2

Physical parameters of $InGaTe_2$ compound

T, K	σ, S/m	α, 10^{-6} V/K	χ, W/(m·K)	R, cm^3/C	μ, $cm^2/(V \cdot s)$	n, cm^{-3}	$Z \cdot 10^{-3}$, K^{-1}
300	6.3	580	0.84	794	780	$8 \cdot 10^{15}$	0.002
400	12	595	0.82	269	479	$2.3 \cdot 10^{16}$	0.005
500	31.6	600	0.79	72.4	160	$8.9 \cdot 10^{16}$	0.015
600	251	595	0.74	7.2	67	$8.7 \cdot 10^{17}$	0.12
700	646	590	0.69	2.02	58	$3 \cdot 10^{18}$	0.32
800	1260	570	0.66	0.98	41	$6.3 \cdot 10^{18}$	0.62
900	2512	540	0.63	0.112	22	$8.9 \cdot 10^{19}$	1.16

It is known that experimental determination of crystal unit cell parameters is a labor-consuming job. In this connection, here we have theoretically calculated the unit cell parameters of $InGaTe_2$ using the results of calculation of $InGaTe_2$ band structure [22]. The calculations were made by density functional method, using ABINIT software package, with the help of the Troullier-Martins pseudopotentials in the plane wave basis [27]. In the expansion of wave function we used plane waves with maximum kinetic energy 30 Ha*. The lattice parameters were determined by full energy minimization, and structure parameters were optimized using the Hellmann-Feynman forces. The process of forces minimization proceeded till scalar forces $\left|\vec{F}\right| < 3\frac{\text{mRy}}{\text{a.u.}}$.

The external influence is known to cause crystal deformation. In this case, both lattice parameters and parameters that determine position of atoms (their coordinates) are changed as well. So, calculation of these parameters with a given deformation value is an important task. It is considered that pressure is determined by full energy derivative with respect to pressure at constant entropy S $P = -(\partial E/\partial V)_S$, and compression modulus – by pressure derivative with respect to volume at constant temperature $B = -V(\partial P/\partial V)_T$. In practice a derivative of compression modulus is found with small changes of pressure $B' = (\partial B/\partial P)_T$. Assuming that $B' = B_0'$, then $B = B_0 + B_0'P$

Then

$$\frac{dV}{V} = -\frac{dP}{B_0 + B_0'P}. \tag{3}$$

By integration of this expression we get

$$P(V) = \frac{B_0}{B_0'}\left(\left(\frac{V_0}{V}\right)^{B_0'} - 1\right). \tag{4}$$

Whence we have

$$V(P) = V_0\left(1 + B_0'\frac{P}{B_0}\right)^{-1/B_0'}. \tag{5}$$

* Hartree energy

As is known, solid bodies have a certain equilibrium volume of the unit cell V_0, and, with a change in this volume by small value, full crystal energy is increased. The Murnaghan equation of state [26] describes the dependence of full energy E on the change in volume V of the unit cell.

$$E(V) = E_0 + \left[\frac{B_0 V}{B_0'} \left(\frac{(V_0/V)^{B_0'}}{B_0' - 1} + 1 \right) - \frac{B_0 V}{B_0' - 1} \right] \frac{1}{14703.6}. \qquad (6)$$

Here $E_0 = E(V_0)$ is the energy corresponding to equilibrium volume V_0 (i.e. to energy minimum), $B = - V(\delta P/\delta V)_T$ is compression modulus, B_0 is the same parameter in equilibrium state corresponding to pressure $P = 0$, $B' = (\delta B/\delta P)_T$ is its first pressure derivative at constant temperature. Multiplier 1/14703.6 in the equation was introduced to obtain the value of full energy in Ry (volume is calculated in atomic units – a.u.).

To determine crystal lattice parameters, we changed the unit cell parameter within ±8 % and calculated the respective values of full energy. Parameters in the Murnaghan equation of state were selected such that a dependence of full energy on the unit cell volume $E(V)$ (Fig. 4), obtained from the equation (shown in Fig. 4 as a solid line) passed through the calculated points.

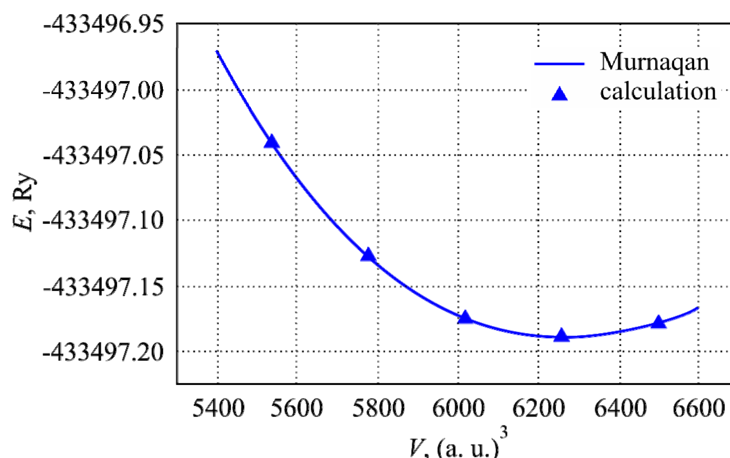

Fig. 4. Dependence of full energy on the unit cell volume of $InGaTe_2$.

According to calculation results, the unit cell volume in equilibrium state V_0 = 6268.1419 a.u., compression modulus B = 40.2392 GPa, its pressure derivative B' = 4.5588.

These results are in good agreement with the calculations made according to the Birch-Murnaghan equation [28] (Table 3).

Table 3

Parameters of the Murnaghan and Birch-Murnaghan equations of state

Parameter	According to Murnaghan	According to Birch-Murnaghan
$V_{0,}$ a.u	6268.1419	6267.8101
E_0, Ry	-433437.189425	-433497.189401
B, Gpa	40.2392	40.1350
B'	4.5588	4.7886

$$E(V)=E_0+\frac{9V_0B_0}{16}\left\{\left[\left(\frac{V_0}{V}\right)^{\frac{2}{3}}-1\right]^3 B_0'+\left[\left(\frac{V_0}{V}\right)^{\frac{2}{3}}-1\right]^2\left[6-4\left(\frac{V_0}{V}\right)^{\frac{2}{3}}\right]\right\}\frac{1}{14703.6}. \qquad (7)$$

Owing to the fact that unit cell volume is $V = abc$ and the resulting equilibrium volume is $V_0 = 6268.1419$ a.u., calculations make it possible to find lattice parameters.

Crystal lattice parameters $a = 8.3945$ Å; $c = 6.8352$ Å that we calculated and coordinates of atoms $x = 0.1730$ in the unit cell agree well with our experimental data and the data in [10]. It should be noted that the results obtained allow further calculation of the phonon spectrum and to study the influence of deformation on the electron and optical properties of $InGaTe_2$, to calculate theoretically the unit cell parameters of other compounds with a known band structure.

The effective mass is known to be the main characteristic of the electron properties of semiconductors. The effective mass is used for studying the electric and magnetic properties, in the calculation of kinetic parameters and in the analysis of critical points of optical parameters.

The tensor components of the inverse effective mass are calculated by the formula:

$$\left[\frac{m_0}{m^*}\right]_{ij}=\delta_{ij}+\frac{2}{m_0}\sum_{n'\neq n}\frac{\left\langle n_1k_0\left|P_i\right|n_1'k_0\right\rangle\left\langle n_1'k_0\left|P_j\right|n_1k_0\right\rangle}{E_n(k_0)-E_{n'}(k_0)}, \qquad (8)$$

m_0 is mass of electron at rest; δ_{ij} is Kronecker sign, $\left\langle n_1k_0\left|P_i\right|n_1'k_0\right\rangle$ is magnetic element of momentum operator, $P_i=-i\hbar\frac{\partial}{\partial x_i}$ at extreme point k_0. n, n' are electron bands. $\left|n_1k_0\right\rangle$ is electron wave function.

$$\left\langle n_1k_0\left|P_i\right|n_1'k_0\right\rangle=\frac{1}{\lambda}\int_{\lambda}\varphi^*_{nk_0}(r)P_i\varphi_{n'k_0}(r)d^3r, \qquad (9)$$

λ is unit cell volume.

The energy spectrum $E_n(k_0)$ and the respective wave function $\varphi_{nk0}(r)$ at extreme point k_0 are found from a one-electron Schrödinger equation. In the plane wave basis

$$\sum_{G'}\left[\frac{\hbar(k_0+G')}{2m_e}\delta_{GG'}+V(k_0+G_1k_0+G')\right]\phi_n(k_0+G')=E_{nk_0}\phi_n(k_0+G)-V(k_0+G_1k_0+G') \qquad (10)$$

is the Fourier image of crystalline pseudopotential.

In $InGaTe_2$, valence band maximum and conduction band minimum are at high-symmetry point T, $\kappa_0 = 0.5b_1 - 0.5b_2 + 0.5b_3$($b_1$, b_2, b_3) are basic translations of the reciprocal lattice [22]. In our calculations, the tensor components of the inverse electron effective mass are calculated to an accuracy of $0.01m_0$

$$\left(\frac{m_0}{m_n}\right)=\begin{pmatrix}3.09 & 0 & 0\\ 0 & 3.09 & 0\\ 0 & 0 & 4.59\end{pmatrix}. \qquad (11)$$

The tensor components of the inverse hole effective mass

$$\left(\frac{m_0}{m^*_{p\perp}}\right)=\begin{bmatrix}-2.31 & 0 & 0\\ 0 & -2.31 & 0\\ 0 & 0 & -0.11\end{bmatrix}. \qquad (12)$$

The tensor components of the inverse effective mass of both electrons and holes are of a

diagonal form, so constant-energy surfaces are ellipsoids of revolution. From the symmetry of $InGaTe_2$ crystal it also follows that constant-energy surfaces must be ellipsoids of revolution.

Conclusions

1. In this paper, using experimental investigations of the temperature dependences of the electric conductivity, the Hall coefficient, the Seebeck and thermal conductivity coefficients, we have determined the energy gap, the concentration of charge-carrier Hall mobility and the thermoelectric figure of merit of $InGaTe_2$ compound and established that the energy gap found by the electric conductivity (0.74 eV) and by the Hall coefficient (0.76 eV) are in good agreement.
2. For the first time, using the results of calculation of $InGaTe_2$ band structure through use of ABİNİT software package, we have theoretically calculated the unit cell parameters of this phase and established that the the calculated and experimentally determined values of these parameters are in good agrement, and have calculated the tensors of the inverse effective mass of electrons and holes.

References

1. H. Hahn, B. Weltman, Uber ternare Chalkogenide des Thalliums mit Gallium und Indium, *Naturwissenschaften* **54** (2), 42 – 48 (1967).
2. D. Muller, G. Eulenberger, und H. Hahn, Uber ternare Thalliumchalkogenide mit thalliums-selennid-structur, *Z. Anorg. Allg. Chem*. **398** (2), 207 – 220 (1973).
3. E. Mooser, W.B. Pearson, The Chemical Bond in Semiconductors, *J. Electronics* **1** (6):629 – 645 (1956).
4. G.D. Guseynov, Search for and Physical Research on Compound Semiconductor Analogs: *Synopsis of a Doctoral Dissertation in Physics and Mathematics* (Vilnius, 1972), 81 p.
5. E.M. Godzhayev, Structure, Electronic and Thermal Properties of Compound Semiconductors Based on sp and 4*f* Elements: *Synopsis of a Doctoral Dissertation in Physics and Mathematics* (Baku: Institute of Physics of the Academy of Sciences of the Azerbaijan SSR, 1985), p. 31.
6. G.D. Guseynov, E.M. Kerimova, E.M. Godzhayev, et al., Physical-Chemical Investigations of $A^{III}X^{VI}$-$B^{III}X^{VI}$ Systems, *Russian J. of Physical Chemistry* **45** (5), 1458 – 1463 (1971).
7. G.D. Guseynov, F.M. Seidov, and A.M. Pashayev, Research on *TlS-GaS* System, *Izvestia AN SSSR, Inorganic Materials* **8** (11), 170–174 (1972).
8. G.D. Guseynov, F.M. Seidov, and H.Ya. Khalilov, On the Pseudobinary System, *Russian Journal of Physical Chemistry* **46** (3), p. 803 – 806 (1972).
9. A.A. Kuliev, Z.G. Kagramanian, Study of *TlSe-GaSe* System, *Izvestia Vuzov, Chemistry and Chemical Technology* 20 (4), 606 – 608 (1977).
10. M. Mobarak, H. Berge, G.F. Lorusso et al., The Growth and Properties of Single Crystals of $GaInTe_2$, a Ternary Chalkogenide Semiconductor, *J. Phys. D: Appl. Phys*. **31**, 1433 – 1437 (1998).
11. V.A. Aliev, Real Structure, Photoelectric Effects in Crystals of $TlA^{III}B_2^{VI}$, *Synopsis of a Doctoral Dissertation in Physics and Mathematics* (Baku, 1997), p. 34.
12. N.A. Abdullayev, Peculiarities of Thermal Expansion in Layered Crystals, *Synopsis of PhD Thesis in Physics and Mathematics* (Baku, 1985), p. 22.
13. V.I. Tkachenko, Yu.V. Voroshilov, L.V. Kostyukov, and A.M. Fantits, Formation Enthalpies and Heat Capacities of $TlGaSe_2$ and $TlGaS_2$ Compounds, *Reports of the Academy of Sciences of Ukr. SSR, series (B), Geological, Chemical and Biological Sciences* **12**, 64 – 66 (1980).
14. E.M. Godzhayev, A.E. Bakhyshov, and A.B. Nagiev, Thermoelectric Figure of Merit of Solid

Solutions of $TlInTe_2$-$TlPrTe_2$ System, *Izvestiya: Inorganic Materials* **23** (10), 1750 – 1753 (1987).
15. E.M. Godzhayev, Kh.O. Sadygova, Thermoelectric Figure of Merit of $InTl_xGa_{1-x}Te_2$ ($0 \leq x \leq 0.2$) Solid Solutions, *Izvestiya: Inorganic Materials* **28**(10/11), 2238 – 2241 (1992).
16. E.M. Godzhayev, G.S. Dzhafarova, and S.I. Safarova, Band Structure of $TlInTe_2$ and Thermoelectrric Figure of Merit of Solid Solutions on its Basis, *J. Thermoelectricity* **1**, 28 – 33 (2013).
17. E.M. Godzhayev, R.A. Kerimova, Thermoelectric Properties of $TlIn_{1-x}Yb_xTe_2$ ($0.01 \leq x \leq 0.04$) Crystals, *Izvestiya: Inorganic Materials* **40** (11), 1314 – 1316 (2004).
18. G. Orudzhev, N. Mamedov, H. Uchiki, N. Yamamoto, S. Iida, H. Toyota, E.M. Godzhayev, and F. Hashimzade, Band Structure and Optical Functions of Ternary Chain *TlInSe*2, *Journal of Physics and Chemistry of Solids* **64**,703 – 1706 (2003).
19. E.M. Godzhayev, G.S. Orudzhev, R.A. Kerimova, and E.A. Allakhyarov, Band Structure and Optical Properties of Chained Compound *TlInTe*, *Physics of the Solid State* **48**, 40 – 43 (2006).
20. E.M. Godzhayev, G.S. Orudzhev, and D.M. Kafarova, Band Structure and Dielectric Permittivity of $TlGaTe_2$ Compound, *Physics of the Solid State* 46(5), 811 – 813 (2004).
21. G. Orudzhev, Y. Shim, K. Wakita, N. Mamedov, S. Jafarova, and F. Hashimzade, Linearized Augmented Plane Wave Band Structure Calculations and Dielectric Function of Layered $TlGaSe_2$, *Jap. J. of Applied Physics* **47** (10), 8182 – 8187 (2008).
22. E.M. Godzhayev, Z.A. Dzhakhangirli, E.A. Allakhyarov, D.M. Kafarova, and A.R. Ibragimova, Cultivation, Phase Analysis and Band Structure of a Monocrystal of *InGaTe*, *Inorganic Materials* **47** (10), 1162 – 1165 (2011).
23. E.M. Godzhayev, U.S. Abdurahmanova, Z.A. Dzhakhangirli,, S.M. Mehdieva, Optical Functions and Effective Masses of Electrons and Holes in $InGaTe_2$, *Physical Science International Journal* **4** (5), 699 – 707(2014).
24. L.P. Pavlov, *Methods for Measurement of Semiconductor Material Parameters* (Moscow: Vyschaya Shkola, 1987), p. 7 – 42.
25. A.F. Ioffe, *Selected Works, Vol. 2* (Leningrad: Nauka, 1975), 468 p.
26. F.D. Murnaghan, The Compressibility of Media under Extreme Pressures, *Proc. of the National Academy of Sciences* **30**, 244 – 247 (1944).
27. X. Gonze, B. Amadon, P.-M. Anglade, J.-M. Beuken, F. Bottin, P. Boulanger, F. Bruneval, et al., ABINIT: First-Principles Approach of Materials and Nanosystem Properties, *Computer Phys. Comm*. **180**, 2582 – 2615 (2009).
28. F. Birch, Finite Elastic Strain of Cubic Crystals, *Physical Review* **71**, 809 – 824 (1947).

Submitted 20.12.2013.

V.A. Romaka[1,2], P. Rogl[3], Yu.V. Stadnyk[4], L.P. Romaka[4], R.O. Korzh[2], D. Kaczorowski[5], V.Ya. Krayovskyy[2], O.I. Lakh[6]

[1]Ya. Pidstryhach Institute for Applied Problems of Mechanics and Mathematics National Academy of Sciences of Ukraine, 3-b, Naukova Str., Lviv, 79060, Ukraine;
[2]National University "Lvivska Polytechnika", 12, S. Bandera Str., Lviv, 79013,Ukraine;
[3]Institut für Physikalische Chemie, Universität Wien, 42, Währinger Str., Wien, A-1090, Österreich;
[4]Ivan Franko National University of Lviv, 6, Kyryla and Mefodiya Str., 79005, Lviv, Ukraine;
[5]Institute of Low Temperature and Structural Research Polish Academy of Sciences, 2, Okólna Str., Wroclaw, 50-422, Poland;
[6]Closed JSC V.I. Lakh "NVO "Thermoprylad", 3, Naukova Str., Lviv, 79060, Ukraine

STRUCTURAL, ENERGY AND KINETIC CHARACTERISTICS OF $Hf_{1-x}Lu_xNiSn$ THERMOELECTRIC MATERIAL

The crystal and electronic structures, the temperature and concentration dependencies of resistivity, the Seebeck coefficient and magnetic susceptibility of $Hf_{1-x}Lu_xNiSn$ thermoelectric material were studied in the range $T = 80 \div 400$ K, $N_A^{Lu} \approx 1.9 \cdot 10^{20}$ cm^{-3} ($x = 0.01$) $\div$ $1.9 \cdot 10^{21}$ cm^{-3} ($x = 0.10$) $H \leq 10$ T. The mechanisms of a simultaneous generation of donor- and acceptor-nature defects in a crystal were established. They change the compensation degree of semiconductor material and determine the mechanism of conduction predicted by the $Hf_{1-x}Lu_xNiSn$ electronic structure calculations.

Key words: electronic structure, resistivity, the Seebeck coefficient.

Introduction

Interest in thermoelectric materials based on intermetallic semiconductors *n-ZrNiSn*, *n-HfNiSn*, *n-TiNiSn* and *p-TiCoSb*, crystallized as structural type *MgAgAs* (space group $F\bar{4}3m$) [1] is caused by simultaneously high values of the electric conductivity and the Seebeck coefficient, which assures high efficiency of thermal into electric energy conversion and makes these semiconductor materials some of the most studied thermoelectric materials [2, 3]. This paper, contributing to further research into the effect of heavy doping of *MgAgAs* ($N_{A,D} \sim 10^{19} \div 10^{21}$ cm^{-3}) semiconductors making them heavily doped and strongly compensated [4] on the change in structural, energy, kinetic and magnetic characteristics, studies thermoelectric material $Hf_{1-x}Lu_xNiSn$ obtained by doping *n-HfNiSn* with atoms of rare-earth *Lu* metal.

These investigations are caused by the fact that optimization of thermoelectric material parameters to obtain maximum values of thermoelectric figure of merit depends on a series of factors, in particular, carrier concentration, scattering mechanisms, thermal conductivity, etc., and one of the methods of such optimization is doping of semiconductor with donor and/or acceptor impurities [5].

Investigation procedures

The object to be investigated included crystalline structure, electron density distribution (DOS), electrokinetic and energy characteristics of $Hf_{1-x}Lu_xNiSn$. The samples were synthesized in the

laboratory of Institute for Physical Chemistry, Vienna University. The *X*-ray structural analysis with employment of Fullprof program [6] was used to obtain the values of $Hf_{1-x}Lu_xNiSn$ crystal lattice periods. The data arrays obtained by the powder method (diffractometer Guinier-Huber image plate system, $CuKa_1$-radiation; $8° \leq 2\theta \leq 100°$) were used for the calculation of structural characteristics. The chemical and phase compositions of samples were controlled by scanning electron microscope (SEM, Zeiss Supra 55VP) and microprobe analyzer (EPMA, energy-dispersive *X*-ray analyzer). The electronic structure calculations were performed by the Korringa-Kohn-Rostoker (KKR) methods in coherent potential approximation (CPA) and local density approximation (LDA) [7]. For the calculations use was made of lattice constant values on *k*-net of size 10 × 10 × 10 and parametrization type of Moruzzi-Janak-Williams exchange-correlation potential [8]. The width of energy window covered by the loop is 16 eV. The number of energy values for the calculation of DOS was 1000. The accuracy of calculation of the Fermi level position was ±8 meV. The temperature and concentration dependences of the electrical resistivity (ρ) and the Seebeck coefficient (α) were measured with respect to copper and magnetic susceptibility (χ) by the Faraday method of $Hf_{1-x}Lu_xNiSn$ samples in the ranges: $T = 80 \div 400$ K, $N_A^{Lu} \approx 1.9 \cdot 10^{20}$ cm^{-3} ($x = 0.01$) ÷ $1.9 \cdot 10^{21}$ cm^{-3} ($x = 0.10$) and magnetic field induction $H \leq 10$ T.

Research on structural features of *Hf₁₋ₓLuₓNiSn*

The microprobe analysis of the concentration of atoms on the surface of $Hf_{1-x}Lu_xNiSn$ samples has shown their conformity to the initial charge compositions, which is one of the experimental proofs of a predicted substitution of *Hf* atoms by *Lu* atoms. In turn, the *X*-ray phase and structural analyses have shown that all $Hf_{1-x}Lu_xNiSn$ samples up to the composition $x = 0.35$ inclusive have no traces of other phases (Fig. 1, inset). The research has also confirmed the result of [9] as regards the disorder of *n-HfNiSn* crystal structure which consists in partial, up to ~ 1 %, occupation by *Ni* ($3d^84s^2$) atoms of crystallographic position 4 *a* of *Hf* ($5d^26s^2$) atoms, which generates donor-nature structural defects in a crystal, and electrons are major current carriers. As was expected, replacement of smaller-size *Hf* atoms ($r_{Hf} = 0.158$ nm) by larger-size *Lu* atoms ($r_{Lu} = 0.173$ nm) leads to increase in the values of $Hf_{1-x}Lu_xNiSn$ unit cell period (Fig. 1).

Refinement of $Hf_{1-x}Lu_xNiSn$ crystalline structure by powder method with a simultaneous refinement of isotropic parameters of atomic substitution and occupancy of crystallographic position of *Hf* (4 *a*) has shown that the lowest value of coefficient of nonconformity between a model of crystalline structure and an array of Bragg reflections ($R_{Br} = 2.7$ %) was obtained for a model where the occupancy of position of *Hf*(*Lu*) atoms for $x \geq 0.01$ is 100 %. In other words, *Lu* atoms introduced into the structure put in order crystalline structure of $Hf_{1-x}Lu_xNiSn$ semiconductor, which creates prerequisites for preparation of material with unambiguous and predicted kinetic characteristics.

Note the availability of two linear areas on the dependence $a(x)$ $Hf_{1-x}Lu_xNiSn$: $0 \leq x \leq 0.01$ and $x \geq 0.03$. Such, at first sight, minor peculiarity of $a(x)$ behaviour is typical of all previously studied related $Zr_{1-x}R_xNiSn$ solid solutions (*R* is rare-earth metal) [10] and served as additional proof of the correctness of proposed model of *n-HfNiSn* crystalline structure [9]. Indeed, if in the output structure of *HfNiSn* compound the positions of *Hf* atoms are partially occupied by smaller-size *Ni* atoms [1], then on doping of semiconductor with atoms of rare-earth metal on the area $0 \leq x \leq 0.01$ there is a displacement of smaller-size *Ni* atoms ($r_{Ni} = 0.124$ nm) by *Lu* atoms of considerably larger size (by ~ 40 %). At impurity concentrations $x \geq 0.01$ all *Ni* atoms will be displaced from the position of *Hf* atoms, and *Hf* atoms will be substituted by *Lu* atoms, where the difference in atomic radii is

considerably smaller. In that case the amplitude of change in the values of $Hf_{1–x}Lu_xNiSn$ unit cell period in the areas $0 \le x \le 0.01$ and $x \ge 0.03$ will be different; in the former case this change will be greater, as evidenced by a larger slope of dependence $a(x)$, which is only possible with displacement of smaller-size *Ni* atoms from the position of larger-size *Hf* atoms.

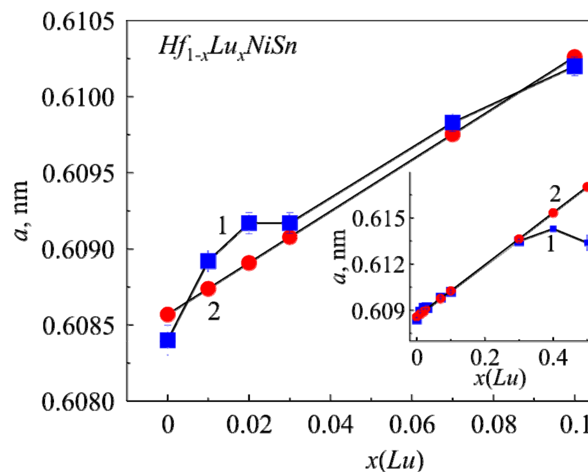

Fig. 1. Change in the values of unit cell period a(x) of $Hf_{1-x}Lu_xNiSn$: 1 – experiment; 2 – calculation.

Proceeding from the assumption that doping of *n-HfNiSn* with *Lu* atoms is accompanied by crystal structure ordering, and *Lu* impurity atoms displace *Hf* atoms from position 4 *a*, we calculated a change in the values of unit cell period (Fig. 1, curve 2). In the calculations we assumed that the initial compound *HfNiSn* is ordered, that is, all the atoms occupy only their own crystallographic positions. Exactly for this reason the calculated value of unit cell period for the initial compound *HfNiSn* is larger than the experimental one, as long as in a real compound, as we mentioned before, ~ 1 % of *Hf* atoms are displaced by smaller-size *Ni* atoms. Comparison of the calculated and experimental values of unit cell period of $Hf_{1–x}Lu_xNiSn$ (Fig. 1) vividly demonstrates structural changes that we investigated in the refinement of crystal structure by powder method.

The process of semiconductor crystal structure ordering on doping with *Lu* atoms, apart from structural peculiarities, contributes essentially to electron density redistribution. Thus, if in the initial compound *HfNiSn* there are donor-nature structural defects as a result of displacement of up to ~ 1 % of *Hf* atoms by smaller-size *Ni* atoms, the process of semiconductor doping with *Lu* atoms and ordering its crystal structure is accompanied, on the one hand, by the reduction of the number of donor-nature structural defects, since *Ni* atoms leave the position of *Hf* atoms (“healing: of donor-nature structural defects in position 4 *a*). On the other hand, since *Lu* ($5d^16s^2$) atom possesses one 5*d*-electron less than *Hf* atom, such doping will generate acceptor-nature structural defects in a crystal.

Thus, doping of *n-HfNiSn* with the atoms of rare-earth metal *Lu* by substitution of *Hf* atoms is accompanied by crystal structure ordering and makes it resistant to temperature and time changes, which is a necessary condition of possible material use for production of sensitive elements of thermal converters. Moreover, such ordering is accompanied by a simultaneous reduction of the number of donor-nature defects (*Ni* atoms in position 4*a* of *Hf* atoms) and increase in the number of acceptor-nature structural defects (Lu atoms in position 4*a* of *Hf* atoms), which must lead to a change in semiconductor compensation degree and the type of major current carriers as a result of a change in the ratio of donor- and acceptor-nature defects.

Research on the electron structure of $Hf_{1-x}Lu_xNiSn$

To predict the behaviour of the Fermi level ε_F, the energy gap ε_g and the kinetic characteristics of *n-HfNiSn* doped with *Lu* atoms, the electron density distribution (DOS) of $Hf_{1-x}Lu_xNiSn$, $0 \le x \le 0.10$ was calculated (Fig. 2 a). Taking into account the results of structural research, namely that introduction of *Lu* atoms into *HfNiSn* compound puts in order its crystal structure, the calculation of DOS was performed for the case of ordered structure variant.

As mentioned above, introduction of *Lu* atoms into the structure of *HfNiSn* compound is attended by generation of acceptors. In that case, doping of *n-HfNiSn* semiconductor by the lowest concentrations of acceptor impurity can be expected to be attended by increase in semiconductor compensation degree [6].

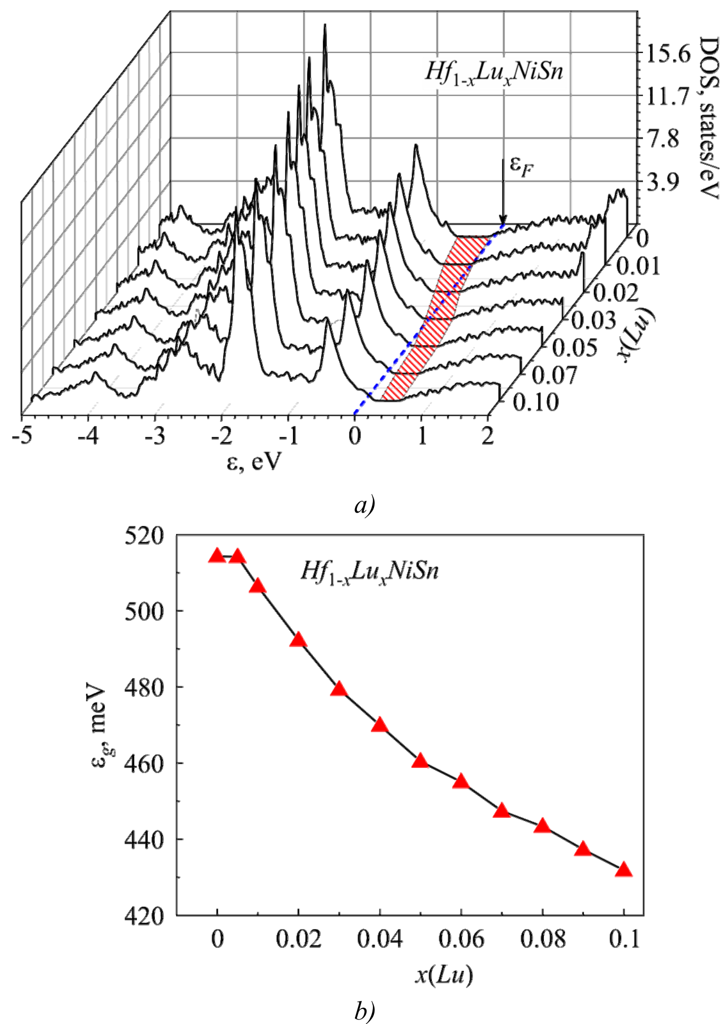

Fig. 2. Calculation of the electronic density of states DOS (a) and change in the values of energy gap ε_g (b) of $Hf_{1-x}Lu_xNiSn$.

As can be seen from Fig. 2 *a*, on introducing into *n-HfNiSn* the least attainable in the experiment concentrations of *Lu* acceptor impurity, the Fermi level ε_F starts drifting from conduction band from which it was spaced ~ 81.3 meV [9], to the mid of the energy gap ε_g (hatched area in Fig. 2 *a*), and then to valence band which will be crossed at certain *Lu* concentrations. Crossing by the Fermi level ε_F of the mid energy gap and its further motion towards valence band will change semiconductor conduction type, and holes will become major current carriers. In that case further doping of now

p-type semiconductor with acceptors must be accompanied by a decrease in compensation degree.

Apart from the drift caused by a change in semiconductor compensation degree, there is also a reduction in the values of energy gap ε_g (Fig. 2 *b*) from the values of of ε_g $(x = 0) = 514.3$ meV and ε_g $(x = 0.05) = 460.4$ meV to ε_g $(x = 0.10) = 431.8$ meV. The predicted behaviour of the Fermi level ε_F is accompanied by interesting processes of change in DOS values on the Fermi level (Fig. 3 *a*, curve 2). Thus, doping of *n-HfNiSn* semiconductor with *Lu* acceptor impurities will expectedly result in the reduction of DOS on the Fermi level, and the minimum of dependence $g(\varepsilon_F)$ corresponds to crossing by the Fermi level the mid energy gap of semiconductor. At concentrations of *Lu* impurity, when the Fermi level will cross the mid energy gap and approach the valence band, there will be a predicted growth of DOS on the Fermi level.

The above results of calculations of change in the electron density distribution and, in particular, the density of states on the Fermi level, agree with the results of experimental measurement of the magnetic susceptibility χ of $Hf_{1-x}Lu_xNiSn$ (Fig. 3 *a*, curve 1). Investigations have shown that $Hf_{1-x}Lu_xNiSn$, $x > 0.01$ semiconductors are Pauli paramagnetics whose magnetic susceptibility is determined exclusively by the electron gas and is proportional to the density of states on the Fermi level. As can be seen from Fig. 3 *a*, curve 1, dependence $\chi(x)$ has a plateau in the concentration area $x = 0.02 \div 0.03$ which we attribute, as shown by calculations, exactly to a change in the density of states on the level of $g(\varepsilon_F)$. In this context it should be noted that basic semiconductor *n-HfNiSn* is not Pauli paramagnetic, but a weak diamagnetic, as testified by the negative values of magnetic susceptibility: $\chi(x = 0) = -0.082$ cm^3/g [11]. So, the alleged growth of dependence $\chi(x)$ in the concentration area $x = 0 \div 0.02$ cannot be attributed to increase in DOS on the Fermi level.

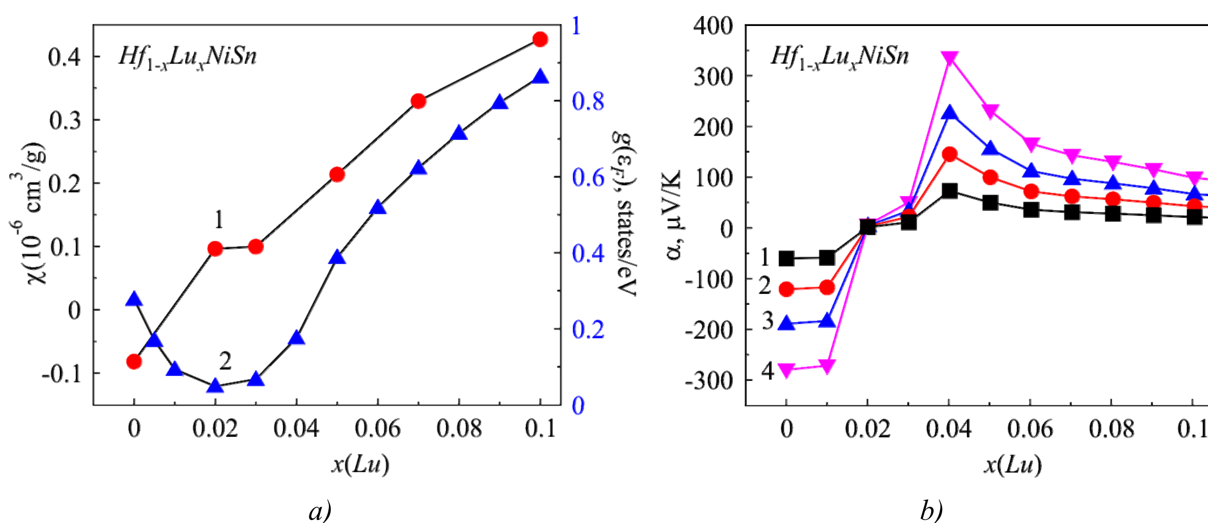

Fig. 3. Change in the values of magnetic susceptibility χ *(curve 1) and density of states on the Fermi level* $g(\varepsilon_F)$ *(curve 2) (a) and the Seebeck coefficient* α *(calculation) (b) of* $Hf_{1-x}Lu_xNiSn$ *at the temperatures: 1 – 80 K; 2 – 160 K; 3 – 250 K; 4 – 380 K.*

Having calculated the electronic structure of $Hf_{1-x}Lu_xNiSn$ thermoelectric materials, we obtained the mechanism for prediction of the kinetic characteristics of a semiconductor, in particular, the Seebeck coefficient, the electric resistivity, etc. For the calculation of the Seebeck coefficient α as a working formula the relationship [12] was used:

$$\alpha = \frac{2\pi^2}{3}\frac{k^2 T}{e}\left(\frac{d}{d\varepsilon}\ln g(\varepsilon_F)\right),$$

where $g(\varepsilon_F)$ is the density of states on the Fermi level.

As an example, Fig. 3 *b* shows a change in the values of the Seebeck coefficient $\alpha(x)$ of $Hf_{1-x}Lu_xNiSn$ at different temperatures. Changing the concentration of *Lu* atoms, we can purposefully obtain in thermoelectric material both positive and negative high values of the Seebeck coefficient and conductivity, which serves one of the conditions for obtaining high values of thermoelectric figure of merit.

Thus, the results of calculation of the density of electronic states of $Hf_{1-x}Lu_xNiSn$ based on the results of structural investigations confirm the predicted acceptor nature of structural defects generated in a crystal on substitution of *Hf* atoms by *Lu*. The results of experimental research presented below will show the conformity of calculated results to real processes in thermoelectric material.

Research on the electrokinetic and energy characteristics of $Hf_{1-x}Lu_xNiSn$

The temperature dependences of electric resistivity ρ and the Seebeck coefficient $\alpha(1/T)$ for the samples of $Hf_{1-x}Lu_xNiSn$, $0 \le x \le 0.1$ are shown in Fig. 4. The dependences $\ln\rho(1/T)$ and $\alpha(1/T)$ are typical for doped and compensated semiconductors with high- and low-temperature activation areas, which is indicative of the presence in them of several activation conductivity mechanisms. From the activation areas of dependences $\ln\rho(1/T)$ we calculated the values of activation energies from the Fermi level ε_F to percolation level of conduction band (valence band) ε_1^{ρ} and electron jumps ε_3^{ρ} in the states with energies close to the Fermi level ε_F, and from the activation areas of dependences $\alpha(1/T)$ – the values of activation energies ε_1^{α} and ε_3^{α}, which yield, respectively, the values of modulation amplitude of continuous energy bands and small-scale fluctuation of heavily doped strongly compensated semiconductors [13].

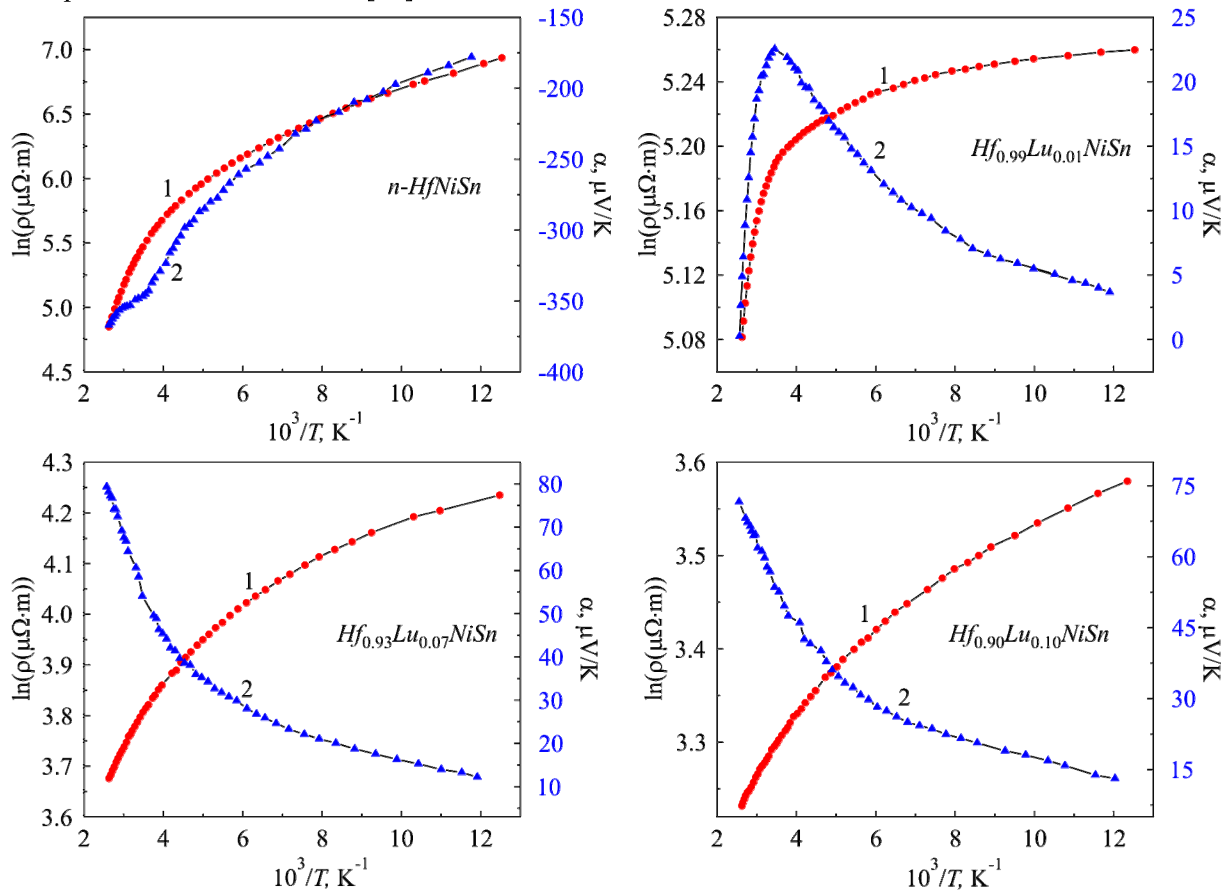

Fig. 4. Temperature dependences of resistivity ρ (1) and the Seebeck coefficient α (2) of $Hf_{1-x}Lu_xNiSn$.

As is shown in Figs. 4 and 5 *b*, the Seebeck coefficient of $Hf_{1–x}Lu_xNiSn$, $x = 0$, has negative values, and electrons are the main current carriers. This is a well known and expected result related to donor nature of structural defects of *n-HfNiSn* semiconductor [1].

Introduction to *HfNiSn* compound of the lowest concentration of *Lu* atoms leads to a change in conduction type of $Hf_{1–x}Lu_xNiSn$ semiconductor: at $x \geq 0.01$ the values of the Seebeck coefficient become positive over the entire temperature range, indicating that the Fermi level is now closer to the valence band than to conduction band (Fig. 4 and 5 *b*). Such a behavior of the Fermi level had been anticipated by the calculations of semiconductor electron structure and results from the appearance in a crystal of acceptor-nature structural defects at introduction of *Lu* atoms.

The fact that *Lu* atoms introduced into *HfNiSn* compound result in generation in a crystal of acceptor-nature structural defects is shown by the dependences of change in the values of electric resistivity over the entire temperature and concentration ranges (Fig. 5 *a*). Thus, introduction of the lowest in the experiment concentration of *Lu* atoms is accompanied by a drastic reduction in the values of electric resistivity, for instance, at 80 K, from the values of $\rho(x = 0) = 1029.1$ μΩ·m to $\rho(x = 0.01) = 192.4$ μΩ·m and $\rho(x = 0.1) = 35.9$ μΩ·m. The point is that the concentration of acceptors generated in a crystal on introducing the lowest concentration of *Lu* ($x = 0.01$) is too high, and we jump over the concentration gap whereby the Fermi level would move from the edge of conduction band to the mid of the energy gap, which would be attended by growth in the electric resistivity values due to a reduction of density of states on the Fermi level in the *n*-type semiconductor doped with acceptors.

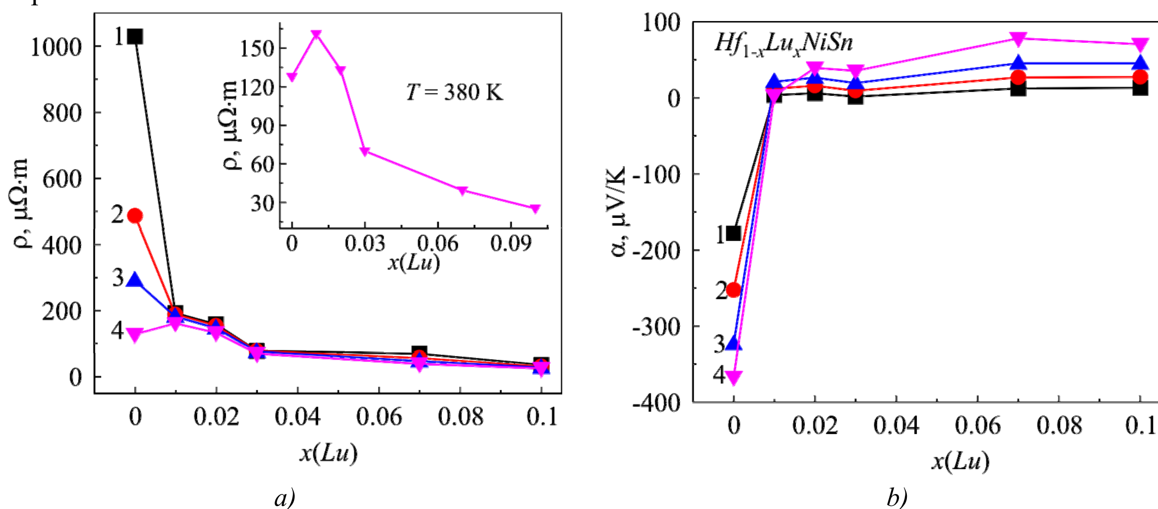

Fig. 5. Change in the values of resistivity ρ(x) (a) and the Seebeck coefficient α(x) (b) $Hf_{1-x}Lu_xNiSn$ at the temperatures: 1 – 80 K; 2 – 160 K; 3 – 250 K; 4 – 380 K.

We draw attention to the fact of appearance of maximum on the dependence $\rho(x)$ at a temperature of $T = 380$ K (Fig. 5 *a*). A similar picture of maximum $\rho(x)$ displacement to the area of high impurity concentrations was observed in [11, 14] on doping of *n-HfNiSn* with acceptor impurities *Rh* and *Co*. This effect was explained by generation in a crystal of acceptor-nature defects concurrently with donor-nature structural defects whose ionization occurs at higher temperatures.

The proof of the fact that the Fermi level crossed the mid of the energy gap and is moving exactly in the direction of valence band on doping of *n-HfNiSn* with *Lu* atoms is a behaviour of the dependence of the Seebeck coefficient $\alpha(x)$ of $Hf_{1–x}Lu_xNiSn$ (Fig. 5 *b*). Thus, the values of the Seebeck coefficient, for instance, at 80 K, vary from the values of $\alpha(x = 0) = –178.1$ μVK^{-1} to $\alpha(x = 0.01) = 3.7$ μVK^{-1} and $\alpha(x = 0.1) = 13.2$ μVK^{-1}, which testifies to a change in the type of major

current carriers in $Hf_{1-x}Lu_xNiSn$ – from electrons at $x = 0$ to holes at $x \geq 0.01$.

We also focus on the behaviour of dependence of the Seebeck coefficient $\alpha(x)$ of $Hf_{1-x}Lu_xNiSn$ at $T = 380$ K. The value of the Seebeck coefficient at temperature $T = 380$ K varied with a change in concentration of *Lu* impurity atoms at follows: from $\alpha(x = 0) = -367.2$ μVK^{-1} to $\alpha(x = 0.01) = 0.2$ μVK^{-1} and $\alpha(x = 0.02) = 39.4$ μVK^{-1}. We can see that at concentration $Hf_{1-x}Lu_xNiSn$, $x = 0.01$ and temperature $T = 380$ K the concentrations of ionized acceptors and donors became practically the same, as indicated by the Seebeck coefficient value close to zero. This result completely agrees with the nature of behaviour of $\rho(x)$ at temperature $T = 380$ K exactly in the region of acceptor concentrations $x = 0.01$. And this, in turn, also points to the fact of appearance in a crystal of donors by so far unknown mechanism on doping with acceptor impurity.

Therefore, the two experimental results, namely change in the values of electric resistivity $\rho(x)$ and the Seebeck coefficient $\alpha(x)$ of $Hf_{1-x}Lu_xNiSn$ point to the presence in a crystal of a complicated mechanism of generation of structural defects of both acceptor and donor nature.

In this context it is interesting to follow the nature of change in the energy characteristics of $Hf_{1-x}Lu_xNiSn$, obtained from the experimental research (Fig. 6), from which it can be also concluded that introduction of *Lu* impurity atoms into the structure of *HfNiSn* compound is accompanied by generation of both acceptor- and donor-nature structural defects. Thus, from Fig. 6 *a* it is seen that doping of semiconductor results in the reduction of the values of activation energy $\varepsilon_1^{\rho}(x)$. It is important to explain that the value of energy $\varepsilon_1^{\rho}(x)$ for undoped semiconductor *n-HfNiSn* reflects the energy gap between the position of the Fermi level ε_F and the edge of conduction band. At the same time, the values of activation energy $\varepsilon_1^{\rho}(x)$ for the lowest and all succeeding concentrations of *Lu* atoms reflect the energy gap between the Fermi level position and the edge of valence band. The fact that the value of activation energy $\varepsilon_1^{\rho}(x = 0)$ fits in the dependence $\varepsilon_1^{\rho}(x)$ is quite casual.

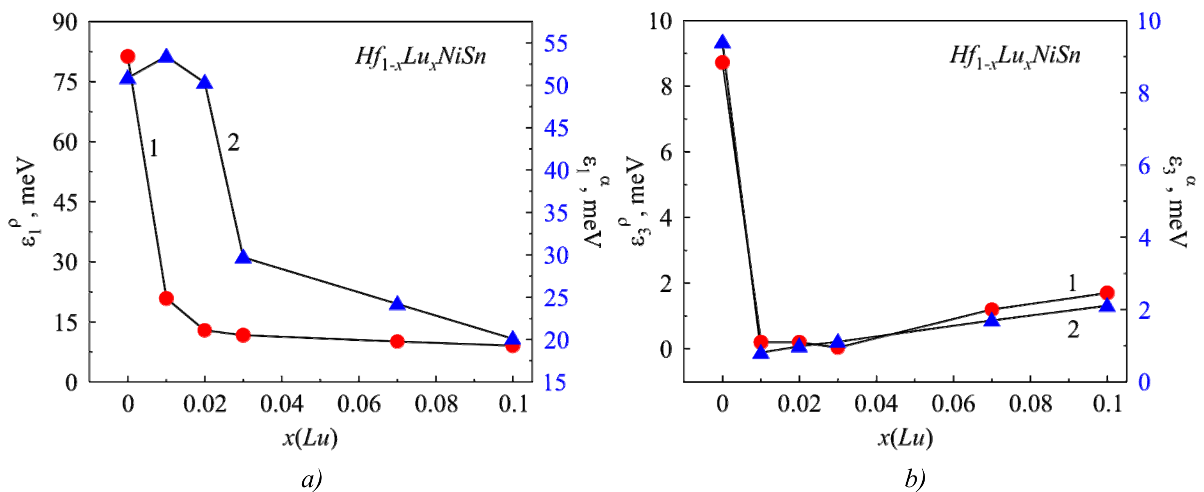

Fig. 6. Change in the values of activation energies $\varepsilon_1^{\rho}(x)$ (1) and $\varepsilon_1^{\alpha}(x)$ (2) (a) and $\varepsilon_3^{\rho}(x)$ (1) and $\varepsilon_3^{\alpha}(x)$ (2) (b) $Hf_{1-x}Lu_xNiSn$.

The nature of behaviour of $\varepsilon_1^{\rho}(x)$ implies the following interesting peculiarity. We can see that starting from the concentration of *Lu* impurity $x = 0.01$ to $x = 0.10$ the rate of motion of the Fermi level ε_F to the edge of valence band each time is reduced and is as follows: in the concentration area $x = 0.01 \div 0.02$ the rate of motion is $\Delta\varepsilon_F/\Delta x = 8$ meV/%*Lu*, in the area $x = 0.02 \div 0.03$ the rate of motion is $\Delta\varepsilon_F/\Delta x = 1.2$ meV/%*Lu*, in the area $x = 0.03 \div 0.07$ the rate of motion is $\Delta\varepsilon_F/\Delta x = 0.4$ meV/%*Lu* and

in the area $x = 0.07 \div 0.10$ the rate of motion is $\Delta\varepsilon_F/\Delta x = 0.3$ meV/%*Lu*. In connection with the above values of drift velocity of the Fermi level ε_F in various concentration areas of *Lu* impurity atoms, quite a logical question arises. As long as we increase the concentration of *Lu* acceptor impurities by the linear law, which generate in a crystal the acceptor-nature structural defects by the same law, then why does the Fermi level not move by the same law to the edge of valence band? Which serves the restraining factor of such motion, and the dependence resembles the exponent?

Answering this question, it is logical to assume that apart from acceptors, donors are also generated in a crystal, whose generation velocity increases with increasing concentration of *Lu* atoms introduced into a crystal. This conclusion coincides with that made from the nature of electric resistance and the Seebeck coefficient behaviour.

On the other hand, simultaneous generation in a crystal with different velocity of donor- and acceptor-nature structural defects will be attended by a change in semiconductor compensation factor, as well as by a change in modulation amplitude of continuous energy bands of heavily doped strongly compensated semiconductor by the law that reflects the ratio of ionized acceptors and donors in a crystal. Fig. 6 *a* shows a change in the values of activation energy $\varepsilon_1^{\alpha}(x)$ which is proportional to modulation amplitude of continuous energy bands $Hf_{1-x}Lu_xNiSn$. We can see that in the case of undoped semiconductor *n-HfNiSn* the modulation amplitude is $\varepsilon_1^{\alpha}(x = 0) = 50.9$ meV. Introduction into *n*-type semiconductor of the lowest in the experiment concentration of *Lu* impurity that corresponds to composition $x = 0.01$ is accompanied by increase in semiconductor compensation factor, as indicated by the value of modulation amplitude $\varepsilon_1^{\alpha}(x = 0.01) = 53.4$ meV. Moreover, at concentration $x = 0.01$ the type of semiconductor conductivity is changed, namely holes become major current carriers.

Adding to now *p*-type $Hf_{1-x}Lu_xNiSn$ semiconductor, $x = 0.01$, of *Lu* acceptor impurity naturally reduces the degree of compensation, that is, the difference in the number of ionized acceptors and donors will be increased. This effect is reflected in the reduction of modulation amplitude values of $\varepsilon_1^{\alpha}(x = 0.02) = 50.3$ meV, and a maximum appears on the dependence $\varepsilon_1^{\alpha}(x)$. It is clear that further doping of *p*-type semiconductor with acceptor impurity will only reduce the compensation factor, and the value of modulation amplitude of continuous energy bands will be reduced as well (Fig. 6 *a*). As long as we monotonously increase acceptor concentration in a semiconductor, where holes are major current carriers, it would be quite logical to expect the same reduction in the values of modulation energy of continuous energy bands of $Hf_{1-x}Lu_xNiSn$. However, as is seen from Fig. 6 *a*, a change in the values of $\varepsilon_1^{\alpha}(x)$ dependence for the cases of $x > 0.01$ does not follow the linear law, but reminds the case of $\varepsilon_1^{\rho}(x)$, indicating simultaneous generation, along with acceptors, of donors by unknown mechanisms.

Changes in the values of hopping conductivity activation energy $\varepsilon_3^{\rho}(x)$ and activation energy $\varepsilon_3^{\alpha}(x)$ of $Hf_{1-x}Lu_xNiSn$ (Fig. 6 *b*) also point to generation in a crystal of donor-nature defects by unknown mechanism. And indeed, a monotonous increase in the number of acceptor-nature defects in *p*-type semiconductor was to cause a reduction in the values of activation energy of hopping conduction $\varepsilon_3^{\rho}(x)$, as long as electron localization radius would have to be reduced. However, in the experiment, starting from concentration $x \geq 0.03$, we observe increased values of activation energy of hopping conductivity from the values of $\varepsilon_3^{\rho}(x = 0.03) = 0.04$ meV to $\varepsilon_3^{\rho}(x = 0.07) = 1.2$ meV and $\varepsilon_3^{\rho}(x = 0.1) = 1.7$ meV. Such a behaviour of hopping conductivity activation energy $\varepsilon_3^{\rho}(x)$ is possible only in the presence of donors, which increases electron localization radius [4].

Increase in the values of modulation amplitude of small-scale fluctuation from the values of $\varepsilon_3^{\alpha}(x = 0.01) = 0.8$ meV to $\varepsilon_3^{\alpha}(x = 0.07) = 1.7$ meV and $\varepsilon_3^{\alpha}(x = 0.1) = 2.1$ meV is also possible only under condition of generation of donors alongside with acceptors, which will change semiconductor

compensation degree. It can be predicted that with a certain number of acceptors the rate of donor generation will be the same as that of acceptors and even greater, which will again change semiconductor compensation degree.

Thus, the results of kinetic investigations of $Hf_{1-x}Lu_xNiSn$ allow speaking about a complex mechanism of a simultaneous generation in a crystal of acceptor- and donor-nature structural defects on introducing atoms of rare-earth metal *Lu* into the structure of *HfNiSn* compound by substitution of *Hf* atoms. Such a mechanism will be proposed below.

Refinement of the crystal and electron structures of $Hf_{1-x}Lu_xNiSn$

In [1] we proposed a procedure for getting information on crystal structure which is unavailable when using *X*-ray investigation methods. The essence of this procedure lies in seeking for such spatial arrangement of atoms in the nodes of semiconductor crystal lattice that provides the adequacy of the results of calculation of electron structure distribution and the results obtained from the experimental research, in particular, a change in the Fermi level position.

Using binding to numerical values of activation energy ε_1^{ρ} from the Fermi level to the level of percolation of valence band of $Hf_{1-x}Lu_xNiSn$, we sought for a compensation factor that would provide experimentally established velocity of the Fermi level motion shown in Fig. 7 *a*, curve 1. Calculations of DOS were performed for various variants of atoms arrangement in the nodes of unit cell, and the degree of occupancy of crystallographic position of $Hf_{1-x}Lu_xNiSn$ by intrinsic or extrinsic atoms. It turned out that the most acceptable variant of atoms arrangement foresees the appearance of vacancies in the position of *Sn* atoms (4 *b*). In this case compound formula will change for $Hf_{1-x}Lu_xNiSn_{1-y}$, and crystalline structure will remain ordered. The dynamics of change in the concentration of vacancies in crystallographic position 4 *b* of *Sn* atoms in $Hf_{1-x}Lu_xNiSn_{1-y}$ is shown in Fig. 7 *b*. The velocity of the Fermi level motion towards the valence band is shown in Fig. 7 *a*, curve 1, which within the limits of calculation errors coincides with the results of motion of the Fermi level (Fig. 7 *a*, curve 2), obtained from the temperature dependences of electric resistivity (Fig. 4).

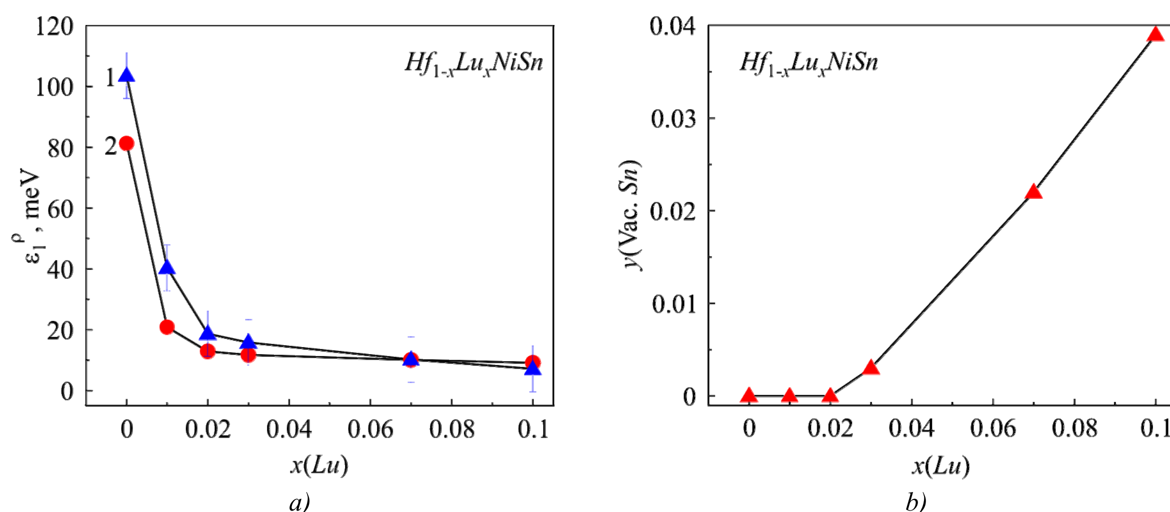

Fig. 7. Calculated (1) and experimentally obtained (2) dependence of activation energy ε_1^{ρ} (a) in $Hf_{1-x}Lu_xNiSn$ and dynamics of change in the concentration of vacancies in crystallographic position of Sn (b).

Conclusions

Thus, as a result of a comprehensive research on crystal and electron structures, the electrokinetic and magnetic characteristics of intermetallic semiconductor *n-HfNiSn*, heavily doped with the atoms of rare-earth metal *Lu*, the mechanisms of simultaneous generation in a crystal of acceptor- and donor-nature structural defects have been established that change thermoelectric material compensation factor and determine the mechanisms of electric conductivity.

The work was performed in the framework of grant of the National Academy of Sciences, № 106U000594.

References

1. V.A. Romaka, V.V. Romaka, and Yu.V. Stadnyk, *Intermetallic Semiconductors: Properties and Applications* (Lviv, Lvivska Polytechnika, 2011), 488 p.
2. T.M. Tritt, M.A. Sabramanian, Thermoelectric Materials, Phenomena, and Applications: A Bird’s Eye View, *MRS Bulletin* **31** (3), 188 – 198 (2006).
3. G.S. Nolas, J. Poon, and M. Kanatzidis, Recent Developments in Bulk Thermoelectric Materials, *MRS Bulletin* **31** (3), 199 – 205 (2006).
4. B.I. Shklovsky, A.L. Efros, *Electronic Properties of Doped Semiconductors* (Moscow: Nauka, 1979), 416 p.
5. L.I. Anatychuk, *Thermoelements and Thermoelectric Devices* (Kyiv: Naukova Dumka, 1979), 768 p.
6. T. Roisnel, J. Rodriguez-Carvajal, WinPLOTR: a Windows Tool for Powder Diffraction Patterns Analysis, *Mater. Sci. Forum, Proc. EPDIC7* **378-381**, 118 – 123 (2001).
7. M. Schruter, H. Ebert, H. Akai, P. Entel, E. Hoffmann, and G.G. Reddy, First-Principles Investigations of Atomic Disorder Effects on Magnetic and Structural Instabilities in Transition-Metal Alloys, *Phys. Rev. B* **52**, 188 – 209 (1995).
8. V.L. Moruzzi, J.F. Janak, and A.R. Williams, *Calculated Electronic Properties of Metals* (NY: Pergamon Press, 1978), 348 p.
9. V.V. Romaka, P. Rogl, L. Romaka, Yu. Stadnyk, A. Grytsiv, O. Lakh, and V. Krajovsky, Peculiarites of Structural Disorder in *Zr*- and *Hf*- Containing Heusler and Half-heusler Stannides, *Intermetallics* **35**, 45 – 52 (2013).
10. V.A. Romaka, D. Fruchart, E.K. Hlil, R.E. Gladyshevskii, D. Gignoux, V.V. Romaka, B.S. Kuzhel, and R. Krayjvskii, Features of an Intermetallic *n-ZrNiSn* Semiconductor Heavily Doped with Atoms of Rare-Earth Metals, *Semiconductors* **44** (3), 293 – 302 (2010).
11. V.A. Romaka, P. Rogl, V.V. Romaka, Yu.V. Stadnyk, E.K. Hlil, V.Ya. Krajovsky, and A.M. Horyn, Features of Conduction Mechanisms in *n-HfNiSn* Semiconductor Heavily Doped with *Rh* Acceptor Impurity, *Semiconductors* **47** (9), 1145 – 1152 (2013).
12. N. Mott, T. Davis, *Electronic Processes in Noncrystalline Substances* (Moscow: Mir, 1982), 368 p.
13. V.A. Romaka, Yu.V. Stadnyk, V.V. Romaka, D. Fruchart, Yu.K. Gorelenko, V.F. Chekurin, and A.M. Horyn, Features of Electrical Conductivity in the *n-ZrNiSn* Intermetallic Semiconductor Heavily Doped with the In Acceptor Impurity, *Semiconductors* **41** (9), 1041 – 1047 (2007).
14. V.A. Romaka, P. Rogl, Yu.V. Stadnyk, V.V. Romaka, E.K. Hlil, V.Ya. Krayovskii, and A.M. Horyn, Features of the Conduction Mechanisms of the *n-HfNiSn* Semiconductor Heavily Doped with the *Co* Acceptor Impurity, *Semiconductors* **46** (9), 1106 – 1113 (2012).

Submitted 06.03.2014.

V.A. Barabash[1], S.A. Glyazer[1], G.G. Gromov[1], I.A. Drabkin[2], L.B. Ershova[1], S.A. Molchanova[1]

[1]RMT Ltd, 22 d, Larin Str., Nizhny Novgorod, 603152, Russia;
[2]State Scientific-Research and Design Institute of Rare-Metal Industry ("GIREDMET" JSC), 5/1 B. Tolmachevsky lane, Moscow, 119017, Russia

MATCHING OF EXTRUDED MATERIALS BASED ON BISMUTH-ANTIMONY CHALCOGENIDES FOR A THERMOELEMENT

Extruded thermoelectric materials of different conductivity types based on bismuth and antimony chalcogenides, according to the reported experimental data, are much different in their thermoelectric properties. This paper deals with matching of thermoelement legs of such materials. It is shown that condition of equality of the absolute values of Seebeck coefficient at room temperature is a good criterion for matching of materials in a thermoelement assuring maximum temperature difference on it.

Key words: extruded thermoelectric material, thermoelement, maximum temperature difference.

Introduction

Crystalline antimony-bismuth chalcogenides in their physical properties are anisotropic materials. Their characteristics in the direction of triad axis and normal to it may differ several times. In the design of thermoelements of zone-melted materials based on antimony-bismuth chalcogenides, the problem of *n*- and *p*-type legs matching does not arise, since thermoelectric characteristics of legs cut of oriented crystals in the direction normal to trigonal axis (along cleavage planes) are very close. Therefore, for matching of legs it is sufficient to take legs of different types with close electric conductivity or Seebeck coefficient values.

In extrusion of such materials, a deformation texture is formed where the major part of grains is located such that their trigonal axis is directed normal to extrusion axis. In *p*-type crystalline materials, the ratio between electric conductivity in the direction normal to trigonal axis and electric conductivity in the direction of trigonal axis (electric conductivity anisotropy) is 2 – 2.5 [1, 2], thermal conductivity anisotropy is the same as electric conductivity anisotropy; Seebeck coefficient anisotropy is absent. This results in the absence of thermoelectric figure of merit anisotropy. Therefore, in *p*-type extruded materials with ideal contacts between the grains the thermoelectric figure of merit must be the same as in a single crystal. In *n*-type materials electric conductivity anisotropy is about 4, whereas thermal conductivity anisotropy is 2. Seebeck coefficient anisotropy is absent. The difference in thermal conductivity and electric conductivity anisotropy leads to the fact that in extruded materials the lines of electric current and thermal flow may not coincide locally, which will result in formation of eddy currents [3] reduction of thermoelectric figure of merit. Therefore, in extruded materials the thermoelectric figure of merit of *n*-type materials should be lower than that of *p*-type materials, and selection of thermoelement couples becomes a topical issue.

Thermoelectric parameters of extruded materials

Temperature dependences of thermoelectric properties of extruded thermoelectric materials produced by company RMT were measured on RMT DX8080 plant. In the measurements, the six-wire

Harman method was used [4, 5]. The dimensions of the samples were (length × width × height) 2 × 2 × 1.6 mm^3. Galvanic anti-diffusion *Ni* coatings were applied on the end faces of the samples by the technique used for mass production of thermoelectric modules.

The results of measurements are given in Figs. 1 – 3.

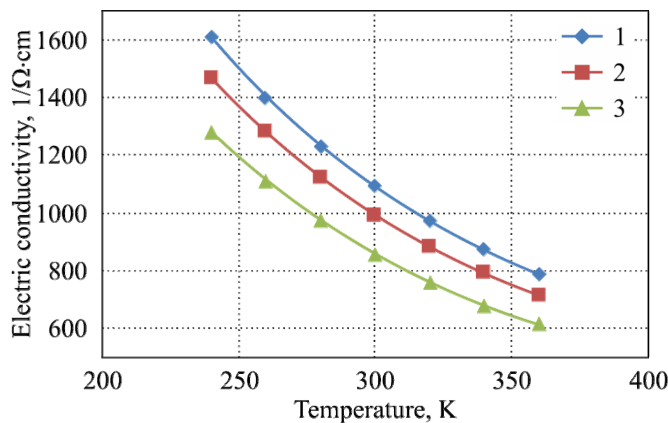

a)

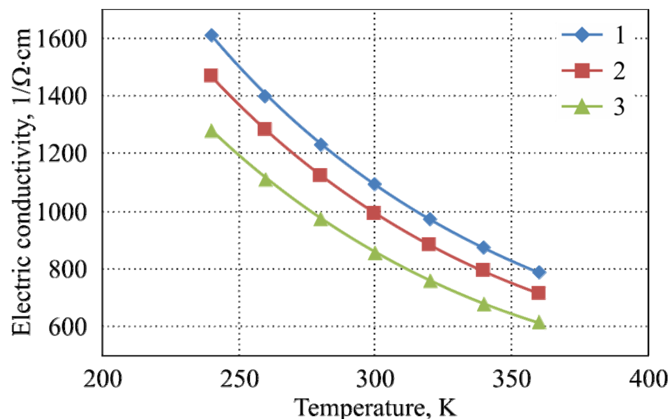

b)

Fig. 1. Temperature dependences of electric conductivity a) for p-type $Bi_{0.4}Sb_{1.6}Te_3$ ($1 – \alpha_{300} = 200$ µV/K, $2 – \alpha_{300} = 210$ µV/K, $3 – \alpha_{300} = 216$ µV/K) and b) for n-type $Bi_2Se_{0.15}Te_{2.85}$ ($1 – \alpha_{300} = –208$ µV/K, $2 – \alpha_{300} = –213$ µV/K, $3 – \alpha_{300} = –219$ µV/K).

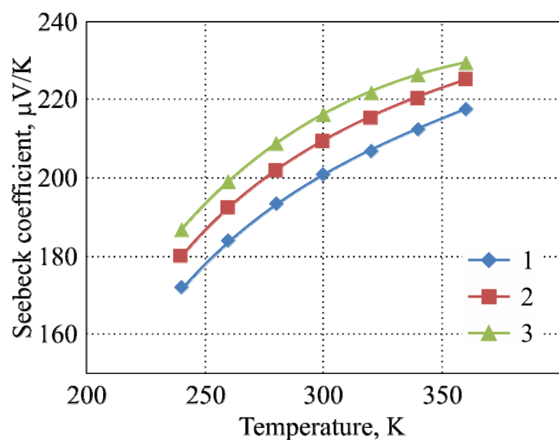

a)

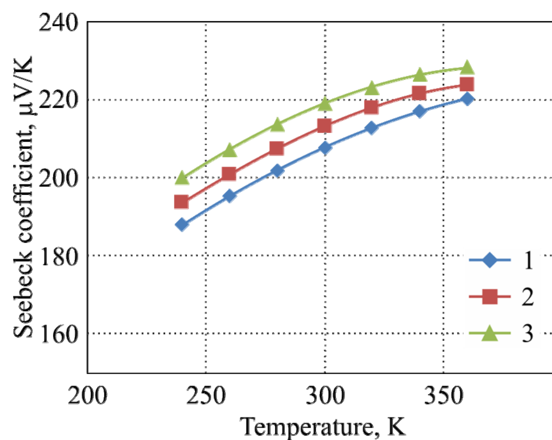

b)

Fig. 2. Temperature dependences of Seebeck coefficient a) for p-type $Bi_{0.4}Sb_{1.6}Te_3$ and b) for n-type $Bi_2Se_{0.15}Te_{2.85}$. The designations are the same as in Fig. 1.

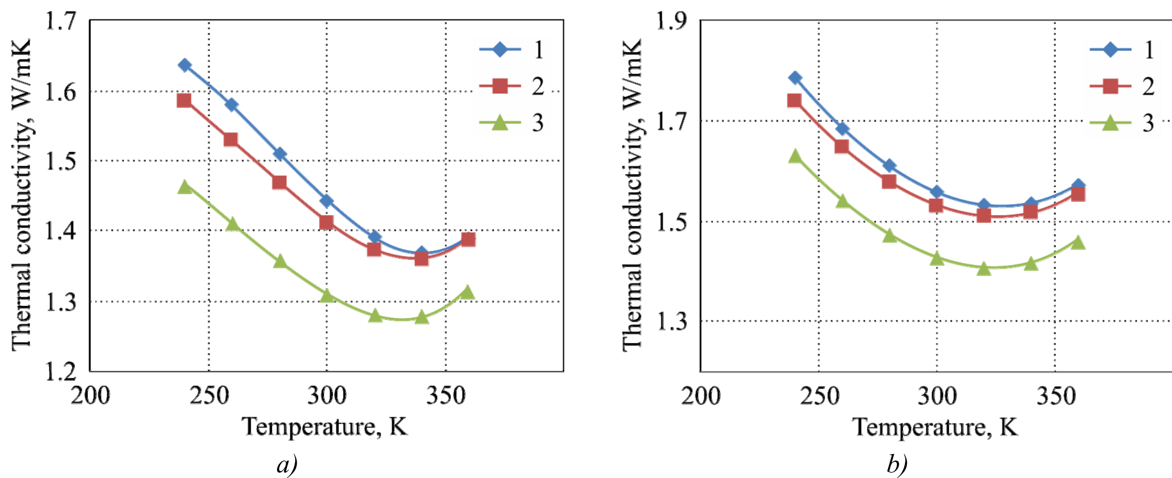

Fig. 3. Temperature dependences of thermal conductivity a) for $Bi_{0.4}Sb_{1.6}Te_3$ of p-type and b) for $Bi_2Se_{0.15}Te_{2.85}$ of n-type. The designations are the same as in Fig. 1.

The temperature dependences of the thermoelectric figure of merit are given in Fig. 4.

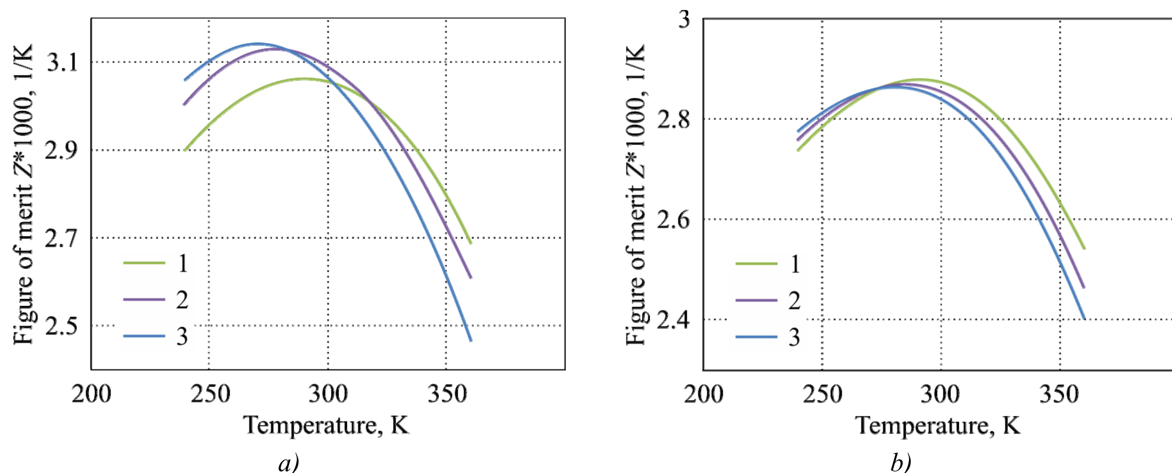

Fig. 4. Temperature dependences of thermoelectric figure of merit Z a) for p-type $Bi_{0.4}Sb_{1.6}Te_3$ and b) for n-type $Bi_2Se_{0.15}Te_{2.85}$. The designations are the same as in Fig. 1.

For the investigated samples the thermoelectric figure of merit at 300 K was $(3.05 - 3.13)\cdot10^{-3}$ K^{-1} for *p*-type and $(2.83 - 2.87)\cdot10^{-3}$ K^{-1} for *n*-type. These values are slightly below for *p*-type than published in the literature [6, 7], which may be due to a low elongation ratio (≈ 10) in extrusion tool employed. From the figure it is seen that at 300 K in *n*-type material the figure of merit grows with increase of Seebeck coefficient, and in *p*-type material it first grows and then drops. The average values of thermoelement figure of merit lie within $(2.95 - 2.98)\cdot10^{-3}$ K^{-1}.

It should be noted that we had in our possession the samples prepared by other manufacturers. According to the results of our measurements, their thermoelectric figure of merit did not exceed that obtained on our samples.

In the Harman measurements, contact resistance proves to be included into measured leg resistance. One would think that this automatically solves the problem of account of contact resistance in thermoelectric processes. For temperature-independent thermoelectric parameters such is indeed the case, but actually the situation is more complicated. The point is that temperature field inside the leg is

determined, among other things, by the Joule heat released inside the leg. And it is related to the temperature dependence of material resistivity without regard to contact resistance. Contact resistance becomes apparent only during the processes of heat release on the ends of the leg. Therefore, when measuring by the Harman method, to single out the electric conductivity of material, one should first determine contact resistance.

Contact resistance is most evidently manifested in the leg height dependence of $\Delta T_{\max}$. It is convenient to estimate contact resistance ρ_c by the variation of maximum temperature difference for modules with the different height of legs. If with a change of leg height from l to l' maximum temperature difference varies from $\Delta T_{\max}$ to $\Delta T'_{\max}$, then in the approximation of temperature-independent thermoelectric parameters

$$\rho_c = \frac{\rho}{2}\frac{A}{(\frac{1}{l}-\frac{1}{l'})-\frac{1}{l'}A}, \tag{1}$$

where ρ is material resistivity and

$$A = \frac{\left(\Delta T'_{\max} - \Delta T_{\max}\right)\left(T + \Delta T_{\max}\right)}{\left(T - \Delta T_{\max}\right)\Delta T_{\max}}. \tag{2}$$

From the data for modules of company RMT contact resistance is equal to $2 - 2.5 \cdot 10^{-6}$ $\Omega \cdot$cm^2. Material electric conductivity σ_m in this case is found from electric conductivity σ_H, measured by the Harman method by means of relation

$$\sigma_m = \frac{\sigma_H}{1-\frac{2\rho_c}{l}\sigma_H}, \tag{3}$$

where l is the height of leg measured by the Harman method. Because of contact resistance, the data on electric conductivity given in Fig. 1 are underrated by 3 – 5 %. The data on the thermoelectric figure of merit are underrated respectively.

Characteristics of thermoelectric modules

Maximum temperature difference on a thermoelement will correspond to its maximum figure of merit Z_{th}. In the approximation of temperature-independent thermoelectric parameters for thermo-element legs having identical section, a condition for matching of couples for reaching maximum Z_{th} is given by the ratio [8]:

$$\sigma_n \kappa_n = \sigma_p \kappa_p. \tag{4}$$

To compare the type of dependences of electric conductivity of n- and p-type materials, Fig. 5 shows dependences of electric conductivity at 300 and 320 K on the absolute value of Seebeck coefficient at 300 K.

From the above data it is seen that the curves for n-type materials are located somewhat higher than the respective curves for p-type materials. That is, n-type materials have higher specific power than p-type materials. Thermal conductivity of n-type materials is even somewhat higher than thermal conductivity of p-type materials with the identical values of Seebeck coefficient. And in n-type materials the relative excess of thermal conductivity proves to be higher than the relative excess of

electric conductivity, as a result of which the thermoelectric figure of merit for *n*-type material proves lower than thermoelectric figure of merit of *p*-type material. But on the whole, to satisfy equation (4), it is necessary that a thermoelement be formed by materials with close absolute values of Seebeck coefficient.

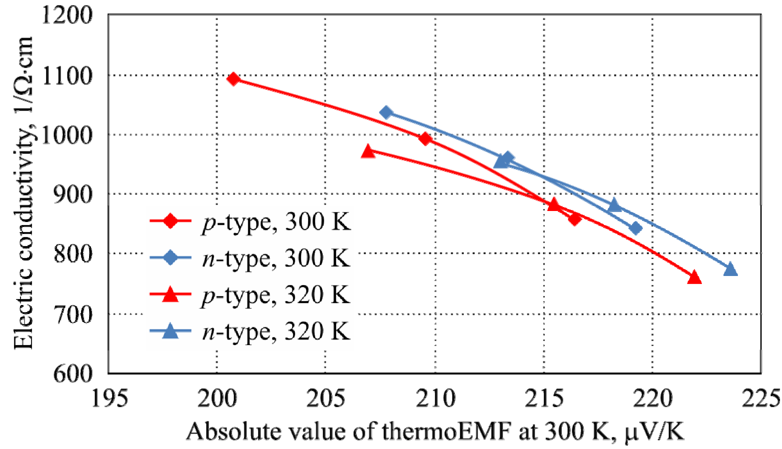

Fig. 5. Dependences of electric conductivity on the absolute value of thermoEMF at 300 K.

However, the temperature dependences of thermoelectric parameters can seriously disturb the validity of (4). Account of temperature dependences can be taken most consecutively by optimal control methods [9]. However, with such a calculation it is difficult to trace a connection to thermal balance equations used with temperature-independent thermoelectric parameters. Therefore, in the calculation we used a model of effective values of thermoelectric parameters [10] that allows keeping the form of thermal balance equation which on the cold end with a zero thermal flow to the cold end of the leg is of the form:

$$\alpha_{c\,eff\,t} T_c I - \frac{1}{2} I^2 R_{c\,eff\,t} - K_{eff\,t} = 0, \tag{5}$$

where T_c is temperature of the cold end of the leg, I is current through the leg, and

$$K_{eff\,t} = \bar{K} = \frac{s}{\int_0^L \frac{dx}{\kappa(T_x)}}, \quad t = n, p, \tag{6}$$

where L is leg length, and s is cross-sectional area of t type conductivity leg.

$$R_{c.eff\,t} = \frac{2\bar{K}}{s^2} \int_0^L \rho(T_y) dy \int_y^L \frac{dx}{\kappa(T_x)}, \quad t = n, p. \tag{7}$$

$$\alpha_{c.eff\,t} = \alpha(T_C) + \frac{\bar{K}}{sT_c} \int_0^L T_y \frac{d\alpha(T_y)}{dT} \frac{dT}{dy} dy \int_y^L \frac{dx}{\kappa(T_x)}, t = n, p. \tag{8}$$

T_x, T_y is function of temperature distribution along a thermoelement leg. The results of calculation by methods [9] and [10] were compared in [11] and shown to be identical. In order to use formulae (4) – (9), it is necessary to know temperature distribution along the legs. For this purpose, one should first solve thermal conductivity equation, being given by certain initial boundary conditions, and then, using successive approximations method, find at given hot end temperature of leg T_h minimum achievable temperature T_c.

The results of calculation are given in Table 1.

Table 1

Results of calculation of $\Delta T_{\max}$ for different combinations of n- and p-type couples at the hot end temperature of thermoelement T_h = 300 K

α_p at 300 K / α_n at 300 K	200 μV/K	210 μV/K	216 μV/K
	$\Delta T_{\max}$, K		
−208 μV/K	73.6(72.39)	74.5	74.6
−213 μV/K	73.7	74.6(74.27)	74.9
−219 μV/K	73.5	74.6	75.2(74.35)

It is seen that the difference in $\Delta T_{\max}$ achieves two degrees, whereas, based on the average value of thermoelement efficiency, it should not exceed 0.3 K. Condition (4) for matching of the electrical properties of legs with account of temperature dependences takes on the form:

$$\sigma_{ceff\,n}\kappa_{ceff\,n} = \sigma_{ceff\,p}\kappa_{ceff\,p}, \tag{9}$$

where the respective values of electric conductivity and thermal conductivity are found from (6) and (7). Table 2 lists the calculated values of legs mismatch parameter δ

$$\delta = \frac{\sigma_{ceff\,n}\kappa_{ceff\,n}}{\sigma_{ceff\,p}\kappa_{ceff\,p}} - 1. \tag{10}$$

Table 2

Results of calculation of legs mismatch parameter δ for different combinations of n- and p-type couples

α_p at 300 K / α_n at 300 K	200 μV/K	210 μV/K	216 μV/K
	δ, %		
–208 μV/K	–6.3	7.0	37
–213 μV/K	–16.1	–4.1	22.7
–219 μV/K	–32.6	–23.4	–1.5

From the table it is evident that an ideally matched couple includes materials with α_n = –219 μV/K and α_p = 216 μV/K, yielding the highest value of $\Delta T_{\max}$ according to Table 1. The diagonal elements of the table are best matched. In so doing, the absolute value of Seebeck coefficient of *n*-type is several units higher than Seebeck coefficient of *p*-type. The data in Table 1 agree with these results. Thus, criterion of proximity of the absolute values of Seebeck coefficient for a couple of thermo-element legs is sufficiently valid and convenient for practical use.

Experimental verification of the compatibility of thermoelement leg couples was done by direct measurement of $\Delta T_{\max}$ for modules specially assembled of legs with different properties. The measured results are also given in Table 1 in brackets. Comparison of the experimental and calculated data shows sufficiently good agreement of the results. And the calculation correctly reflects the experimentally observed tendency to $\Delta T_{\max}$ increase with growth of the absolute values of Seebeck coefficient.

Conclusions

The temperature dependences of thermoelectric parameters of extruded thermoelectric materials mass-produced by company RMT (Russia) have been measured by the Harman method. The thermoelectric figure of merit at 300 K was $(3.05 – 3.13)\cdot10^{-3}$ K^{-1} for *p*-type and $(2.83 – 2.87)\cdot10^{-3}$ K^{-1} for *n*-type. Unlike crystalline materials based on bismuth and antimony chalkogenides, the thermoelectric properties of *n*- and *p*-type extruded materials vary notably. Consideration of matching in thermoelement of legs of such materials shows that similarity of absolute Seebeck coefficient values at room temperature for a couple of thermoelement legs is sufficiently good and convenient condition for practical application.

References

1. L.D. Ivanova, Yu.V. Granatkina, and Yu.A. Sidorov, Electrophysical Properties of Antimony Telluride Single Crystals Doped with Selenium and Bismuth, *Inorganic Materials* **1**, 44 – 52 (1999).
2. V.A. Kutasov et al., Anisotropy of Properties of $Bi_2Te_{3-x}Se_x$ Single Crystals, *Physics of the Solid State* **29**(10), 3008 – 3011 (1987).
3. V.N. Abrutin, I.A. Drabkin, and L.B. Ershova, Curl Currents Occurrence in Homogeneous Isotropic Thermoelectric Elements, *Proc. of 5th European Conference on Thermoelectrics* (Odessa, September 10-12, 2007), pp. 163 – 165.
4. T.C. Harman, J.M. Honig, Special Techniques for Measurement of Thermoelectric Properties, *J. Appl. Physics* **29**, 1373 – 1375 (1959).
5. V. Abrutin, I. Drabkin, and V. Osvenski, Corrections Used when Measuring Materials Thermoelectric Properties by Harman Method, *Proc. of 2nd European Conference on Thermoelectrics* (Krakov, September 15-17, 2004).
6. D. Vasilevsky, N. Kukhar, S. Turenne, and R.A. Masur, Hot Extruded $(Bi, Sb)_2(Te, Se)_3$ Alloys for Advanced Thermoelectric Modules, *Proc. of 5th European Conference on Thermoelectrics* (Odessa, September 10-12, 2007), pp. 64 – 67.
7. L.D. Ivanova, L.I. Petrova, and Yu.V. Granatkina, Extruded Materials of Solid Solutions of Bismuth and Antimony Chalcogenides, *Thermoelectrics and Their Applications* (Saint-Petersburg, 2008), pp. 246 – 251.
8. *Thermoelectric Coolers*, Ed. by A.L. Vainer (Moscow: Radio and Sviaz, 1983), 173 p.
9. L.I. Anatychuk, V.A. Semenyuk, *Optimal Control over the Properties of Thermoelectric Materials and Devices* (Chernivtsi: Prut, 1992).
10. I.A. Drabkin, Z.M. Dashevsky, Basic Energy Relations for the Cooling Leg with Regard to Temperature Dependences of Thermoelectric Parameters, *Thermoelectrics and their Applications* (Saint-Petersburg, 2000), pp. 292 – 297.
11. I.A. Drabkin, L.B. Ershova, Comparison of Different Approaches to Optimization of Single-Stage Thermoelectric Modules, *Thermoelectrics and Their Applications* (Saint-Petersburg, 2006), pp. 378 – 390.

Submitted 04.06.2014.

L.I. Anatychuk, R.V. Kuz

L.I. Anatychuk

Institute of Thermoelectricity of the NAS and MES
Ukraine, 1, Nauky Str., Chernivtsi, 58029, Ukraine

R.V. Kuz

EFFECT OF AIR COOLING ON THE EFFICIENCY OF THERMOELECTRIC GENERATOR IN A DIESEL-ENGINED CAR

A model of a car with thermoelectric generator (TEG) was created with regard to the fact that TEG must assure power supply to heat removal system of its own. The results of optimization of the hot side temperature of TEG and the electric supply power of heat removal system are given. The effective efficiency and the electric power of TEG for a 75 kW diesel engine are calculated. The necessity of optimal design of TEG heat removal system is shown.

Key words: heat recovery, thermoelectric generator, internal combustion engines.

Introduction

The use of waste heat from the internal combustion engines is one of the critical tasks of thermoelectricity [1 – 6]. World producers of vehicles, as well as companies of thermoelectric profile, give much prominence to the development of efficient thermoelectric generators for vehicles. The purpose is to increase fuel saving due to the use of engine exhaust heat for electric energy generation.

The largest companies making it their mission to create industrial prototypes of generators and their large-scale production are Hi-Z [7], BSST [8] and General Motors [9] in the USA. In Japan, the problems of creating automotive generators are most widely addressed by companies Komatsu [10], Nissan [11] and Shiroki [12]. In Germany, company Volkswagen [13] and company BMW together with DLR (German Airspace Centre) represented their developments of thermoelectric automotive generators [13]. Nevertheless, it should be noted that the majority of the above works disregard the effect of thermoelectric generator itself on the operation of a vehicle. However, as is known, the presence of a thermoelectric generator has a considerable impact on the operation of a car due to at least three factors, namely additional hydraulic resistance in vehicle exhaust system, mechanical expenditures of engine on the transportation of additional mass of TEG proper and the expenditures related to the necessity of heat removal from thermoelectric generator. In [4-6] the efficiency of TEG with regard to transportation costs is discussed in detail. It is shown that for cars these costs can exceed the effective work of TEG. As regard heat removal, for the purpose of noninterference to automotive cooling system, heat removal from TEG should be done due to TEG own power.

The purpose of this work is to estimate the effective power and efficiency of an automotive thermoelectric generator with regard to provision of TEG heat removal.

Physical model of a car with thermoelectric generator

The work of thermoelectric generator as part of modern car can be represented by a schematic shown in Fig. 1.

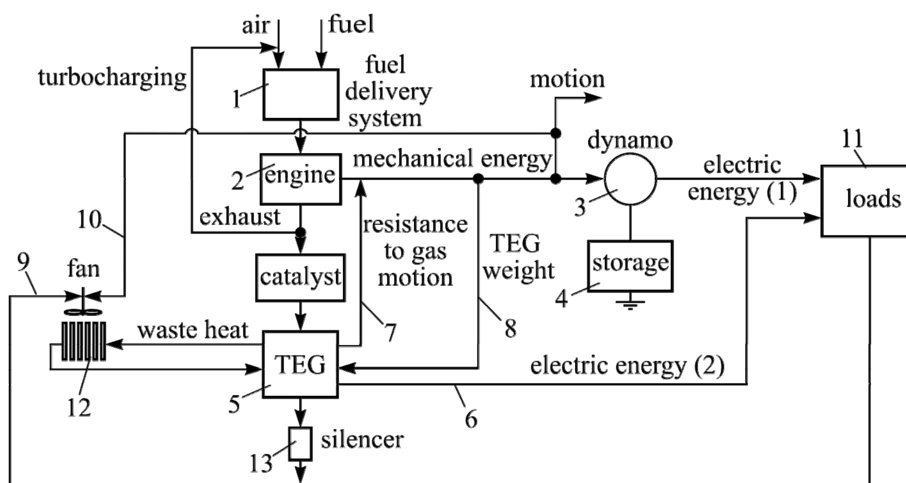

Fig. 1. Schematic of energy distribution in a car with TEG.

Fuel delivery system 1 feeds into engine 2 fuel mixture whose combustion provides for mechanical power of engine P. This power is spent on driving the car itself P_A and on the work of dynamo 3 that generates electric power W_D at efficiency η_D. The electric power is spent on the work of all car electric loads 11 and on charging storage 4.

The thermoelectric generator 5 will offer an additional advantage of generated electric power W_{TEG} 6. Additional expenditures will include: mechanical power P_{gas} 7 related to pressure increase in the exhaust system; mechanical power P_m 8 related to car weight increase due to TEG; electric 9 (or mechanical 10) power P_c necessary for provision of TEG cooling system operation.

Thus, the energy balance in a car without TEG is of the form:

$$P = P_A + W_D / \eta_D. \tag{1}$$

The energy balance in a car with thermoelectric generator is given below

$$P + W_{TEG} / \eta_{TEG} = P_A + W_D / \eta_D + P_c + P_m + P_{gas}, \tag{2}$$

where η_{TEG} is thermoelectric generator efficiency, P_c is mechanical power spent on provision of TEG cooling system operation, P_m is mechanical power spent on the transportation of TEG, P_{gas} is mechanical power spent on overcoming additional pressure in exhaust system due to the existence of TEG.

Let us consider a simplified model of a car with TEG with regard to provision of heat removal from TEG (Fig. 2) that will enable us to reveal in general terms the basic features of heat removal from TEG.

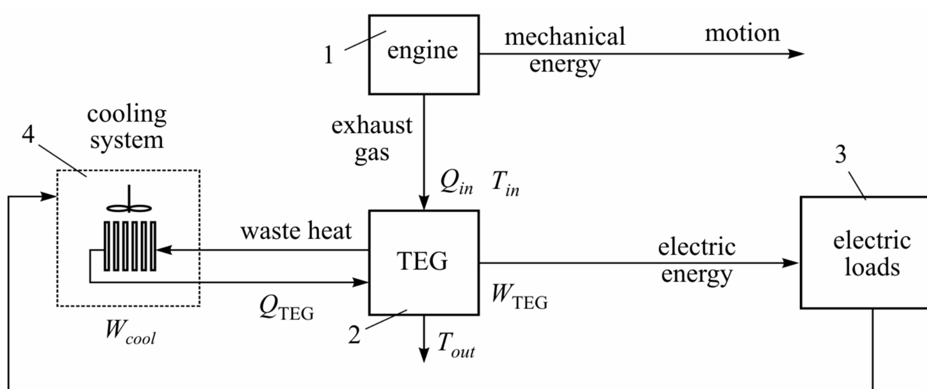

Fig. 2. A simplified model of a car with TEG.

Exhaust gas of thermal power Q_{in} from engine 1 comes to thermoelectric generator 2 of thermal resistance R_t at temperature T_{in} and leaves the generator at temperature T_{out}. The TEG generates electric energy W_{TEG} at efficiency η_{TEG}. A case is considered when part of this electric energy W_{cool} is spent on the operation of cooling system 4 which removes thermal power Q_{TEG} from the TEG. The ambient temperature is T_{amb}. The problem thus stated brings into existence two values that should be optimized, namely the hot side temperature of TEG and the power spent on the operation of cooling system.

The model is concerned with a one-sectional TEG and ignores the effect of other vehicle systems on the engine performance.

Mathematical description of thermoelectric generator operation

Equation for finding the optimal hot side temperature of TEG will be found from the heat balance in TEG:

$$Q_{in} = Q_{out} + Q_{TEG}, \tag{3}$$

$$Q_{in} = cm\left(T_{in} - T_{amb}\right), \tag{4}$$

$$Q_{out} = cm\left(T_{out} - T_{amb}\right), \tag{5}$$

$$Q_{TEG} = \frac{T_{out} - T_0}{R_t}, \tag{6}$$

where c is exhaust gas heat capacity, m is exhaust gas mass flow rate, T_0 is the cold side temperature of TEG.

Substituting (4) – (6) into (3), we obtain an equation for finding the hot side temperature of TEG:

$$T_{out}\left(R_t\right) = \frac{Q_{in}\left(1 + \dfrac{T_{amb}}{T_{in} - T_{amb}}\right) + \dfrac{T_0}{R_t}}{\dfrac{1}{R_t} + \dfrac{Q_{in}}{T_{in} - T_{amb}}}\ . \tag{7}$$

TEG efficiency will be calculated by the formula

$$\eta_{TEG}(R_t) = \frac{T_{out} - T_0}{T_{out}} \frac{M - 1}{M + T_0 / \mathrm{T}_{out}}\ , \tag{8}$$

$$M = \sqrt{1 + Z\frac{(T_{out} + T_0)}{2}}, \tag{9}$$

The effective efficiency of TEG was found as follows:

$$\eta_{ef} = \frac{W_{TEG} - W_{cool}}{Q_{TEG}}. \tag{10}$$

The temperature dependence of figure of merit Z in formula (9) was taken into account by using the average integral value in the temperature range (T_0, T_{out}).

To calculate the electric power of TEG with account of heat removal system operation, it is necessary to know the efficiency of air-to-liquid heat exchanger obtained from the experimental studies of heat exchanger:

$$Q_{cool} = f(W_{cool}, T_H, T_C), \tag{11}$$

where Q_{cool} is thermal power of heat exchange system, W_{cool} is electric supply power of heat exchange system, T_H is liquid temperature, T_C is air temperature.

Optimization algorithm was realized in MathCAD mathematical simulation system [14].

TEG parameters calculation example

As an example, we shall calculate the basic parameters of TEG for a 75 kW diesel in continuous operation mode at a car speed 100 km/h. In this operation mode, the exhaust gas temperature is about 420 °C.

Thermoelectric materials. Calculation of TEG efficiency and power was made with the use of a typical temperature dependence of *ZT* [15] of *Bi-Te* based materials which is given in Fig. 3.

Air-to-liquid heat exchanger. The empirical dependence (11) characterizing the work of heat exchange system was found experimentally according to the following schematic (Fig. 4).

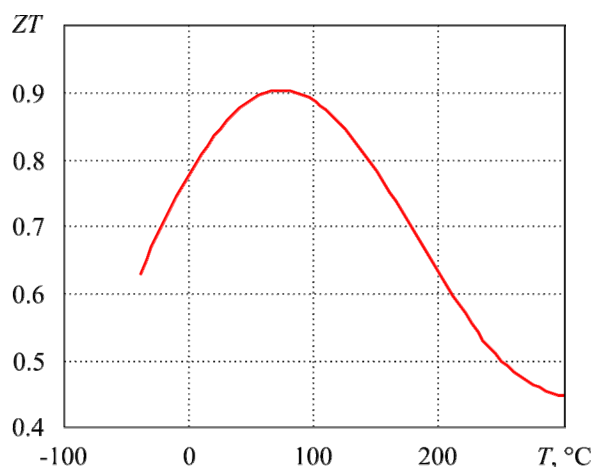

Fig. 3. Temperature dependence of ZT for Bi-Te based materials.

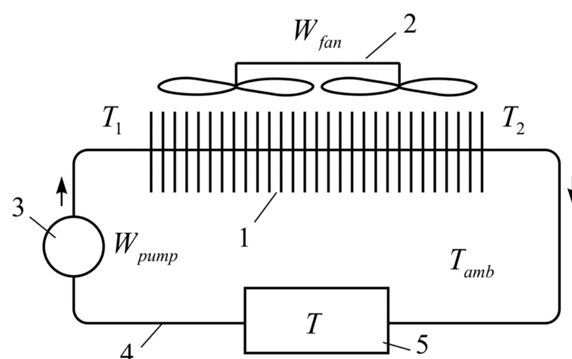

Fig. 4. Schematic of cooling system study: 1 – air-to-liquid heat exchanger, 2 – fan unit, 3 – electric liquid pump, 4 – liquid circuit, 5 – liquid thermostat.

Liquid thermostat 5 was used to create temperature difference between the liquid and the environment. Pump 3 pumped the liquid through heat exchanger 1 blown over by fan unit 2. The difference in temperatures T_1 and T_2 was used to determine power Q removed by the heat exchanger depending on liquid temperature T, supply power of fan unit W_{fan} and supply power of pump W_{pump}.

The results of experimental study of heat removal system are given in Fig. 5.

A series of such dependences of heat exchanger thermal power for different supply powers of fans and pump was polynomial approximated and used in optimization algorithm.

As a rule, the efficiency of fans, just as the efficiency of pumps, is not very high (50 – 65 %). So, the use of direct cooling from the incoming flow can assure a smaller expenditure of engine energy on cooling system (by a factor of ~2 – 2.5). Many works predict the use of liquid heat exchangers (radiators) existing in vehicles for cooling of thermal generator. However, in this case it should be noted that such heat exchangers are designed for provision of heat removal from the engines under the most complicated conditions, namely high temperature of incoming air flow, low motion speeds, extreme powers. Under such conditions, the existing radiators can be unable to remove heat from thermal generator without disturbance of engine thermal conditions. Therefore, it may be necessary to use special heavy-duty radiators that will assure heat removal from thermal generator, or to use an

additional heat exchanger for heat removal from TEG. In so doing, it should be expected that the use of electric fans for the operation of heat removal system makes this operation mode more flexible and can assure minimum electric energy consumption.

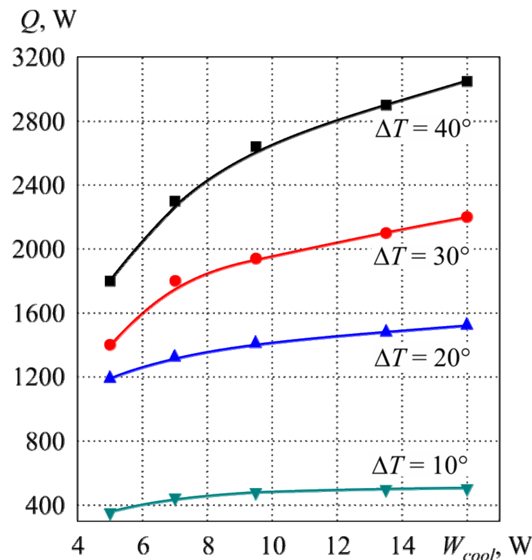

Fig. 5. Dependences of heat removal power of air-to-liquid heat exchanger on the supply power of fans. Pump power is 2 W.

Heat removal system optimization. In the beginning, optimization of the hot side temperature of TEG took place. The results of this optimization are shown in Figs. 6 – 7. As is obvious, there exists TEG power optimum which is due to the effect of two competing factors. With a reduction of TEG thermal resistance, the thermal power passing through the generator is increased. At the same time, the hot side temperature of TEG is reduced.

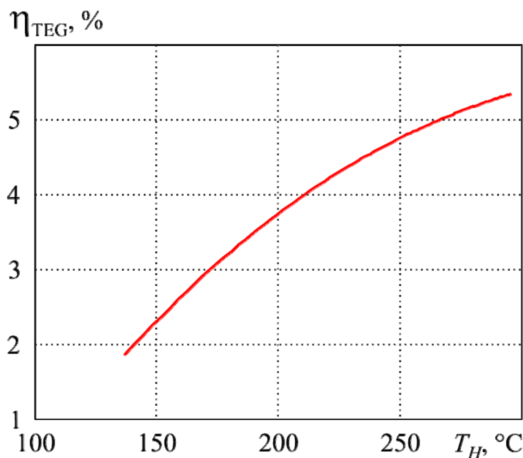

Fig. 6. Dependence of TEG efficiency on the hot side temperature of TEG. T_c = 90 °C.

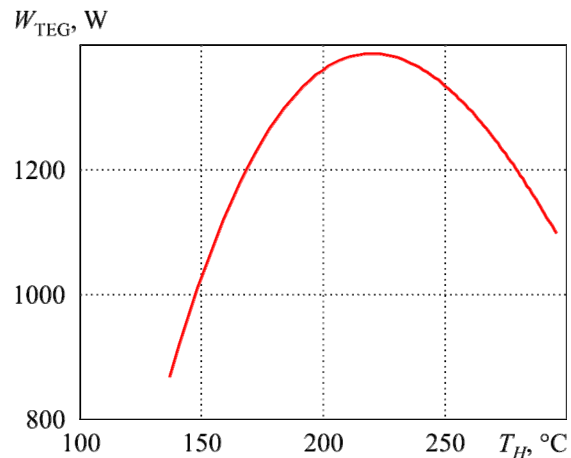

Fig. 7. Dependence of TEG electric power on the hot side temperature of TEG. T_c = 90 °C.

Calculation of the effective efficiency and power of TEG with regard to expenditures on heat removal was performed according to Eqs. (6 – 8).

Figs. 8 – 9 show the results of optimization of heat removal system. The effective efficiency and electric power of TEG were calculated with consideration that part of TEG power is removed to provide for the operation of TEG heat removal system. From the plots it is evident that there exist pronounced optimal operating conditions of heat removal system. From Fig. 8 it is seen that with a reduction of

ambient temperature, the efficiency of TEG increases from ~3.8 % at a temperature of +50 °C to ~ 7.2 % at a temperature of –40 °C. It corresponds to the extreme values of TEG electric power 1.2 kW and 3.1 kW, respectively. From Fig. 9 it is seen that TEG yields additional 1.5 – 4 % of engine power in the form of electric energy. With regard to dynamo efficiency, it will correspond to 2 – 6 % of fuel saving.

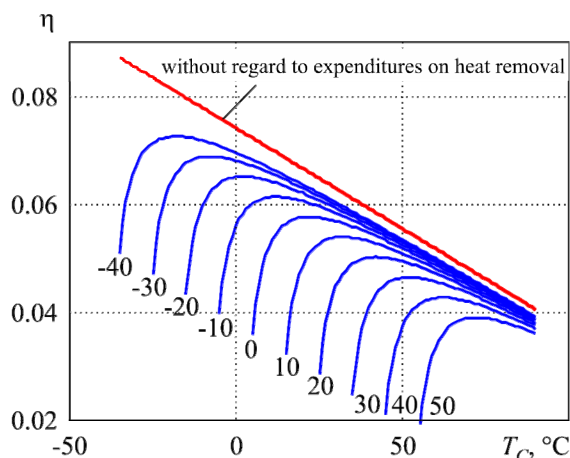

Fig. 8. Dependence of TEG effective efficiency on the cold side temperature of TEG. Ambient temperature is indicated beside the plots.

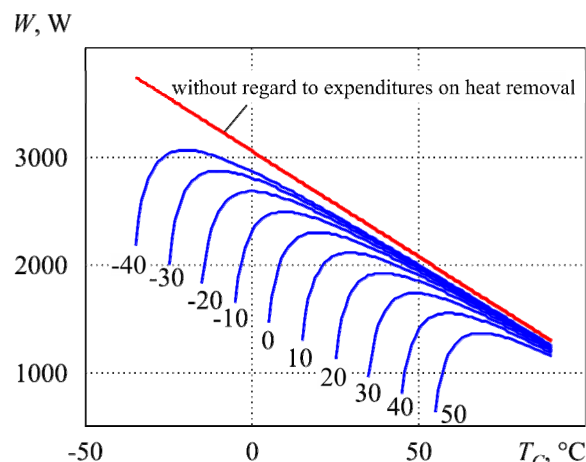

Fig. 9. Dependence of TEG effective electric power on the cold side temperature of TEG. Ambient temperature is indicated beside the plots.

Table 1 lists the data on the optimal values of TEG efficiency and power, as well as thermal power that must be removed from TEG and expenditures on cooling system operation. As can be seen, with a rise in ambient temperature, the optimal effective efficiency and power decrease, and expenditures on cooling system operation increase from ~ 15 % to ~ 25 % with the use of electric fans. If the fans are driven by engine mechanical energy, then with regard to average electric fan efficiency, expenditures on cooling system operation will make 6 – 12 %.

Table 1

Basic characteristics of TEG with heat removal system

Ambient temperature, °C	Thermal power that must be removed from TEG, kW	TEG power, kW	Electric power of heat removal system, kW	Electric expenditures on heat removal operation, %	Effective efficiency of TEG, %
-40	42.7	3.12	0.477	15.4	7.25
-30	41.1	2.84	0.462	16.5	6.80
-20	40.0	2.61	0.457	17.4	6.53
-10	38.0	2.32	0.432	18.7	6.05
0	36.5	2.15	0.422	20.1	5.75
10	33.9	1.82	0.365	20.4	5.30
20	32.0	1.60	0.337	21.1	5.05
30	31.4	1.41	0.315	22.5	4.61
40	31.5	1.32	0.304	23.4	4.25
50	31.5	1.21	0.297	24.8	3.82

Let us consider what changes can take place in TEG efficiency versus the car location.

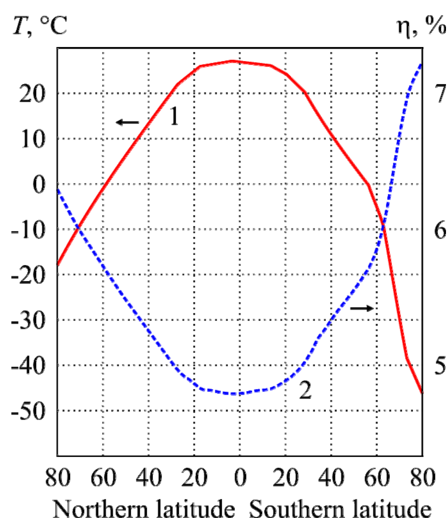

Fig. 10. Dependences of average annual temperature and TEF efficiency on the latitude.

Fig. 10 shows the average annual temperature on the planet (curve 1) depending on the latitude. Another scale shows the latitude dependence of thermoelectric generator efficiency (curve 2) [16].

Conclusions

1. Arrangement of heat removal from an automotive thermal generator is an important factor of its performance deficiency that should be taken into account in the design of such TEG. Thus, for a 75 kW diesel engine the expenditures on heat removal from a one-sectional TEG by heat exchangers with electric fans can reach 15 – 25 % of electric energy generated by TEG, or approximately 6 – 12 % of TEG power in the form of engine mechanical energy which is about 0.1 – 0.4 % of its power.
2. The efficiency of heat removal from an automotive TEG has optimal values that are a function of ambient air temperature. For a diesel engine, with a reduction of ambient air temperature, the efficiency of TEG increases from ~ 3.8 % at a temperature of + 50 °C to ~ 7.2 % at a temperature of – 40 °C, which corresponds to TEG electric power values 1.2 kW and 3.1 kW. So, car operation with TEG is more efficient in climatic zones with reduced air temperatures.
3. The use of TEG with account of expenditures on heat removal from it yields additional 1.5 – 4 % of engine power in the form of electric energy, which, respectively, can effect fuel saving about 2 – 6 % at a car speed 100 km/h.

References

1. L.I. Anatychuk, Yu.Yu. Rozver, K. Misawa, and N. Suzuki, Thermal Generators for Waste Heat Utilization, *Proc. of 16th International Conference on Thermoelectrics* (Dresden, 1997), p. 586 – 587.
2. L.I. Anatychuk, R.V. Kuz, Yu.Yu. Rozver, Efficiency of thermoelectric recuperators of the exhaust gas energy of internal combustion engines, *J. Thermoelectricity* **4**, 80 – 85 (2011).
3. L.I. Anatychuk, R.V. Kuz, Yu.Yu. Rozver, Thermoelectric generator for a petrol engine, *J. Thermoelectricity* **2**, 97 – 104 (2012).
4. G. Min, D.M. Rowe, Conversion Efficiency of Thermoelectric Combustion Systems, *IEEE Transactions on Energy Conversion* 22, 528 – 534 (2007).
5. K.M. Sacr, M.K. Mansour, and M.N. Mussa, Thermal Design of Automobile Exhaust Based on Thermoelectric Generators: Objectives and Challenges, *J. Thermoelectricity* 1, 64 – 73 (2008).

6. X. Zhang, K.T. Chau, and C.C. Chan, Overview of Thermoelectric Generation for Hybrid Vehicles, *J. Asian Electric Vehicles* **6** (2), 1119 – 1124 (2008).
7. N. Elsner, J. Bass, S. Ghamaty, D. Krommenhoek, A. Kushch, and D. Snowden, Diesel Truck Thermoelectric Generator, *Advanced Combustion Engine Technologies, FY 2005 Progress Report*, p. 301 – 305.
8. D. Crane, L. Bell, Progress Towards Maximizing the Performance of a Thermoelectric Power Generator, *Proc. ICT '06, 25th International Conference on Thermoelectrics* (Vienna, Austria), p. 11 – 16.
9. Jihui Yang, F. Seker, R. Venkatasubramanian, G.S. Nolas, C. Uher, and H. Wang, Developing Thermoelectric Technology for Automotive Waste Heat Recovery, *Advanced Combustion Engine Technologies, FY 2006 Progress Report*, p. 227 – 231.
10. T. Kajikawa, Current state of thermoelectric power generation technology in Japan, *J. Thermoelectricity* **2**, 21 – 31 (2007).
11. K. Ikoma, M. Munekiyo, K. Furuya, M. Kobayashi, T. Izumi, and K. Shinohara, Thermoelectric Module and Generator for Gasoline Engine Vehicles, *Proc. ICT'98. XVII International Conference on Thermoelectrics* (Nagoya, Japan, 1998), p. 464 – 467.
12. E. Takanose, H. Tamakoshi, The Development of Thermoelectric Generator for Passenger Car, *Proc. 12th International Conference on Thermoelectrics* (Yokohama, Japan, 1993), p. 467 – 470.
13. *Thermoelektrik-Eine Chance Fur Die Atomobillindustrie* (Berlin, 2008).
14. PTC Mathcad – Engineering Calculations Software. www.ptc.com.
15. L.I. Anatychuk, R.V. Kuz, Materials for Vehicular Thermoelectric Generators, *Proc. of ICT-2011* (Michigan, USA).
16. S.P. Khromov, L.I. Mamontova, *Meteorological Dictionary* (Leningrad: Gidrometeoizdat, 1974).

Submitted 12.06.2014.

Yu.M. Lobunets

Yu.M. Lobunets

Institute of Thermoelectricity of the NAS and MES Ukraine,
1, Nauky Str., Chernivtsi, 58029, Ukraine

CRITERIA FOR PERFORMANCE EVALUATION OF THERMOELECTRIC ENERGY CONVERTERS

Performance analysis problems for thermoelectric energy converters are considered on the base of system approach. Methods to construct the limiting opportunities sets for thermoelectric generators and heat pumps under various restrictions are outlined.
Key words: thermoelectric energy converter, system analysis.

Introduction

The literature on the methods of performance evaluation and comparison of thermoelectric energy converters (TEC) is quite extensive [1-8]. The absolute majority of the existing methods are based on the analysis of extreme modes of TEC under various assumptions. However, such analysis gives no sufficient information for making decisions on the choice of real device parameters, since it does not take into account a relationship between technical and economic characteristics in an explicit form. Moreover, technical criteria of TEC efficiency are often competing, i.e. improvement of one of them with a change in the vector of controlling parameters results in the degradation of another. The uncertainty of optimization purposes is also due to the fact that by virtue of specific features of energy conversion system, any real technical task can be implemented in the infinitely large set of variants differing in specific characteristics and project cost.

The task of optimal design is to assure a choice of this set of variants leading to the achievement of the target goal with minimum expenditures. For solving this task a TEC should be considered as a system consisting of thermoelectric circuit, heat source and sink. Having mathematical models of these units and their interaction conditions, one can formulate target function defining the efficiency of device as a whole and find an optimal solution. In some cases for these purposes one employs the empirical dependences which describe the defining parameters of units with a subsequent numerical solution of optimization problem [9]. Understandably, such approach is acceptable only for solving a narrow class of problems, since it is related to obtaining a large volume of experimental data.

The methods of system analysis are successfully used for solving similar problems in a general form [10, 11]. The essence of the method lies in constructing a set of possible solutions (a set of limiting opportunities) of the problem in a space of defining criteria. Analysis of such sets gives an idea of the basic system properties, the character of interaction between units, allows revealing in this space a set of efficient solutions (Pareto set) of the problem restricting the space of optimal solutions of multi-criteria problem. Problem solutions obtained in the generalized variables are universal, since they cover all possible combinations of primary independent variables and allow evaluating possible performance of TEC at early stages of design.

Generalized variables and TEC efficiency criteria

A mathematical model of TEC in the general form has rather high dimensionality, since it comprises considerable amount of independent variables having wide variation intervals. It is quite difficult to trace the relation between all affecting factors and generalize this data in a space of natural physical variables. Problem dimensionality can be reduced considerably and brought to a generalized form through use of similarity theory methods [12].

In [7] it was shown that the problem of thermoelectric energy conversion can be reduced to a small-size system of generalized variables having clear physical meaning and normalized variation intervals:

$$N = f(I_{o}, \Theta, J, Ki, Bi). \tag{1}$$

Here, $N = Nh/\lambda T_p$ is dimensionless power of thermoelement; $I_o = zT_p$ is the Ioffe criterion characterizing thermoelectric material properties. Dimensionless temperature of thermoelements $\Theta = T/T_p$ is a definable parameter used to calculate the energy characteristics of TEC. Dimensionless current $J = jeh/\lambda$, the Kirpichev criterion $Ki = qh/\lambda T_p$ and the Biot criterion $Bi = \alpha h/\lambda$ characterize duty parameters defining the state of the system.

Special attention should be given to a choice of problem defining temperature T_p which assigns the temperature scale. As a defining temperature for thermoelectric generator (TEG) use is made of maximum acceptable device operating temperature $T_p = T_{\max}$; as a defining temperature for thermoelectric heat pump (THP) the heat sink temperature $T_p = t_o$ is assumed. Such choice of scale restricts the range of possible temperatures to the values of $\Theta \leq 1$.

The examined criteria have a clear physical meaning. The Ioffe criterion characterizes the limiting opportunities of TEC. It can be shown that in TEG mode full dimensionless power of thermoelement in short circuit mode $N_o = I_o\Delta\Theta^2$. That is, the Ioffe criterion characterizes the power of thermoelement of single dimensions with a unit step temperature (at $\Delta\Theta = 1$ $I_o = N_o$). The following relations hold for an idealized schematic of TE heat pump: $J_{opt} = I_o$ and $Ki_{\max} = 0.5I_o$, i.e. the Ioffe criterion characterizes extreme modes of THP (J_{opt} is dimensionless current density assuring the mode of maximum cooling capacity of THP). Taking into account that $qh/\lambda = \Delta T$, the Kirpichev criterion $Ki = \Delta T/T_p$ can be treated as the Carnot efficiency in the temperature range considered. Dimensionless current density is the ratio between maximum possible values of the Peltier heat ($Q_p = jeT_p$) and the flux of net thermal conductivity ($Q_\lambda = \lambda/hT_p$), i.e. $J = Q_p/Q_\lambda$. The Biot criterion is known to represent the ratio between thermal resistances of thermal conductivity $R_\lambda = h/\lambda$ and heat transfer $R_\alpha = 1/\alpha$. In their physical meaning criteria *Ki, J* and *Bi* represent a generalized description of the main system units, namely heat source, thermoelectric converter and heat sink. Having optimal solutions in generalized variables, one can always transfer their results to a concrete project, having received a description of generalized criteria as a function of primary data for each of the system units.

Idealized model of TEC

The relation between TEC characteristics and duty parameters is traced most obviously in the idealized mathematical model of thermoelement which comes down to one-dimensional problem of thermal conductivity under the first-kind boundary conditions [7]:

$$\frac{\partial^2\Theta}{\partial Y^2} + \frac{J^2}{I_o} = 0, \tag{2}$$

$$\begin{cases}\Theta(0)=\Theta_o;\\ \Theta(1)=\Theta_h;\end{cases} \tag{3}$$

Solution of equation (2) is of the form:

$$\Theta(Y)=C_1+C_2Y-\frac{J^2}{2I_o}Y^2, \tag{4}$$

where $C_1 = \Theta_o$; $C_2=\Theta_h-\Theta_o+\frac{J^2}{2I_o}$; $Y = y/h$ is dimensionless coordinate.

In such formulation it is supposed that on the heat-releasing thermoelement junction there is an ideal heat exchange ($Bi_h \to \infty$), and heat flux on the heat-absorbing junction Ki corresponding to the assigned conditions can be found from the heat balance:

$$Ki+Q_\lambda+Q_p=0. \tag{5}$$

Here, $Q_\lambda = -\Theta'(0)$ is thermal conductivity flux and $Q_p = J\Theta(0)$ is the Peltier heat. Hence, with regard to (4), we obtain the main relation for an ideal schematic of TEC:

$$Ki=J\Theta_o-\frac{J^2}{2I_o}-\Delta\Theta. \tag{6}$$

This expression includes two duty parameters Ki and J. In heat pump mode, parameter J is controlling, and Ki – controlled. In energy generator mode, on the contrary, device characteristics are defined by the density of heat flux Ki which is responsible for dimensionless current J.

Heat pump mode

From (6) it follows that dependence of heat flux on supply current for THP mode has the form of a square parabola, i.e. the range of problem definition is restricted by the range of currents at the ends of which cooling capacity goes to zero. The boundary conditions for J are determined as the roots of equation (6):

$$J_{1,2}=I_o\Theta_o\pm\sqrt{(I_o\Theta_o)^2-2I_o\Delta\Theta}; \tag{7}$$

From (7) it follows that the problem has physical meaning at $(\Theta_o^2 - 2I_o\Delta\Theta) \geqq 0$.

Maximum cooling capacity of thermoelement is achieved at current density

$$J_{opt}=I_o\Theta_o. \tag{8}$$

Thus,

$$Ki_{\max}=\frac{I_o\Theta_o^2}{2}+\Theta_o-\Theta_h. \tag{9}$$

Maximum difference between thermoelement junctions in cooling mode is achieved on condition of $Ki_{\max} = 0$. In so doing,

$$\Theta_{\min}=\frac{\sqrt{1+2I_o\Theta_h}-1}{I_o}. \tag{10}$$

Accordingly, maximum possible temperature difference on thermoelement is equal to:

$$\Delta\Theta_{\max} = 1 - \Theta_{\text{o}\min}. \tag{11}$$

Temperature distributions in thermoelement for different supply currents from the permissible range (7) are represented in Fig. 1 *a*.

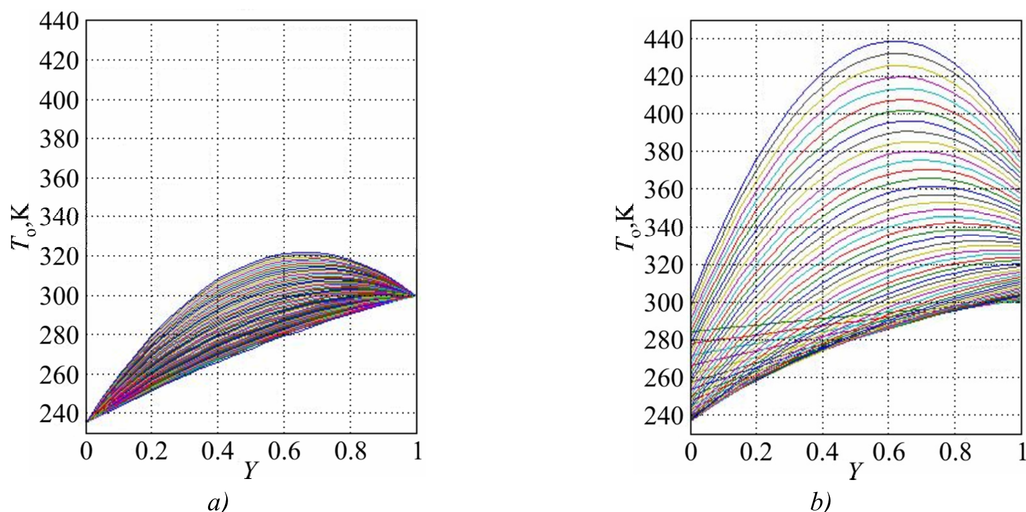

Fig. 1. Temperature distributions in thermoelement, THP mode, 0 ≦ J ≦ J_{max}.
(a – idealized model; b – boundary conditions of II/III kind).

THP efficiency *E* is determined as the ratio between net cooling capacity *Ki* and power *N* consumed by energy source. Consumed power can be determined as

$$N = \frac{J^2}{I_\text{o}} + J\Delta\Theta. \tag{12}$$

With regard to (6) we will get:

$$E = \frac{J\Theta_\text{o} - \dfrac{J^2}{2I_\text{o}} - \Delta\Theta}{\dfrac{J^2}{I_\text{o}} + J\Delta\Theta}. \tag{13}$$

The ratio between *E* and *Ki* in the acceptable range of currents at fixed junction temperatures is illustrated in Fig. 2.

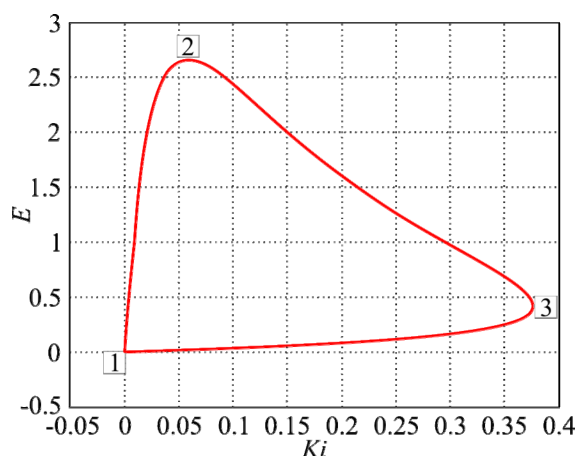

Fig. 2. The ratio between cooling capacity and efficiency of THP in the assigned temperature range.

This set of solutions restricts the range of definition of thermoelectric cooling problem under assumed restrictions. As is seen from the represented data, on the set under consideration one can separate two typical ranges. In the areas 1 – 2 and 1 – 3 one can always find a change in governing parameters resulting in a simultaneous improvement of criteria *E* and *Ki*. This range is called the range of efficient solutions. The area 2 – 3 is related to the range of weakly efficient solutions, since any improvement of one criterion results in the degradation of another. Nevertheless, it is obvious that optimal solutions of the problem should be sought exactly in the range of weakly efficient solutions, since it covers a set of solutions with maximum values of THP efficiency criteria. Having constructed for the range of temperatures ($\Theta_{\text{omin}} - \Theta_h$) the sets of solutions similar to that represented in Fig. 1, we will obtain a vivid presentation of the range of definition of the problem under consideration (Fig. 3 *a*).

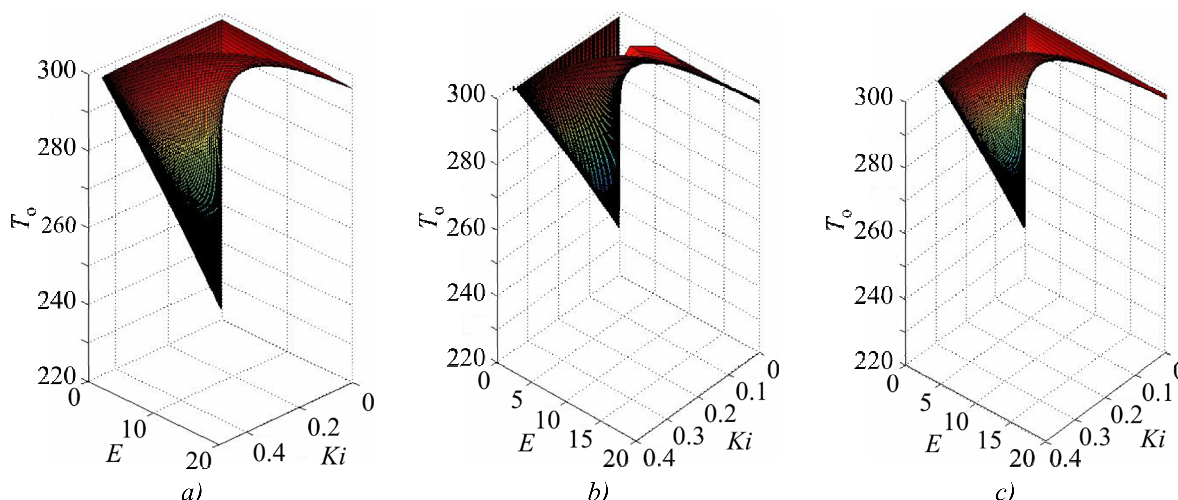

Fig. 3. The range of definition of thermoelectric cooling problem in the space of criteria T_o, Ki, E. (a – boundary conditions of I/I kind; b – of II/III kind; c – of III/III kind).

Electric energy generator mode

In electric energy generator mode the definable parameter is dimensionless current density which in the problem formulation considered (with the assigned material properties and known temperature conditions) depends only on load factor $m = R_n/R$:

$$J = \frac{I_o \Delta\Theta}{2(m+1)}. \tag{14}$$

Here, R_n is load resistance; $R = 2(\rho h/s)$ thermocouple resistance.

Thermocouple power is equal to

$$N = I_o \Delta\Theta^2 \frac{m}{2(m+1)^2} \tag{15}$$

From the last expression it follows that maximum TEG power is achieved at $m_{opt} = 1$:

$$N_{\max} = \frac{I_o \Delta\Theta^2}{8}. \tag{16}$$

The thermoelement efficiency is equal to the ratio between net power and heat flux on the heat-absorbing junction

$$n = \frac{N}{Ki}. \tag{17}$$

The range of change in the net power is determined by expression (16). The corresponding range of change in dimensionless heat fluxes $Ki_{\min} \div Ki_{max}$ meeting the problem conditions can be determined by substituting (14) into (6) at $m = 0$ (short circuit current, $J = J_{\max}$) and at $m = \infty$ (idle current, $J = 0$):

$$Ki_{\min} = \Delta\Theta(\frac{I_o\Theta_o}{2} - \frac{I_o\Delta\Theta}{8} - 1); \tag{18}$$

$$Ki_{\min} = -\Delta\Theta.$$

The behaviour of permissible range of dimensionless heat flux density as a function of temperature of the heat-absorbing junction is illustrated in Fig. 4.

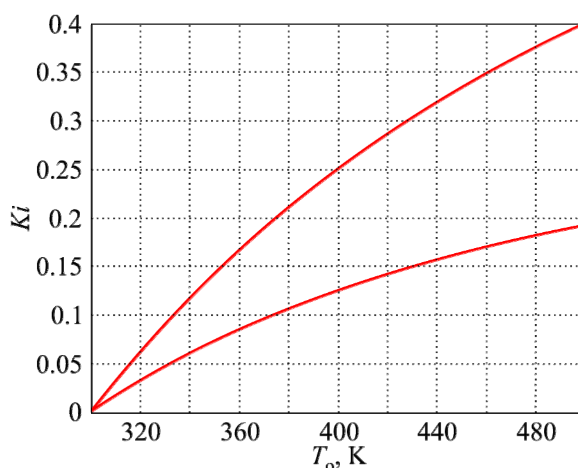

Fig. 4. Acceptable values of Ki in the range of temperatures $T_p \geqq T_o \geqq t_o$.

With regard to (6) from (17) we obtain

$$n = \frac{I_o\Delta\Theta^2 \dfrac{m}{2(m+1)^2}}{J\Theta_o - \dfrac{J^2}{2I_o} - \Delta\Theta}. \tag{19}$$

The ratio between the specific power and thermoelement efficiency with a change in load factor within $0 \leqq m \leqq \infty$ is represented in Fig. 5.

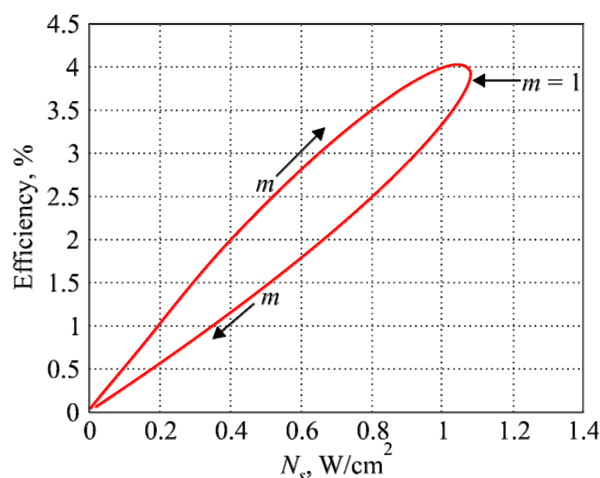

Fig. 5. The ratio between power and efficiency of TEG with a change in load factor within $0 \leqq m \leqq \infty$ (z = 0.003; dT = 100 K, h = 1 mm).

As it follows from the data given in the figure, the area corresponding to the region of $0 \leqq m \leqq 1$ is a set of efficient solutions, as long as with increase in *m,* both efficiency criteria of the problem are increased. The region $1 \leqq m \leqq \infty$ can be characterized as a set of inefficient solutions, since with increase in *m* both criteria are degraded.

Having constructed similar sets for the entire range of operating temperatures, we get a set of possible solutions of the problem under consideration in the space of basic technical and economic criteria (Fig. 6).

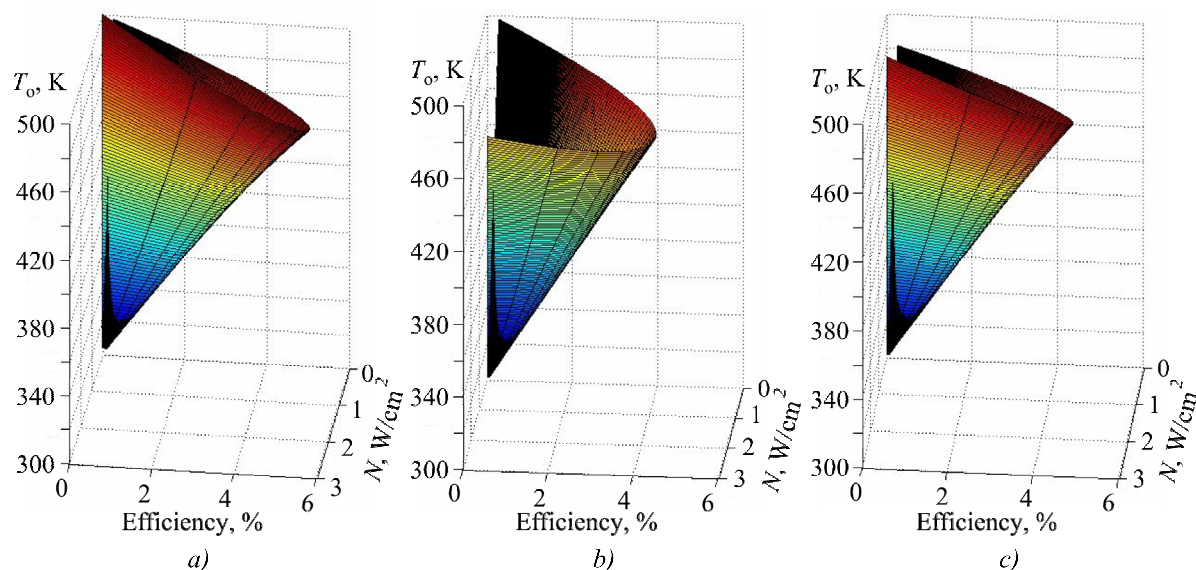

Fig. 6. The range of definition of thermoelectric energy conversion problem.
(a – boundary conditions of I/I kind; b – of II/III kind; c – of III/III kind).

Mathematical model of TEC under the boundary conditions of II/III kind

The above ideal model of TEC under the boundary conditions of I kind gives a vivid presentation of the basic regularities and ratios between criteria in THP and TEG modes, but it is unsuitable for the calculation of real devices, as long as similar abstraction cannot be implemented in practice. In fact, the temperature of TEC junctions is a function of state and is determined by conditions of heat transfer in a system. A more general and real problem formulation is assignment of the boundary conditions of II kind on the heat-absorbing thermoelement junctions (the specific density of heat flux is known) and the boundary conditions of III kind (convective heat exchange conditions) on the heat-releasing thermoelement junctions. In this case the boundary conditions of problem (3) are of the form:

$$\Theta'(0) - J\Theta(0) + Ki(0) = 0, \quad (20)$$

$$Bi[\Theta(1) - \vartheta] + \Theta'(1) - J\Theta(1) = 0.$$

Substituting solution (4) into (20), we get the following system of equations for the determination of integration constants C_1, C_2:

$$C_1 J - C_2 = Ki; \quad (21)$$

$$C_1(J - Bi) + C_2(J - Bi - 1) = \frac{J^2}{2I_o}(J - Bi) - Bi\vartheta - \frac{J^2}{I_o}.$$

Unlike idealized problem formulation, in the case under consideration the temperature mode is completely determined by conditions of heat exchange between thermoelement junctions.

Heat pump mode

Typical temperature distributions along thermoelement height on condition of $\Theta_o \le 1$ are represented in Fig. 1 *b*. As it appears from the above data, the effect of heat exchange conditions is manifested in the reduction of cooling depth as compared to idealized schematic of THP.

It follows from (4) that $C_1 = \Theta_o$. Taking this into account, from (21) we obtain the following expression for finding acceptable values of current density in THP mode:

$$aJ^3 + bJ^2 + cJ + d = 0, \tag{22}$$

where

$$a = -\frac{1}{2I_o};$$

$$b = \Theta_o + \frac{Bi_h}{2I_o} + \frac{1}{I_o};$$

$$c = -\Theta_o Bi_h - Ki;$$

$$d = Ki\left(Bi_h + 1\right) - Bi_h(\Theta_o - \vartheta_h).$$

At $\Theta_o = 1$ the roots of this equation restrict the range of current densities wherein the condition $\Theta_o \le 1$ is met. The problem has a physical meaning in the case when the discriminant of equation (22) $D \geqq 0$. At $D = 0$ the equation has only one real root – this case is limiting for the assumed restrictions. Thus, permissible combinations of problem criteria $\{I_o, Ki, Bi_h, \vartheta_h\}$ restricting the area of possible solutions can be determined from the condition:

$$D = -4b^3d + b^2c^2 - 4ac^3 + 18abcd - 27a^2d^2 = 0. \tag{23}$$

The values of acceptable ranges of J are determined by the ratio between criteria Ki and Bi_h. To each value of Bi_h corresponds an acceptable range of values $0 \leqq Ki \leqq Ki_{max}$, wherein the problem has a physical meaning, i.e. wherein the condition $\Theta_o \le 1$ can be met. Dependence of maximum possible dimensionless cooling capacity Ki_{max} on the intensity of heat exchange Bi_h is given in Fig. 7 *a*. At $Bi_h = \text{const}$ by means of (23) one can determine the range of possible values of $J = f(Ki)$, (Fig. 7 *b*). From the data given in the figure it follows that the range of efficient problem solutions is matched by the values of current in the range of $0 \leqq J \leqq 1/2\, J_{max}$. Maximum cooling depth $\Theta_o = \Theta_{min}$ can be achieved under conditions of $Bi_h \to \infty$, $Ki = 0$.

The efficiency of THP is determined as

$$E = \frac{Ki}{\dfrac{J^2}{I_o} + J\Delta\Theta} \tag{24}$$

and depends on cooling depth Θ_o, cooling capacity Ki and current density J.

The ratio between E and Ki for conditions under consideration is given in Fig. 7 *c*.

Having constructed an array of solutions similar to that represented in Fig. 7 *c*, for the acceptable ranges of changes in the temperature of the heat-absorbing junction we will obtain a

plurality of limiting opportunities of thermoelectric cooling problem in the space of criteria *Ki, E* and Θ_o (Fig. 3 *c*).

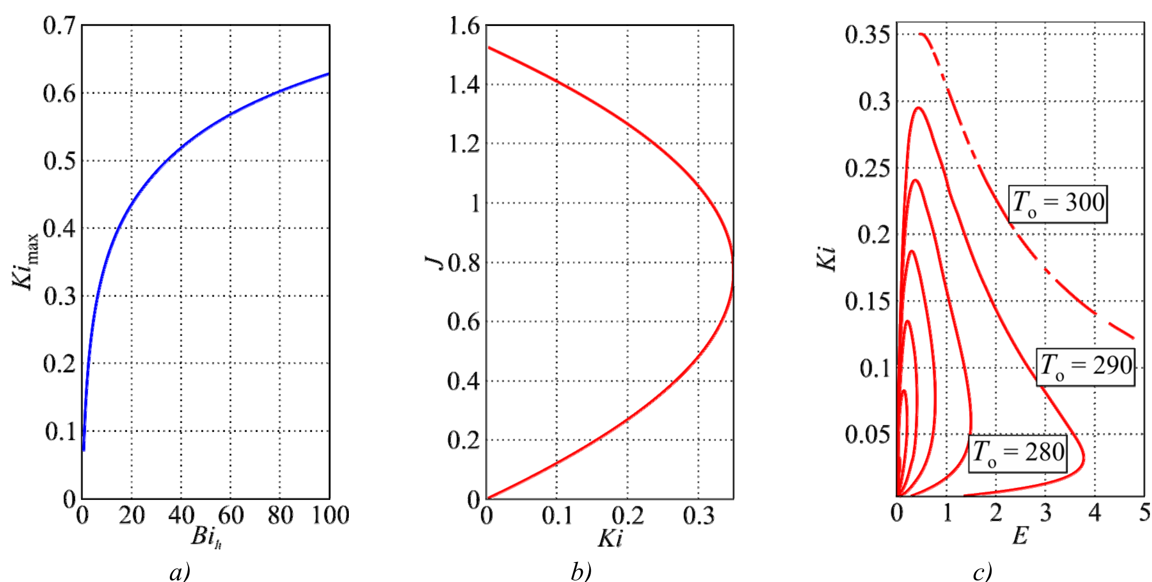

Fig. 7. a) Dependence of maximum possible cooling capacity Ki_{max} on Bi_h criterion.
b) The range of acceptable values of current density J as a function of heat flux Ki at Bi_h = 10.
c) The ratio between efficiency E and cooling capacity Ki.

Electric energy generator mode

For electric energy generator mode the temperature restriction of the heat-absorbing junction is active, i.e. for the achievement of maximum efficiency the condition $\Theta_o = 1$ should be met. With regard to the fact that maximum temperature of the heat-absorbing junction is achieved in idle mode (current equal to zero), assuming in (22, 23) $J = 0$, one can obtain the expression restricting acceptable ratios of Ki and Bi_h for the problem formulation considered:

$$Ki_{\max} = \frac{Bi_h(1-\vartheta_h)}{Bi_h + 1}, \tag{25}$$

from the last expression it follows that in the limiting case ($Bi_h \to \infty$) the dimensionless density of heat flux is restricted by the value

$$Ki_{\max} \le 1 - \vartheta_h \tag{26}$$

Under real conditions the restriction (26) is also active, i.e. to assure maximum efficiency, the condition $Ki = 1 - \vartheta_h$ should be met. The overrunning of this limit of heat flux is impermissible, since at nonstandard switching off the load there is considerable (by 15...20 %) temperature rise of the heat-absorbing layers of TEG (Fig. 8 *a*) that can result in construction damage. This condition restricts markedly the operating temperature difference which in the range of optimal loads is reduced by 20...30 % as compared to the available one (Fig.8 *b*). Since load mode has a pronounced effect on temperature distribution in thermoelements, and the problem becomes highly nonlinear, the mode of maximum TEG power is achieved at $\Delta\Theta < \Delta\Theta_{max}$ (Fig. 9). In so doing, the modes of maximum power and maximum efficiency coincide, since at given heat flux density the maximum efficiency is achieved at $N = N_{max}$.

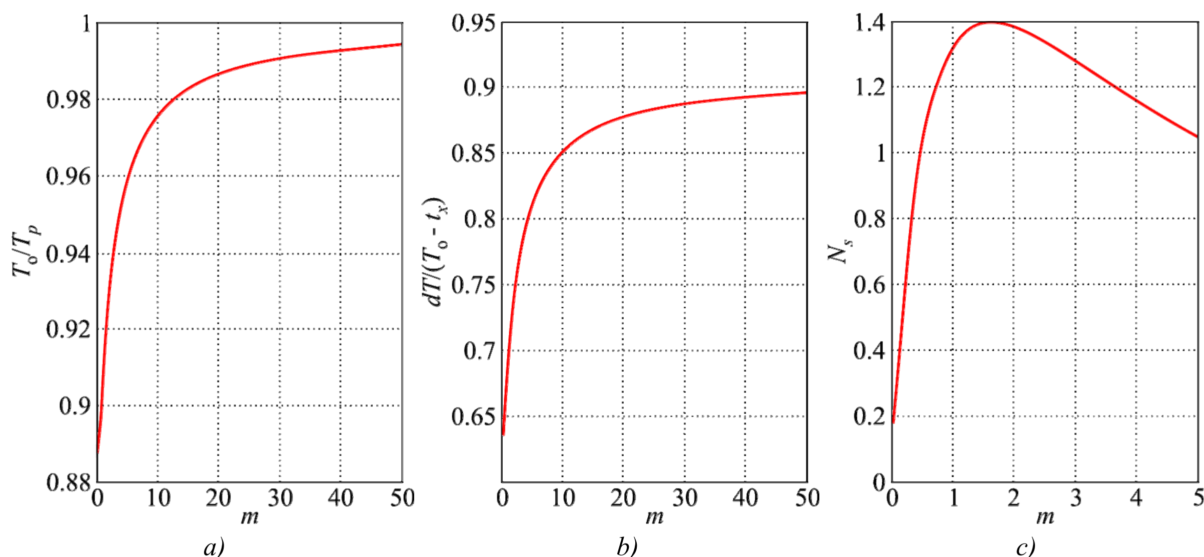

Fig. 8. Effect of load factor on TEG characteristics: a) –dependence of relative temperature of the heat-absorbing junction on m; b) – dependence of relative operating temperature difference on m; c) – dependence of specific power N_s, W/cm^2, on m.

The foregoing implies that in the general case the defining criterion which restricts technical and economic characteristics of TEG at given properties of thermoelectric material is the Biot criterion which characterizes heat removal conditions, namely it limits both the losses in temperature head on cooling of TEG and the range of acceptable densities of heat flux on the side of heat source.

The range of definition of the problem of thermoelectric power conversion in formulation considered is given in Fig. 3 *b*.

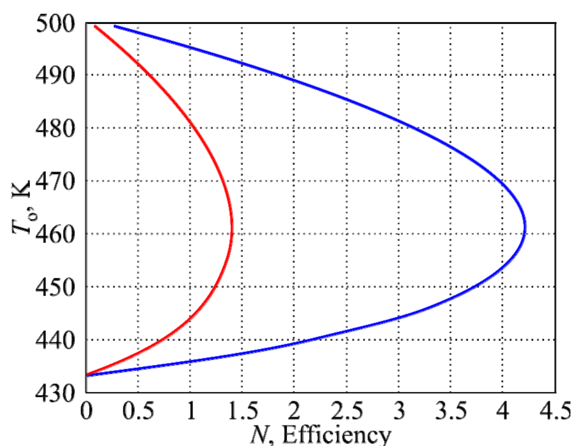

Fig. 9. The ratio between temperature T_o, power and efficiency of TEG at $0 \leqq m \leqq \infty$.
(– efficiency, %; – specific power N, W/cm^2).

The case of using constant-power heat sources (Ki = const), such as radioisotope heat sources, has unique features. As a rule, such sources assure relatively low heat flux densities, but have no restrictions on temperature conditions (within reasonable limits) [7, 8]. At first sight, for such TEG it is optimal to provide for a mode with maximum permissible temperature of heat-absorbing junction ($\Theta_o = 1$). However, in fact, in this case also the decisive influence on the characteristics of TEG is produced by cooling conditions (Bi_h criterion). Figs. 10 *a, b* show the dependences of junction temperatures and temperature differences on Bi_h criterion for the case $Ki < Ki_{\max}$ = const. Significant is the fact that TEG power tends to maximum on achieving minimum possible under conditions concerned temperature value

of the heat-absorbing junction T_o (Fig. 10 *c*). That is, increase in temperature difference (and power) is possible only due to reduction of losses from heat exchange irreversibility. The limiting power of TEG can be achieved only under conditions of $Ki = Ki_{max}$, $Bi_h \to \infty$.

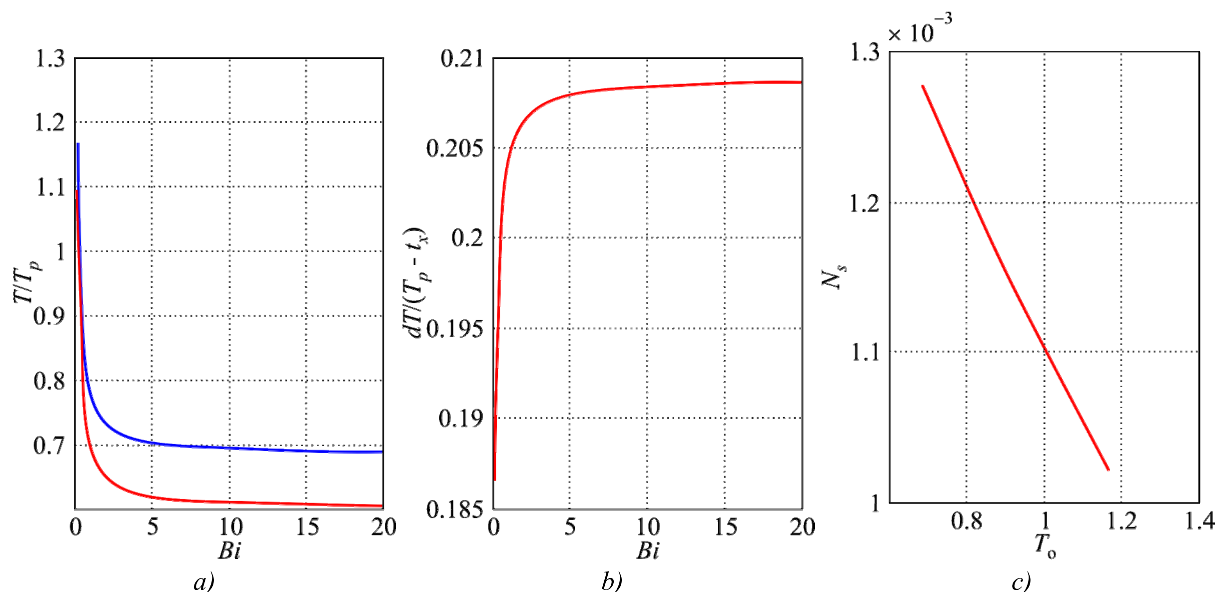

Fig. 10. Characteristics of TEG at Ki < Ki$_{max}$: a) – dependence of junction temperatures on Bi$_h$ (– T_o/T_p ; – T_h/T_p); b) – dependence of relative operating temperature difference $dT/(T_p - t_x)$ on Bi$_h$; c) – the ratio between the specific power of TEG N_s and the temperature of the heat-absorbing junction T_o/T_p.

Mathematical model of TEC under boundary conditions of III/III kind

Quite common is a schematic whereby heat transfer on the heat-absorbing junction of TEC is due to convective heat exchange. In this case the junction temperature is limited by heat carrier temperature. For the analysis of similar schematics it is necessary to use a mathematical model of thermoelement under the boundary conditions of III kind on the heat-absorbing and heat-releasing junctions:

$$Bi_o[\vartheta_o - \Theta(0)] + \Theta'(0) - J\Theta(0) = 0; \qquad (27)$$

$$Bi_h[\Theta(1) - \vartheta_h] + \Theta'(1) - J\Theta(1) = 0.$$

Substituting (4) into (27), we get the following system of equations for the determination of integration constants C_1, C_2:

$$C_1(J + Bi_o) - C_2 = Bi_o\vartheta_o; \qquad (28)$$

$$C_1(Bi_h - J) + C_2(Bi_h - J + 1) = Bi_h\vartheta_h + \frac{J^2}{I_o}(1 + \frac{Bi_h - J}{2}).$$

Heat pump mode

For the schematic under consideration the heat flux on the heat-absorbing junction is equal to:

$$q = \alpha_o(t_o - T_o), \qquad (29)$$

or in the dimensionless form:

$$Ki = Bi_o(\vartheta_o - T_o). \qquad (30)$$

From the last relation it follows that heat pump mode is implemented on condition of

$$T_o \leq \vartheta_o. \tag{31}$$

For arbitrary combinations of problem parameters the range of permissible currents $J_{min} \leq J \leq J_{\max}$ that satisfy condition (31) will be found as the roots of equation

$$\vartheta_o - \Theta_o(J, I_o, Bi_o, Bi_h, \vartheta_o, \vartheta_h) = 0. \tag{32}$$

At the ends of this current interval the temperature of the heat-absorbing junction is equal to the temperature of liquid being cooled, and cooling capacity goes to zero (Fig. 11 *a, b*). It is noteworthy that the intensity of heat exchange on the heat-absorbing junction of Bi_o does not affect the values of acceptable supply currents and their range depends only on the heat carrier temperatures ϑ_o, ϑ_h and heat exchange conditions on the heat-releasing junction of Bi_h. It is due to the fact that changes in Bi_o are compensated by respective changes in T_o according to (30).

Similar to the schematic considered above, the cooling capacity of THP is limited by cooling depth and heat exchange conditions on the heat-absorbing junction of Bi_h. The specific feature of schematic under study is that cooling depth is assigned by the temperature of cooled heat carrier ϑ_o, and cooling capacity, in conformity with (30), is a function of temperature difference between the heat carrier and the heat-absorbing junction. It restricts maximum cooling depth of THP and places the following limitation on the acceptable temperature ratio between the cooled heat carrier and the heat-absorbing junction:

$$\vartheta_o - \Theta_o \geqq \frac{Ki}{Bi_o}. \tag{33}$$

From the last equation it follows that heat flux on the heat-absorbing junction (net cooling capacity) is varied in conformity with a change in junction temperature (Fig. 11 *a, b*). The ratio between cooling capacity and efficiency is given in Fig. 11 *c*, from which it follows that optimal modes of THP correspond to the region of weakly efficient solutions with the values of supply current $J \leq J_{opt.}$

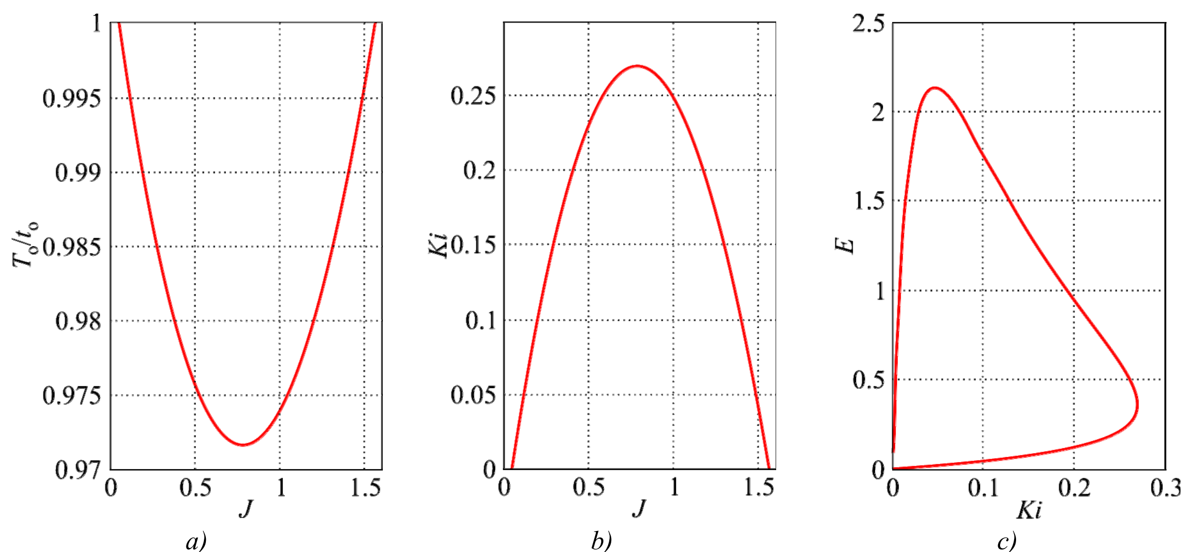

Fig. 11. Characteristics of THP of heat-exchange type: a) – dependence of relative temperature of the heat-absorbing junction (T_o/t_o) on J; b) – dependence of THP heat capacity on J; c) – the ratio between cooling capacity Ki and THP efficiency E.

Electric energy generator mode

In TEG mode, the main limiting factor is the temperature of heating heat carrier ϑ_o. Its maximum acceptable value with regard to (33, 26) is determined as:

$$\vartheta_{o\max} \leqq 1 + \frac{1-\vartheta_h}{Bi_o}. \tag{34}$$

At $\vartheta_o = \vartheta_{o\max}$ the temperature of the heat-absorbing junction in idle mode is equal to T_p, and TEG characteristics achieve maximum possible values. At $\vartheta_o \leqq \vartheta_{o\max}$ the situation is similar to the case with constant-power heat source, namely the governing influence on TEG characteristics is produced by heat exchange conditions on the heat-releasing junctions of thermoelements. However, by virtue of the fact that heat flux and temperature of the heat-absorbing thermoelement junctions depend on load conditions, the acceptable region of schematic under consideration has a greater similarity to characteristics of an idealized TEG (Fig. 12). A set of limiting opportunities of heat-exchange-type TEG is represented in Fig. 6 *c*.

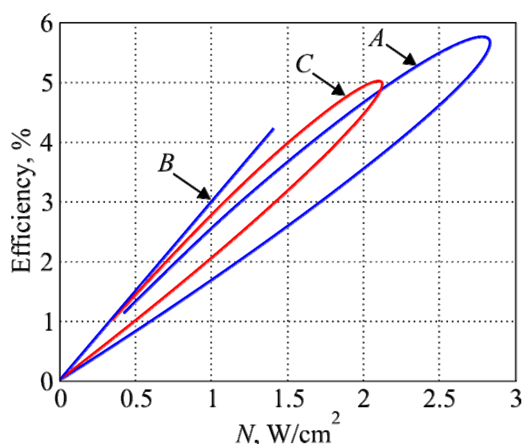

Fig. 12. The ratio between power and efficiency of TEG for different schematics (T_p = 500 K, $0 \le m \le \infty$) A – boundary conditions of I/I kind; B – of II/III kind; C – of III/III kind).

Conclusions

The above results demonstrate the advisability of using system approach for the analysis of TEC characteristics. Solution of thermoelectric energy conversion problem in the generalized form allows clear determination of the effect of the basic system units on the characteristics of thermoelectric devices. Comparative analysis of the sets of limiting opportunities of various TEC schematics allows revealing their peculiarities and obtaining quantitative estimates of each. The obviousness of comparison methods under study is well illustrated in Fig. 12 and Fig. 13 showing characteristics of considered TEC schematics in the space of basic technical and economic criteria (power – efficiency for TEG and cooling capacity – efficiency for THP). Analysis of such characteristics allows objective estimation of actual device losses as compared to an ideal schematic and the specific features of each schematic. The optimal solutions obtained in generalized variables are universal, since they can be transferred to any combination of primary initial data and give unambiguous information on possible characteristics of real TEC with known restrictions on governing parameters (thermoelectric material properties, heat exchange conditions, temperature conditions and device geometry restrictions).

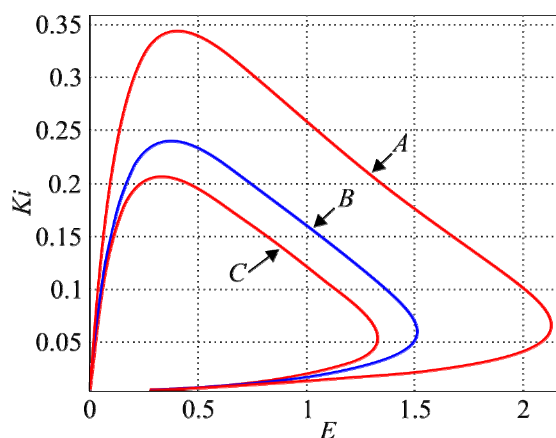

Fig. 13. Comparison of various THP schematics with identical cooling depth (T_o = 280 K). A – boundary conditions of I/I kind; B – of II/III kind; C – of III/III kind.

Symbols

e is the Seebeck coefficient, V/K; σ is electric conductivity, $(\Omega\cdot\text{cm})^{-1}$; λ is thermal conductivity, W/cmK; z is thermoelectric figure of merit, K^{-1}; h is thermoelement height, cm; q is specific density of heat flux, W/cm^2; α is heat transfer coefficient, W/cm^2K; j is current density, A/cm^2; t_h is heat sink temperature, K; t_o is heat source temperature, K; $\Theta = T/T_p$ is dimensionless temperature; T_p is governing temperature, K (for TEG – maximum acceptable temperature $T_p = T_{max}$; for THP – heat sink temperature $T_p = t_h$); $\vartheta_h = t_h/T_p$; $\vartheta_o = t_o/T_p$; ΔT, $\Delta\Theta$ is temperature difference; N is specific power, W/cm^2. In the calculations the following set of initial data was used for illustrations: $z = 3.1\cdot10^{-3}$ K^{-1}; h = 0.1 cm; $Bi_o = Bi_h = 10$; t_h = 300 K; for TEG mode T_p = 500 K; for THP mode T_p = 300 K.

References

1. L.I. Anatychuk, *Thermoelements and Thermoelectric Devices: Handbook* (Kyiv: Naukova Dumka, 1979), 768 p.
2. A.I. Burstein, *Basic Physics for Calculation of Semiconductor Thermoelectric Devices* (Moscow: Fizmatgiz, 1962), 136 p.
3. A.F. Ioffe, *Semiconductor Thermoelements* (Moscow-Leningrad: AN SSSR Publ., 1960), 188 p.
4. I.V. Zorin, E.Ya. Zorina, *Thermoelectric Coolers and Generators* (Leningrad: Energiya, 1973), 135 p.
5. E.K. Iordanishvili, *Thermoelectric Power Sources* (Moscow: Sov.Radio, 1968), 188 p.
6. M.A. Kaganov, M.P. Privin, *Thermoelectric Heat Pumps* (Leningrad: Energiya, 1970), 176 p.
7. Yu.M. Lobunets, *Methods for Calculation and Design of Thermoelectric Power Converters* (Kyiv: Naukova Dumka, 1989), 175 p.
8. A.S. Okhotin et al., *Thermoelectric Generators* (Moscow: Atomizdat, 1976), 320 p.
9. L.I. Anatychuk, R.V. Kuz, and A.V. Prybyla, Heat Exchange Systems and the Efficiency of Thermoelectric Air Conditioner, *J. Thermoelectricity* **1**, 76 – 82 (2013).
10. N.N. Moiseev, *Mathematical Problems of System Analysis* (Moscow: Nauka, 1981), 487 p.
11. I.G. Chernorutsky, *Optimization Methods in Control Theory* (Saint-Petersburg: Piter, 2004), 256 p.
12. A.A. Gukhman, *Use of Similarity Theory for Investigation of Heat and Mass Exchange Processes* (Moscow: Vysshaya Shkola, 1974).328 p.

Submitted 29.04.2014.

NEWS

KIN-ICHI UEMURA

(06.02.1923 – 23.04.2014)

On April 24, 2014, after a short illness, in his 92-nd year of life academician of International Thermoelectric Academy, Doctor of Technical Sciences Kin-ichi Uemura passed away.

Kin-ichi Uemura was born in Saga prefecture Japan. He graduated as a Bachelor of Technical Sciences from Faculty of Engineering, Tokyo University (1946). The scientific interests of Kin-ichi Uemura cover a wide scope of relevant problems of modern thermoelectricity.

Since 1956 Uemura's professional activity has been inseparably related to thermoelectricity. For many years he has studied the electrophysical properties of thermoelectric semiconductor materials, heat exchange processes, developed thermoelectric modules and devices on their basis in Thermoelectric Research Laboratory of Engineering Division, Komatsu Co. Ltd. At Komatsu, Kin-ichi Uemura has been in charge of scientific and development projects on thermoelectric cooling. These studies formed the basis for his doctoral thesis brilliantly maintained in Tokyo University in 1961. Successful completion of the projects brought into being in 1960 a subsidiary company Komatsu Electronics Inc., and Kin-ichi Uemura took charge of its thermoelectric department. From 1960 till 1988 he was responsible for the entire thermoelectric activity of the company.

Kin-ichi Uemura's high international prestige, his remarkable organizing talent, commercial success of his developments resulted in creation in 1990 of Institute for Thermoelectric Technologies Japan (ITTJ) of which he became a director.

Kin-ichi Uemura successfully combined scientific and production, administrative and social activities. He was organizer of the 12-th International Conference on Thermoelectrics (ICT93) and International Short Course on Thermoelectrics (SCT93) in Yokogama, Japan. In 1994 Kin-ichi Uemura was elected academician and Vice-President of International Thermoelectric Academy (ITA). He was editorial board member of "Journal of Thermoelectricity". In 2002 Honorable Golden Prize of International Thermoelectric Academy (ITA) was awarded to him for the fundamental contribution to development of thermoelectricity.

International Thermoelectric Academy, Institute of Thermoelectricity of the NAS Ukraine, "Journal of Thermoelectricity" Publishers are mourning over the death of an outstanding scientist, engineer and teacher, a modest man Kin-ichi Uemura and extend sincere condolences to his near and dear ones. The memory of Kin-ichi Uemura will remain forever in the hearts of his friends, colleagues and disciples.

M.M. Mamedov

M.M. Mamedov

Physics and Mathematics Institute of Turkmenistan Academy of Sciences,
31, Turkmenbashi Str., Ashgabat, Turkmenistan

UNIVERSAL NONEQUILIBRIUM THERMODYNAMICS AND THE SEEBECK EFFECT

In conformity with a book by I. Prigogine and D. Kondepudi "Modern Thermodynamics", this paper describes the Seebeck effect based on Onsager's linear thermodynamics, on the a priori assumption that only a generalized heat flow is different from zero. Moreover, in such situations it is considered that a thermodynamic system is in close to equilibrium state (linear mode). It is proposed to consider the above effect in the framework of universal nonequilibrium thermodynamics, where it is shown that the importance of the Seebeck effect lies in confirming the validity of Onsager's reciprocity relations, since the necessity of making any assumptions as to proximity to equilibrium state is eliminated. The effect is shown to be an illustrative example confirming the adequacy of universal nonequilibrium thermodynamics. Next, a thermodynamically-phenomenological description of the Seebeck effect based on the proposed universal nonequilibrium thermodynamics is provided. The results testify that the Seebeck effect, without experiments, proves not only the validity of Onsager's reciprocity relations, but also the absurdity of Onsager's thermodynamics and of the Prigogine principle of minimum entropy production. Onsager's thermodynamics is absurd because being thermodynamics of reversible processes is called thermodynamics of irreversible processes. And the Prigogine principle is absurd because minimum entropy production being equal to zero is considered to be more than zero.

Key words: universal nonequilibrium thermodynamics, reversibility, irreversibility, Onsager's thermodynamics, Prigogine principle, Seebeck effect, Onsager's reciprocity relations, entropy production, perpetual motion machine, steady-state process, the second law of thermodynamics, scientific revolution.

Introduction

To illustrate the applications of Onsager's reciprocity relations, I. Prigogine and D. Kondepudi in their book "Modern Thermodynamics" consider in detail the thermoelectric effects, specifically, the Seebeck effect [1].

As the first illustration, they consider the thermoelectric effects whereby there is heat flow $\overrightarrow{J_q}$ and electric current $\overrightarrow{J_e}$ in conductors (subscript e means that this refers to electron flow). In this case, entropy production in the unit volume and the related linear phenomenological laws are written as follows [1]:

$$\sigma = \overrightarrow{J_q} \cdot \nabla\left(\frac{1}{T}\right) + \overrightarrow{J_e} \cdot \frac{\vec{E}}{T} \tag{1}$$

$$\overrightarrow{J_q} = L_{qq}\nabla\left(\frac{1}{T}\right) + L_{qe}\frac{\vec{E}}{T}, \tag{2}$$

$$\overrightarrow{J_e} = L_{ee}\frac{\vec{E}}{T} + L_{eq}\nabla\frac{1}{T}, \tag{3}$$

where $\vec{E}$ is electric field. For the one-dimensional system, such as conductors, the vector character of $\overrightarrow{J_q}$ and $\overrightarrow{J_e}$ is of no importance, and the two flows can be regarded as scalars. In order to relate coefficients L_{qq} and L_{ee} to thermal conductivity K and resistance R, one can write equations (2) and (3) in the one-dimensional system as

$$J_q = -\frac{1}{T^2}L_{qq}\frac{\partial T}{\partial x} + L_{qe}\frac{E}{T}, \tag{4}$$

$$J_e = L_{ee}\frac{E}{T} - \frac{1}{T^2}L_{eq}\frac{\partial T}{\partial x}. \tag{5}$$

The Fourier law of thermal conductivity is valid in the absence of electric field, i.e. $E = 0$. Comparison of expression for thermal conductivity

$$J_q = -\left(\frac{1}{T^2}\right)L_{qq}\frac{\partial T}{\partial x} \tag{6}$$

to the Fourier law

$$J_q = -K\frac{\partial T}{\partial x} \tag{7}$$

leads to the relation

$$K = \frac{L_{qq}}{T^2}. \tag{8}$$

To find the correlation between L_{ee} and resistance R, note that electromotive force (EMF) is expressed by the following formula

$$V = -\nabla\varphi = \int_0^l E\mathrm{d}x \ \text{ or } \ J_e l = \frac{L_{ee}}{T}V. \tag{9}$$

Comparison of this equation to Ohm's law

$$J_e = \frac{V}{R} \tag{10}$$

yields

$$L_{ee} = T\frac{l}{R} = \frac{T}{r}, \tag{11}$$

where r is resistance per unit length. As long as Ohm's law can be formulated in general form as

$$\overrightarrow{J_e} = \frac{\vec{E}}{\rho}, \tag{12}$$

where ρ is resistivity, comparing (5) on condition of $\frac{\partial T}{\partial x} = 0$ to (12), we get

$$L_{ee} = \frac{T}{\rho}. \tag{13}$$

In the one-dimensional system ρ is substituted by r, i.e. resistance per unit length.

In the above formulae, cross coefficients L_{qe} and L_{eq} can be also related to the experimentally measured values.

For instance, in the Seebeck effect, the temperature difference between two contacts of different metallic conductors generates EMF. This EMF is measured at the zero current, i.e. at $J_e = 0$. For such a system one can use equations (4) and (5). In (5), assuming that $J_e = 0$, we get

$$0 = L_{ee}ET - L_{eq}\frac{\partial T}{\partial x}. \tag{14}$$

To derive a relationship between the temperature difference ΔT of contacts and the EMF generated by this temperature difference, $\Delta\varphi = -\int E\mathrm{d}x$, let us integrate this equation. In so doing, we suppose that full change in ΔT is small, and one can use the approximation

$$\int TE\mathrm{d}x \approx T\int E\mathrm{d}x = -T\Delta\varphi. \tag{15}$$

Then

$$L_{eq} = -L_{ee}T\left(\frac{\Delta\varphi}{\Delta T}\right)_{J_e=0} \tag{16}$$

The experimentally measured parameter $-(\Delta\varphi/\Delta T)_{Je=0}$, is called thermoelectric power. Using (16), coefficient L_{eq} can be related to the measured values, namely coefficient L_{ee}, temperature T and thermoelectric power $-\Delta\varphi/\Delta T$.

It is noteworthy that formula (16) is meaningful when thermoelectric effects are studied in close to equilibrium states and a linear mode. It means that coefficients L_{qq}, L_{ee} etc. can be regarded as constants. Since $T(x)$ is a function of coordinate x, such an assumption is, strictly speaking, is not correct. Therefore, formula (16) has a meaning not only at $J_e = 0$, but also at $\partial T/\partial x \to 0$ [1, 2].

Description of the Seebeck effect in the framework of universal nonequilibrium thermodynamics

Thus, the aforesaid testifies that the Seebeck effect, on top of everything else, is important for the experimental verification of the validity of Onsager's reciprocity relation [3], at least in close to equilibrium state.

In fact, in the framework of our universal nonequilibrium thermodynamics the importance of the Seebeck effect becomes overwhelmingly greater in confirming the validity of Onsager's reciprocity relation, since the necessity of making any assumptions as to closeness to equilibrium state is eliminated. Moreover, the Seebeck effect is one of the illustrative examples confirming the adequacy of our universal nonequilibrium thermodynamics [4].

Now, to provide proofs for our laudatory comments on the Seebeck effect, we will interpret this effect in terms of universal nonequilibrium thermodynamics. In other words, we will propose a fundamentally new thermodynamic-phenomenological description of the Seebeck effect based on the laws of universal nonequilibrium thermodynamics [5].

For compactness of writing, we introduce the following notations:

$$X_1 = -\frac{1}{T^2}\frac{\partial T}{\partial x},\ X_2 = \frac{E}{T}. \tag{17}$$

Then equations (1) – (3) for the one-dimensional case will take on the form:

$$\sigma = J_q X_1 + J_e X_2, \tag{18}$$

$$J_q = L_{qq} X_1 + L_{qe} X_2, \tag{19}$$

$$J_e = L_{eq} X_1 + L_{ee} X_2. \tag{20}$$

In this case, J_q and J_e are called generalized flows, and X_1 and X_2 – generalized forces.

According to the second law, with regard to (19) and (20), relation (18) will take on the form

$$\sigma = L_{qq} X_1^2 + \left(L_{qe} + L_{eq}\right) X_1 X_2 + L_{ee} X_2^2 \geq 0 \tag{21}$$

that is, in the nonequilibrium state of thermodynamic system the local values of entropy production (σ) are not negative. Within the framework of the Onsager thermodynamics and in the book by I. Prigogine and D. Kondepudi "Modern Thermodynamics" relation (21) was replaced by the following relation [1, 3]

$$\sigma = L_{qq} X_1^2 + \left(L_{qe} + L_{eq}\right) X_1 X_2 + L_{ee} X_2^2 > 0 \tag{22}$$

with imposing the condition

$$L_{qq} > 0, L_{ee} > 0 \text{ and } \left(L_{qe} + L_{eq}\right)^2 < 4 L_{qq} L_{ee} \tag{23}$$

hence, a priori, the possibility of vanishing entropy production (22) under nonequilibrium states of thermodynamic systems was eliminated once and forever, and the feasibility of a perpetual motion machine of the second kind was banned [4]. The seat of the trouble is that nobody else has managed to interpret mathematically and physically adequately the second law of thermodynamics, that is, the equality sign in formula (21) has been referred only to equilibrium state of thermodynamic system, whereby the second law of thermodynamics was from the outset placed on the Procrustean bed of irreversible thermodynamics based on relations (22) and (23) [6].

In fact, according to universal nonequilibrium thermodynamics, for relation (21) to be valid, it is necessary and sufficient to impose on it the following conditions [4]:

$$L_{qq} > 0,\ L_{ee} > 0 \text{ and } \left(L_{qe} + L_{eq}\right)^2 - 4 L_{qq} L_{ee} = 0. \tag{24}$$

Thus, relation (21) with conditions (24) is an adequate mathematical model of the second law of thermodynamics as applied to the description of nonequilibrium irreversible and reversible states of thermodynamic systems with two generalized flows, and here the coefficients of equations (19) and (20) L_{qq}, L_{qe}, L_{eq}, L_{ee} can be the functions of intensive parameters of thermodynamic system. Such situation testifies that in the framework of universal nonequilibrium thermodynamics the linear reversible and linear irreversible thermodynamics, as well as the nonlinear reversible and nonlinear irreversible thermodynamics are partial cases of universal nonequilibrium thermodynamics [4]. Therefore, it appears that reversibility, just as irreversibility, is the inseparable attribute of real nonequilibrium processes, in other words, all steady-state nonequilibrium processes of transfer in thermodynamic systems with two and more generalized flows are reversible due to the fact that in such situations the local values of entropy production in thermodynamic system are equal to zero.

Since in the Seebeck effect the processes of current and heat transfer are steady-state, the nonequilibrium process is reversible because of vanishing local values of entropy production (σ), i.e.

$$\sigma = J_q X_1 + J_e X_2 = 0 \tag{25}$$

or with regard to (19) and (20):

$$\sigma = L_{qq} X_1^2 + \left(L_{qe} + L_{eq}\right) X_1 X_2 + L_{ee} X_2^2 = 0 \tag{26}$$

under conditions

$$L_{qq} > 0, L_{ee} > 0 \quad u \quad \left(L_{qe} + L_{eq}\right)^2 - 4L_{qq}L_{ee} = 0 \tag{27}$$

or relations (27) can be represented as

$$L_{qe} + L_{eq} = \pm 2\sqrt{L_{qq}L_{ee}}. \tag{28}$$

Subsequent analysis showed that in (28) the negative sign before the root must be ignored, and then we have [7]:

$$L_{qe} + L_{eq} = 2\sqrt{L_{qq}L_{ee}}. \tag{29}$$

With regard to (29), relation (26) will take on the form

$$\sigma = \left(X_1\sqrt{L_{qq}} + X_2\sqrt{L_{ee}}\right)^2 = 0. \tag{30}$$

From (30) it follows that:

$$X_1\sqrt{L_{qq}} + X_2\sqrt{L_{ee}} = 0. \tag{31}$$

With regard to (31), equations (19) and (20) will take on the form

$$J_q = \frac{1}{2}\left[L_{qe} - L_{eq}\right]X_2, \tag{32}$$

$$J_e = -\frac{1}{2}\left[L_{qe} - L_{eq}\right]X_1. \tag{33}$$

In so doing, if Onsager's reciprocity relation is fulfilled:

$$L_{qe} = L_{eq}, \tag{34}$$

then thermal flow J_q and electric current J_e go to zero and vice versa. Moreover, according to relations (32) and (33), even if only electric current flow vanishes, i.e. under condition $J_e = 0$, Onsager's reciprocity relation (34) is fulfilled and thermal flow J_q goes to zero.

Thus, fulfillment of traditional condition (14) in the Seebeck effect [1] is the implicit proof of the validity of famous Onsager's reciprocity relations. In its turn, the validity of Onsager's reciprocity relation (34), according to relations (32) and (33), as well as due to the second law of thermodynamics (21), clearly proves the absurdity of Onsager's thermodynamics, since in Onsager's thermodynamics not only local values of entropy production are equal to zero, but due to Onsager's reciprocity relation (34), according to relations (32) and (33), the flows J_q and J_e are also equal to zero.

Thus, the above-stated fundamental theoretical analysis of the Seebeck effect on the basis of its conceptually new thermodynamic-phenomenological description in the framework of our universal nonequilibrium thermodynamics testifies that the Seebeck effect not only proves the validity, without experiments, of famous Onsager's reciprocity relations, but also clearly proves the absurdity of Onsager's thermodynamics and Prigogine's principle of minimum entropy production.

Onsager's thermodynamics is absurd because due to Onsager's reciprocity relations, being thermodynamics of reversible processes, it is called thermodynamics of irreversible processes. Also, Prigogine's minimum entropy production principle is absurd, because minimum entropy production, being equal to zero under steady-state processes, is considered to be more than zero [8, 9].

Summary

The meaning of this paper testifies that thermodynamic scientists, since the time of formulation of the second law of thermodynamics by William Thomson and Rudolf Clausius have followed the wrong path in the development of nonequilibrium thermodynamics science due to inability to interpret adequately the second law of thermodynamics. This is also evidenced by Prigogine's statement in his Nobel Prize lecture "Even one hundred and fifty years after its formulation, the second law of thermodynamics still seems to be a program, rather than a well-developed theory in the usual sense, since nothing precise (except for the sign) is said on entropy production. Even the scope of validity of this inequality remains uncertain".

Summing up, we can say that our universal nonequilibrium thermodynamics and the Seebeck effect, complementing and enriching each other, open a new prospect for the development of nonequilibrium thermodynamics on the basis of adequate interpretation of the second law, more than a century and a half after it was formulated. As regards classical linear thermodynamics of irreversible processes, or, otherwise called Onsager's linear irreversible thermodynamics, it was just a linear thermodynamics of reversible nonequilibrium processes with the zero generalized flows. Thus, it turns out that due to famous Onsager's reciprocity relations, mankind does not possess even a linear thermodynamics of irreversible processes, to say nothing of a linear irreversible thermodynamics. Figuratively speaking, progress of thermodynamic science in the field of nonequilibrium thermodynamics has hindered for more than a century and a half due to the use of incorrect interpretations of the second law of thermodynamics and Onsager's reciprocity relations. Finally, our revolutionary new scientific achievements have made it really possible for the first time to determine correctly and unambiguously the concept of reversibility on the basis of adequate interpretation of the second law of thermodynamics. Namely, nonequilibrium process in thermodynamic system is called reversible, if local values of entropy production in the system are equal to zero, otherwise the process is called irreversible. The class of thermodynamic systems with the zero entropy production includes all thermodynamic systems that are in steady-state nonequilibrium state, therefore, all steady-state nonequilibrium processes are reversible, and the rest of nonequilibrium processes are irreversible. Against the background of these determinations of the reversible and irreversible processes, any engine that works in steady-state mode is perpetual motion machine of the second kind, inasmuch as in such a mode the local values of entropy production in the engine are equal to zero. In this connection, the existing ban on the perpetual motion machine of the second kind is once and forever withdrawn from the agenda, that is, from now on the ban on perpetual motion machine of the second kind in the framework of universal nonequilibrium thermodynamics is out of the question [10].

Thus, our universal nonequilibrium thermodynamics is a scientific revolution non only in nonequlibrium thermodynamics, but also in the historically established world outlook [4, 5].

In view of the aforesaid, from now on using classical linear nonequilibrium thermodynamics based on Onsager's reciprocity relations for solving various theoretical and practical problems from thermodynamics of irreversible processes is out of the question.

Conclusions

1. Traditional quantitative description of the Seebeck effect in the framework of Onsager's thermodynamics is incorrect for high values of transport potential gradients.
2. As a rule, the Seebeck effect is important for the experimental confirmation of the validity of Onsager's reciprocity relations only close to equilibrium.

3. In the framework of universal thermodynamics the Seebeck effect proves the validity of Onsager's reciprocity relations without imposing any restrictions on the values of transport potential gradients.
4. In the framework of universal thermodynamics all steady-state nonequilibrium processes are reversible, and all the rest of nonequilibrium processes are irreversible.
5. Any engine working in steady-state mode is a perpetual motion machine of the second kind, inasmuch as in this mode the local values of entropy production in the engine are equal to zero. In the framework of universal thermodynamics the ban on the perpetual motion machine of the second kind is inadmissible.

References

1. I. Prigogine, D. Kondepudi, Modern Thermodynamics (Moscow: Mir Publ., 2002), 461 p.
2. D.G. Miller, Thermodynamics of Irreversible Processes, Chem.Rev.60, 15 – 37 (1960).
3. L. Onzager, Reciprocal Relations in Irreversible Processes I. Phys. Rev. 37, 405 – 426 (1931).
4. M.M. Mamedov, B.M. Mamedov, Fundamentals of Universal Nonequilibrium Thermodynamics, Aktual'nye Problemy Sovremennoi Nauki 1, 15 – 118 (2012).
5. M.M. Mamedov, B.M. Mamedov, The Laws of Universal Nonequilibrium Thermodynamics, Aktual'nye Problemy Sovremennoi Nauki 5, 133 – 137 (2012).
6. R. Haase, Thermodynamics of Irreversible Processes (Moscow: Mir Publ. 1967), 544 p.
7. M.M. Mamedov, New Linear Nonequilibrium Thermodynamics – Supposed Scientific Revolutionary Discovery, Yestestvennye i Tekhnicheskiye Nauki 4, 56 – 62 (2006).
8. M.M. Mamedov, B.M. Mamedov, Proof of Onsager's Thermodynamics Absurdity on the Basis of Experimental Data, Aktual'nye Problemy Sovremennoi Nauki 3, 175 – 179 (2012).
9. M.M. Mamedov, The Invalidity of Traditional Proof of Prigogine's Minimum Entropy Production Principle, Letters to JETF 29 (8), 69 – 71 (2003).
10. M.M. Mamedov, Universal Nonequilibrium Thermodynamics and a Fundamentally New Scientific Concept of Perpetual Motion Machine of the Second Kind (Open to Discussion), *Proc. XIII Interstate Workshop (November, 2012) "Thermoelectrics and Their Applications"* (Saint-Petersburg, 2013, P. 220 – 225).

Submitted 22.04.2013.

ARTICLE PREPARATION RULES

The article shall conform to the journal profile. The article content shall be legible, concise and have no repetitions.

The article shall be submitted to the editorial board in electronic version.

The text shall be typed in text editor not lower than MS Word 6.0/7.0.

Page setup: "mirror margins"- top margin – 2.5 cm, bottom margin – 2.0 cm, inside – 2.0 cm, outside– 3.0 cm, from the edge to page header – 1.27 cm, page footer – 1.27 cm.

Graphic materials, pictures shall be submitted in color or, as an exception, black and white, in .opj or .cdr formats, .jpg or .tif formats being also permissible. According to author's choice, the tables and partially the text can be also in color.

The article shall be submitted in English on A4 paper sheets; the number of pages shall not exceed 12. By agreement with the editorial board, the number of pages can be increased.

To accelerate publication of the article, please adhere to the following rules:

- the authors' initials and names are arranged in the centre of the first page at the distance of 1 cm from the page header, font Times New Roman, size 12 pt, line spacing 1.2;

- the name of organization, address (street, city, postal code, country) – indent 1 cm below the authors' initials and names, font Times New Roman, size 11 pt, line spacing 1.2, center alignment;

- the title of the article is arranged 1 cm below the name of organization, in capital letters, semi-bold, font New Roman, size 12 pt, line spacing 1.2, center alignment. The title of the article shall be concrete and possibly concise;

- the abstract is arranged 1 cm below the title of the article, font Times New Roman, size 10 pt, in italics, line spacing 1.2 ,center alignment;

- key words are arranged below the abstract, font Times New Roman, size 10 pt, line spacing 1.2, justified alignment. The title "Key words" – font Times New Roman, size 10 pt, semi-bold;

- the main text of the article is arranged 1 cm below the abstract, indent 1 cm, font Times New Roman. size 11 pt, line spacing 1.2, justified alignment;

- formulae are typed in formula editor, fonts Symbol, Times New Roman. Font size is "normal" – 12 pt, "large index" – 7 pt, "small index" – 5 pt, "large symbol" – 18 pt, "small symbol" – 12 pt). The formula is arranged in the text, centre aligned and shall not occupy more than 5/6 of the line width, formulae are numbered in round brackets right;

- dimensions of all quantities used in the article are represented in the International System of Units (SI) with the explication of the symbols employed;

- figures are arranged in the text. The figures and pictures shall be clear and contrast; the plot axes – parallel to sheet edges, thus eliminating possible displacement of angles in scaling;

- tables are arranged in the text. The width of the table shall be 1 cm less than the line width. Above the table its ordinary number is indicated, right alignment. Continuous table numbering throughout the text. The title of the table is arranged below its number, center alignment;

- references should appear at the end of the manuscript. References within the text should be enclosed in square brackets. References should be numbered in order of first appearance in the text. Examples of various reference types are given below.

– L.I. Anatychuk, *Thermoelements and Thermoelectric Devices: Handbook* (Kyiv: Naukova Dumka, 1979), p.766. (Book)
– T.M. Tritt, Thermoelectric Phenomena, Materials, and Applications, *Annual Review of Materials Research* **41**, 433 (2011). (Journal paper)
– U. Ghoshal, *Proceedings of the XXI International Conference on Thermoelectrics* (N.Y., USA, 2002), p. 540. (Proceedings Conference)

The article should be supplemented by:

• letter from the organization where the work was performed or from the authors of the work applying for the publication of the article;

• information on the author (authors): last name and initials; full name and postal address of the institution where the author works; academic degree; position; telephone number; E-mail;

• author's (authors') photo in color or, as an exception, in black and white. With the number of authors more than two their photos are not given;

• author's application to the following effect:

We, the undersigned authors, … transfer to the founders and editors of "Journal of Thermoelectricity" the right to publish the article…in Ukrainian, Russian and English. This is to confirm that the present publication does not violate the copyright of other persons or organizations.

Date Signatures

Below is given an example of article preparation.

Author's
photo
3 × 4 cm

A.I. Casian[1], B.M. Gorelov[2]

Author's
photo
3 × 4 cm

[1]Technical University of Moldova,
168, Stefan cel Mare Ave.,
Chisinau, MD-2004, Moldova;
[2]Institute of Surface Chemistry of National Academy
of Sciences of Ukraine, 17, Gen. Naumov Str.,
Kyiv, 03164, Ukraine

STATE OF THE ART AND PROSPECTS OF THERMOELECTRICITY ON ORGANIC MATERIALS

The aim of the paper is to analyze the expected thermoelectric opportunities of organic materials, including some highly conducting quasi-one-dimensional crystals. It is shown that interest of investigators in these materials has been growing recently. Quasi-one-dimensional organic crystals have high prospects for thermoelectric applications. These materials combine the properties of multi-component systems with more diverse internal interactions and of quasi-one-dimensional quantum wires with increased density of electronic states. It is shown that the values of the thermoelectric figure of merit ZT ~ 1.3 – 1.6 at room temperature are expected in really existing organic crystals of tetrathiotetracene-iodide, TTT_2I_3, if the crystal parameters are approaching the optimal ones.

Key words: thermoelectricity, tetrathiotetracene-iodide, polarizability.

Introduction

It is known that conducting organic materials usually have much lower thermal conductivity than the inorganic materials. Moreover, the organic materials can be fabricated by simpler chemical methods, and it is expected that such materials will be less expensive in comparison with the inorganic ones. Exactly these properties attracted attention to such materials for the use in thermoelectric (TE) applications long time ago [1, 2]. In spite of relatively high value of the thermoelectric figure of merit $ZT = 0.15$ at room temperature observed in polycopper phthalocyanine [2] as early as 1980, the thermoelectric properties of organic materials are still weakly investigated. This situation has the only explanation that thermoelectricians are still weakly interested in organic materials, and organic chemists are also weakly interested in thermoelectric materials. Moreover, in order to seek good organic thermoelectrics, it is necessary to organize multidisciplinary consortiums of physicists, organic chemists and engineers in the field of thermoelectricity. …

The aim of this paper is to present briefly the state-of-the-art of investigations in the area of new organic thermoelectric materials and to describe the nearest expected results for really existing quasi-one-dimensional organic crystals of tetrathiotetracene-iodide, TTT_2I_3.

Quasi-one-dimensional organic crystals of TTT_2I_3

The structure of quasi-one-dimensional organic crystals of tetrathiotetracene-iodide, TTT_2I_3, has been briefly described in [34]. These needle-like crystals are formed of segregate chains or stacks of planar molecules of tetrathiotetracene *TTT*, and iodine ions. The chemical compound TTT_2I_3 is of mixed-valence: two molecules of *TTT* give one electron to the iodine chain which is formed from I_3^- ions. The

conductivity of iodine chains is negligibly small, so that only *TTT* chains are electrically conductive and holes serve as carriers. The electrical conductivity σ along *TTT* chains at room temperature varies between 10^3 and 10^4 Ω^{-1}cm^{-1} for crystals grown by gas phase method [35], and between 800 and 1800 Ω^{-1}cm^{-1} for crystals grown from solution [36]. Thus, the conductivity is very sensitive to crystal impurity and perfection which depends on growth method. In the direction perpendicular to chains σ is by three orders of magnitude smaller than in the longitudinal direction and is neglected. …

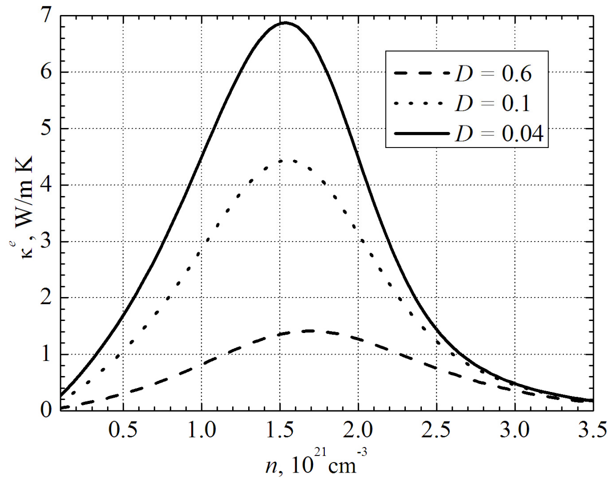

Fig. 1. Dependences of electron thermal conductivity κ^e *on n.*

$$\sigma = R_0,\ S = R_1 / eTR_0,\ \kappa^e = \left(e^2 T\right)^{-1}\left(R_2 - R_1^2 / R_0\right), \tag{1}$$

Thermoelectric properties

Expressions (2) – (3) have been calculated in order to determine the thermoelectric properties of quasi-one-dimensional organic crystals of TTT_2I_3 with different degrees of purity….

Conclusions

The state-of-the-art of research on new organic materials for thermoelectric applications is analyzed. It is shown that the interest of investigators in these materials has been growing in recent years. The highest value of $ZT \sim 0.38$ at room temperature has been measured in doped acetylene, with the only problem that this material is not stable. Accurate control of the oxidation level in poly (3, 4-ethylenedioxythiophene) (PEDOT) gave the power factor 324 μW·m^{-1}K^{-2} and in combination with its low intrinsic thermal conductivity ($\kappa = 0.37$ W·m^{-1}K^{-1}) yielded $ZT = 0.25$ at room temperature, and this material is air-stable….

References

1. Ali Shakouri, Recent Developments in Semiconductor Thermoelectric Physics and Materials, *Annu.Rev.Mater.Res.***41**, 399-431 (2011).
2. L.I. Anatychuk, *Thermoelectricity, Vol.2, Thermoelectric Power Converters* (Kyiv, Chernivtsi: Institute of Thermoelectricity, 2003), 376p.
3. M.E. Bengen, *German Patent Appl*. OZ 123, 438, 1940; *German Patent* 869,070, 1953, Tech. Oil Mission Reel, 143,135, 1946.